ENZYMATIC SYNTHESIS AND PHOTOPHYSICAL CHARACTERIZATION OF DUALLY FLUORESCENT FLAVIN ADENINE DINUCLEOTIDE COFACTORS

A Dissertation
Submitted to
the Temple University Graduate Board

In Partial Fulfillment
of the Requirements for the Degree
DOCTOR OF PHILOSOPHY

---

by
Kimberly J. Jacoby
July 2016

Examining Committee Members:

Robert J. Stanley, Advisor, Chemistry
Ann M. Valentine, Chemistry
Vincent A. Voelz, Chemistry
Charles T. Grubmeyer, External Member, Medical Genetics and Molecular Biochemistry, Temple University

©
Copyright
2016

by

Kimberly J. Jacoby
All Rights Reserved

ABSTRACT

Many enzymes require cofactors in order to carry out specific functions. Flavins, which are naturally fluorescent, compose a unique group of redox cofactors because they have the ability to transfer one or two electrons and are therefore found in three different oxidation states. A specific flavin, flavin adenine dinucleotide (FAD), is a crucial cofactor that facilitates electron transfer in many flavoproteins involved in DNA repair, photosynthesis, and regulatory pathways.

One example of a FAD-containing DNA repair protein is DNA Photolyase (PL). *E. coli* PL is a monomeric flavoprotein that facilitates DNA repair via a photoinduced electron transfer reaction. The catalytic cofactor, FAD, transfers an electron to a thymidine dimer lesion, to cleave the cyclobutane ring and restore the DNA strand. Although the mechanism of repair has been partially elucidated by our group, it is still unclear whether or not the electron is transferred directly from the isoalloxazine moiety to the dimer or if the electron hops from the isoalloxazine moiety to the adenine moiety to the dimer. This sequential hopping mechanism should have excited state absorption features for the reduced flavin species, an adenine radical anion, and the semiquinone flavin species. To investigate the mechanistic role of adenine, *E. coli* PL has been reconstituted with ε-FAD, an FAD analogue in which the adenine was substituted via chemical means with 1,N^6 – ethenoadenine dinucleotide. ε-FAD was selected due to its ease of synthesis and because its structure changes the thermodynamic driving force for the electron transfer reaction, by lowering the energetic gap (LUMO-LUMO) between the isoalloxazine ring and the modified adenine. In order to characterize the excited state

dynamics of the mutant chromophore, the transient absorption measurements were made of each free flavin in solution. These measurements indicate the pathway of electron transfer must be mediated via superexchange rather than a hopping mechanism. This important result shows that the role of adenine in photolyase is to facilitate a superexchange electron transfer mechanism, and a modified flavin can act as a reporter under these experimental conditions.

By exploiting *Corynebacterium ammoniagenes* FAD synthetase adenylation promiscuity, we have enzymatically-synthesized and purified a novel dually fluorescent flavin cofactor. This new flavin adenine dinucleotide (FAD) analogue, flavin 2-aminopurine (2Ap) dinucleotide (F2ApD), can be selectively excited through the 2Ap moiety at 310 nm, a wavelength at which flavins have intrinsically low extinction. The dinucleotide 2Ap emits at 370 nm with high efficiency. This emission has excellent overlap with the absorption spectra of both oxidized and reduced hydroquinone flavin (Fl_{OX} and Fl_{HQ} respectively), which emit at ~525 and ~505 nm respectively. We have characterized the optical properties of this dually fluorescent flavin, iFAD. Steady state fluorescence excitation and emission spectra were obtained and contrasted with the other flavins. Temperature- and solvent-dependent emission spectra suggest that F2ApD stacking interactions are significantly different compared to FAD and etheno-FAD (εFAD). The optical absorption spectra of these dinucleotides were compared with FMN to explore electronic interactions between the flavin and nucleobase moieties. To probe the evolution of the different excited state populations, femtosecond transient absorption measurements were made on the iFADs, revealing that F2ApD exhibited unique transient

spectra as compared to either FAD or εFAD. The significance of these results to flavins, flavoprotein function, and bioimaging are discussed.

The reconstituted ε-FAD in *E.coli* photolyase was catalytically active and actually repaired more efficiently than the FAD-reconstituted photolyase. To validate that an enzymatically synthesized iFAD could be reconstituted into a flavoprotein, this work shows a DNA repair assay using F2ApD that was reconstituted into *E. coli* photolyase, generating the reconstituted analogue, ApPL. Activity assays were compared between FAD-PL and ApPL. This comparison further elucidates the importance of the driving force on the electron transfer reaction in PL. A comparison of fluorescence spectroscopies between the reconstituted PLs highlights their applicability as biosensors and/or mechanistic reporters.

DEDICATION

For my grandparents

ACKNOWLEDGMENTS

My academic accomplishments over the past six years would not have been possible without the guidance and support of my advisor, Dr. Robert Stanley. I will be forever grateful that he accepted me into his lab. Dr. Stanley has been and will always be a great mentor. He may never know how appreciative I am for the countless hours he spent with me in the lab, but I am grateful for every minute of his time. He pushed me to be a better scientist. His patience and passion for teaching science will always be inspirational to me.

I would like to thank Dr. Ann Valentine, Dr. Vincent Voelz, and Dr. Charles Grubmeyer for their willingness to serve on my doctoral advising committee. It was Dr. Grubmeyer's Enzymes and Proteins class that made me fall in love with enzymology. I appreciate all of the thought-provoking conversations and guidance throughout my years at Temple University.

All of the FAD synthetase experiments I worked on would not have been possible without the generous provision of plasmids from our collaborators Dr. Maria Barile and Dr. Milagros Medina. I would like to especially thank Dr. Barile for her help concerning the purification and isolation of the hFADs isoform 2 protein. I am also very appreciative of Dr. Richard Waring's donation of phosphodiesterase, which proved to be active and very useful for our steady state fluorescence measurements.

During my time in graduate school I was fortunate enough to have a supportive family and a great group of friends. My grandparents were always invested in my education and I hope I have made them proud. My husband, Rob, has been so compassionate and understanding of my academic journey. Rob, thank you for encouraging me every day. My friends Dr. Vincent Spata, Dr. Elizabeth Cerkez, Jae Eun Cheong, Steph Kumor and Dr. Kate Buettner thank you for being there for me in the best and worst of times.

It is very important to me that I acknowledge my current and past lab members. The Stanley Lab members have been my family during my time in graduate school. I cannot thank them enough for all of their support. I learned very quickly that every person has some piece of knowledge or expertise that they can contribute to the lab. Even though our skillsets varied widely, we were always united on a mission to answer questions. I've become a better teacher and a better student because of these people. Whether I needed a shoulder to cry on or a victory lap of celebration, my colleagues were always there for me. They are Dr. Madi Narayanan, Dr. Vijay Singh, Dr. Manasa Mammunooru, Dr. Raymond Pauszek, Dr. Sudipto Munshi, David Barnard, Steven Meckel, Rylee McBride, Emily Mattes, Kim Tran, My Nguyen, and Jaqi Kakalecik. I would especially like to thank Ray, David, and Rylee without your help I would have never written this document. I am so lucky to call you my friends.

I would like to thank my mentors, Dr. Linda Mascavage, Dr. Vladi Wilent, Dr. Roy Keyer, Dr. Jason Cross, and Dr. Gretchen Maurer for their kind words of reassurance. Thank you for helping me develop new experiments and ironing out some organic mechanisms.

I am very thankful to have been fortunate enough to receive financial support from teaching assistantships funded by the Temple University Department of Chemistry, FSRI grant and Dissertation Completion grant funded by the Temple University Graduate School, and a research assistantship funded by NASA.

TABLE OF CONTENTS

Page

LIST OF TABLES

Table Page

LIST OF FIGURES

Table Page

CHAPTER 1

INTRODUCTION

1.1 Overview

Enzymes are folded chains of amino acids that perform biological catalysis. Some of these polypeptides accomplish this task using nothing more than salts, water, and their particular active fold. A wide class of enzymes, however, utilize accessory molecules known as cofactors or coenzymes to carry out specific functions. Flavins, vitamin B_2 derivatives which are naturally fluorescent, compose a unique group of redox cofactors because they have the ability to transfer one or two electrons and are therefore found in three different oxidation states. A specific flavin derivative, flavin adenine dinucleotide (FAD), is a crucial cofactor that facilitates electron transfer in many flavoproteins[1]. These flavoproteins are involved in metabolic and biosynthetic processes, photosynthesis, regulatory signaling pathways, and DNA repair. One specific DNA repair enzyme is *E.coli* DNA photolyase. *E.coli* DNA photolyase is a monomeric flavoprotein that facilitates DNA repair via a photoinduced electron transfer reaction. The catalytic cofactor, FAD, transfers an electron to the cyclobutylpyrimidine dimer (CPD), the site of ultraviolet light-induced damage, to cleave the lesion and restore the DNA strand[2]. Although the mechanism of repair has been elucidated by our group, it is still unclear whether or not the electron is transferred directly from the isoalloxazine moiety to the dimer or if the electron hops from the isoalloxazine moiety to the adenine moiety to the dimer[3–5]. This sequential hopping mechanism should have excited state absorption features for the reduced flavin species, an adenine radical anion, and the semiquinone flavin species. This dissertation addresses the role of adenine in the electron transfer

mechanism by using a dually fluorescen-t modified adenine 1,N^6 – ethenoadenine dinucleotide (εFAD). This dually fluorescent FAD was selected because its structure changes the thermodynamic driving force for the electron transfer reaction, by lowering the energetic gap (LUMO-LUMO) between the isoalloxazine ring and the modified adenine. Since both the adenine and flavin are capable of fluorescent emission, these FAD analogs could act as fluorescent reporters on a wide variety of enzymatic reactions, include metabolic processes. For this reason we have coined the term "iFAD" with the goal that after we have characterized the photophysical properties of the analogs we will use them to image metabolism in real time in living cells.

As part of this goal we present the characterization of the excited state dynamics of the chromophore before complicating the system by adding protein. Transient absorption measurements were made of the chemically synthesized flavin in solution and compared to FAD in the oxidized and reduced oxidation states.

The *E.coli* DNA photolyase/εFAD system proves that iFADS have unique photophysical properties giving insight to photoinduced electron transfer mechanisms. After characterizing the oxidized and reduced excited states of εFAD, there was motivation to expand the library of iFADS with different fluorescent adenine analogues. A library of iFADS could be used for bioimaging, drug therapeutics, and mechanistic reconstitution studies. This dissertation validates that iFADS may be generated enzymatically. FAD synthetase (FADS) is a ubiquitous enzyme responsible for the production of flavin adenine dinucleotide via an adenylation reaction of flavin mononucleotide (FMN) from adenosine triphosphate (ATP). In *Corynebacterium ammoniagenes*, *Ca*FADS is bifunctional, also producing FMN via the phosphorylation of

riboflavin[6–9] with ATP. It has been shown that *Ca*FADS will not accept any other triphosphate nucleosides (i.e. GTP, CTP), but here we demonstrate that *Ca*FADS will accept the fluorescent base analogue aminopurine-2'-riboside-5'-triphosphate (2ApTP) for the production of F2ApD, a dually fluorescent flavin analogue.

The implications of adenylation active site promiscuity points towards potential drug targets and therapeutic design. Therefore, we overexpressed and purified human isoform-2 FAD synthetase (hFADS2) to compare *Ca*FADS nucleotide promiscuity in a mammalian adenyl transferase active sites. Human FAD (*h*FADS) synthetases are monofunctional and perform the only adenylation reaction[10,11]. We discovered that *h*FADS2 did not display the same promiscuous behavior as *Ca*FADS. The turnover of 2ApTP with FMN did not yield F2ApD and, in fact, 2ApTP appears to be a competitive inhibitor of *h*FADS. This surprising result highlights the divergent evolution of adenyl transferase sites. It is extremely promising for drug design because of the specific selectivity for native substrates in the human enzyme as compared to the bacterial enzyme. The structural differences leading to this change in activity are discussed.

F2ApD was isolated and purified from a large scale bacterial enzymatic reaction to afford characterization of the iFAD. Spectroscopic tools such as steady-state fluorescence and ultrafast time-resolved transient absorption were utilized. F2ApD exhibits a long excited state lifetime compared to FAD, suggesting that it has the potential to be a bright reporter of FAD-dependent protein activity. The chromophore is significantly more emissive than FAD, making it an attractive single molecule imaging candidate. These results are compared to εFAD, FAD, and their unadenylated precursor FMN.

In order to support the idea that the new enzymatically synthesized iFAD could be used as a modified flavin cofactor in flavoproteins, F2ApD was reconstituted in *E.coli* DNA photolyase. The reconstitution was deemed successful by UV-vis absorption spectroscopy and affinity chromatography. DNA repair activity of F2ApD-reconstituted photolyase, ApPL, was examined. The last component of this dissertation shows the successful steady-state turnover kinetics of ApPL CPD repair.

1.2 Flavins

Organic compounds containing 7,8-dimethylisoalloxazine are classified as flavins. This tricyclic heterocycle is comprised of fused xylene, pyrazine, and pyrimidine rings. This class of chromophore can be found in all domains of life and they are responsible for many biochemical reactions when incorporated into proteins as coenzymes or cofactors[12]. Unlike nicotinamide, which is a 2*e*- redox coenzyme, flavins are unique in that they can undergo both one and two electron transfer reactions. The oxidation states and structures of flavins are included for reference in Figure 1.1. Flavins as cofactors are prominent mediators of biosensing and signaling pathways such as phototropism and nitrogen fixation[13]. Flavin containing proteins, flavoproteins, are also participants in metabolic redox reactions in the mitochondria and can repair DNA in bacteria[1,14,15]. Although many of the reactions that flavins help facilitate are electron transfer mediated, approximately 10% of flavoproteins do not catalyze redox reactions.

Vitamin B_2, riboflavin, does not act as a cofactor in any enzyme, although it has been shown to be the preferred form of cofactor storage (riboflavin-binding protein in

chicken eggs and dodecin in archaeons)[16]. In bacteria, riboflavin can be synthesized *de novo* while mammals must rely on dietary uptake of riboflavin. [17,18]. Riboflavin is a precursor to the prevalent flavin cofactor flavin mononucleotide which is synthesized in an ATP-dependent reaction in bacteria. Flavin mononucleotide can be adenylated using ATP and FAD synthetase to form the abundant flavin adenine dinucleotide cofactor, discussed in detail in section 1.2[6,7,9,10]. Macheroux *et al* identified 374 flavin-dependent proteins, the majority of which (75%) utilize flavin adenine dinucleotide over flavin mononucleotide (25%) (see Figure 1.2 for cofactor structure). The adenine moiety is of significant importance in the noncovalent binding and stabilization of FAD in a protein, but an enzymatic role of the adenine has not been established. Several studies incorporate flavin analogues into flavoproteins, such as *E.coli* DNA photolyase (*Ec*PL) and FAD synthetase with the motivation to understand the mechanisms at hand and identify potential drug targets for "flavin intensive" pathogens[16,19]. These studies show that the reconstituted proteins maintain overall activity and the modified flavins gave insight to the excited state character of the cofactor[20–23]. The work presented in this dissertation shows successful incorporation of adenine analogues of FAD into *Ec*PL and discusses the implications that modifications to the adenine moiety have on the excited state of the flavin and the overall activity of the reconstituted enzyme.

1.3 Excited State Characterization of Flavins in Simple Solvents

Flavin mononucleotide in solution has been well characterized in all three oxidation states. The reported quantum yield for fluorescence is Φ_f=0.27 in the oxidized state[24,25]. This value is more than ten times higher than that of the FAD fluorescence

quantum yield. The ultrafast excited state dynamics for FMN are long lived as compared to FAD, which complements the steady-state fluorescence quantum yields[25–28].

The quenching mechanism is attributed to the photoinduced electron transfer, PET, between the adenine moiety and the isoalloxazine ring. In aqueous solution 80% of the FAD population is in the stacked conformation and 20% of the population is in an unstacked conformation[29,30]. The stacked population is assumed to be quenched due to PET[24,28]. In spite of decades of work, definitive evidence for this quenching mechanism (e.g. observation of radical ions) has not been presented.

Like FAD, the oxidized spectra of εFAD, the structure of which can be seen in Figure 1.3, exhibits excited state energy transfer and quenching. In this case energy transfer between the ethenoadenine moiety and the isoalloxazine ring is readily observed as confirmed by Barrio *et al* in which both εAde and flavin emissions were enhanced by the addition of phosphodiesterase, resulting in phosphodiester bond cleavage and release of the ethenoadenine [29]. This useful modified oxidized cofactor has been used to replace FAD_{OX} in several flavoproteins[31,32].

The excited state quenching mechanism of reduced $FADH^-$ is not as well studied. There is no spectral evidence in the literature that clearly identifies a PET quenching mechanism for the reduced FAD. No radicals have been observed after excitation of the flavohydroquinone or its anion. However computational modeling supports the hypothesis that the adenine moiety mediates excited state catalytic electron transfer processes in the protein EcPL[3,12,26,27,33–40]. While all experimental data seems to support two state sequential decay kinetics with a picosecond(s) lifetime and a longer lived (ns) component for $*FADH^-$ in solution, data on the charge redistribution of reduced $FADH^-$

in the excited state raises questions about previous experimenters fitting parameters and calculations performed[4,12,26,27,39,41,42]. The electron density is localized on the xylene ring in the excited state[43,44]. Previous computational analysis performed distance calculations from the N10 position to the adenine ring[45]. Electron transfer is exponentially dependent on distance so this error is detrimental to the conclusions made about adenine's role in electron transfer[46,47]. This dissertation addresses the excited state dynamics of both $FADH^-$ and $\varepsilon FADH^-$ in solution with implications on the role of adenine in DNA photolyase.

1.4 Biosynthesis of Flavin Adenine Dinucleotide in Bacteria

FAD synthetase (FADS) is a ubiquitous enzyme responsible for the production of the essential cofactor flavin adenine dinucleotide (FAD) via an adenylation reaction of flavin mononucleotide (FMN) from adenosine triphosphate (ATP). In bacteria, this enzyme is bifunctional, also producing FMN via the phosphorylation of riboflavin; see Figure 1.4 for reaction scheme[6,48]. In the bacterium *Corynebacterium ammoniagenes*, 38 kDa FAD synthetase folds into two modules, a kinase module and an adenylation module[8,49]. Both activities are Mg^{2+}-dependent and the order of reactant binding and product release follows a bi-bi mechanism. A crystal structure (PDB ID 2X0K) unveiled a hexameric quaternary structure comprised of a dimer of trimers, see Figure 1.5 [8].

The N-terminal residues 1-186 correspond to the FMN adenyl transferase (FMNAT) active site, which takes on an α/β dinucleotide binding domain with a typical Rossman fold composed of a parallel β-sheet of six strands and five α-helices in a twisted conformation. There is an additional small subdomain made of a β-hairpin and two short α-helices. This structure is not homologous to mammalian or yeast FMNATs; however it

does belong to the nucleotidyltransferase superfamily[8]. The module is responsible for adenylation of FMN to form FAD, but also catalyses the reverse reaction to form FMN and ATP from FAD and pyrophosphate (PPi).

The C-terminal residues (187-338) share sequence and structural homology with monofunctional riboflavin kinases (RFK). This domain makes FMN from riboflavin and ATP. The RFK domain folds into a β-barrel with six anti-parallel β-strands and a long α-helix with seven interconnecting loops.

The FMNAT domain consists of three motifs that are highly conserved in the FAD synthetase and NT families i.e. 28-HxGH-31, 123-Gx(D/N)-125 and 161-xxSSTxxR-168[19,50]. If the sequence is truncated the FMNAT module cannot act independently from the RFK module. It is also important to note that the quaternary structure of caFADS (a dimer of trimers) may facilitate ligand shuttling between the two active sites of contiguous protomers[49]. In this dissertation, the promiscuity of the FMNAT active site is exploited and characterized. Homology and structural differences are discussed to explain the results.

1.5 Biosynthesis of Flavin Adenine Dinucleotide in Humans

In humans, FAD synthesis from riboflavin is dependent on a sequential catalysis of two independent proteins, riboflavin kinase and FAD synthetase, also known as FAD synthase. FAD synthetase is a monofunctional enzyme that exists in two isoforms. The FAD synthetase human isoform 2 (hFADS2) is localized in the cytosol and human isoform 1 (hFADS1) is localized in the mitochondria[51]. All work in this dissertation corresponds to hFADS2 only. The 57 kDa hFADS2 enzyme folds into two domains, a phosphoadenosine phosphosulfate reductase at the C-terminus and a molybdo-pterin-

binding domain at the N-terminus[10,11]. While the molybdo-pterin-binding domain function is not known, the phosphoadenosine phosphosulfate reductase domain is responsible for FAD synthesis and shares over 60% similarity and 34% identity with corresponding FMN adenyl transferase Fad1p protein domain from eukaryotic *S. cerevisiae* [11,52]. Similarly to *C. ammoniagenes* the reaction is Mg^{2+} dependent and the order of reactant binding and product release follows a bi-bi mechanism. To date, the crystal structure of hFADS2 remains unsolved, the FAD synthetase crystal structure from eurkaryotic yeast is shown in Figure 1.6[52]. A comparative analysis of the promiscuity between caFADS and hFADS is discussed in Chapter 3.

1.6 *E. coli* DNA Photolyase

E. coli DNA photolyase is a 54 kDa monomeric DNA repair flavoprotein, see Figure 1.7. This enzyme is responsible for repairing UV damaged DNA lesions called cyclobutylpyrimidine dimers (T<>T or CPDs). These T<>T dimers are bound as substrate to the enzyme and then repaired via a photoinduced electron transfer mechanism catalyzed by a fully reduced anionic flavin, $FADH^-$. EcPL also contains an antenna cofactor methenyltetrahydrofolate (MTHF) that is not essential for catalysis but can improve the efficiency of repair under light limiting conditions[53,54]. Although the catalytic cycle for this enzyme has been solved the reaction intermediates are still highly debated[3,4,55]. Computational studies indicate that the adenine mediates the electron transfer process via a virtual intermediate[34–36]. However, Glusac *et al.* argue that a real radical adenine anion intermediate exists for free flavin in solution[41].

1.7 Ultrafast Transient Absorption Spectroscopy

Ultrafast dynamics are readily unveiled using the transient absorption experimental technique. This technique is used to study both biological and chemical photoinduced excited state properties[56]. The transient absorption technique is used to examine excited-state energy transfer, electron and/or proton transfer, intersystem crossing, isomerization and charge separation. These processes observed do not have to be emissive, they can be representative of dark states evolving in time[57].

The subpicosecond experiments described in this dissertation use short laser pulses to achieve time resolution 200 fs-3,500 ps. A small fraction (~5%) of the sample is photoexcited to an electronically excited state via a short pump pulse[57]. A low intensity probe pulse consisting of either a white light continuum pulse or one with narrower bandwidth (generated in a noncolinear optical parametric amplifier) probes the evolution of the transmittance of the sample over time by delaying the pump arrival relative to the probe pulse using an opto-mechanical delay line[56,58]. This information is collected on a charged coupled device camera and then a difference absorption spectra is calculated.

$$\Delta A = A_{excited\ state} - A_{ground\ state} = \log(\Delta I_0/\Delta I)$$

Equation 1. Difference Absorption

A difference absorption spectra is comprised of several contributions from different processes. The ground-state bleach (GSB) is a negative ΔA corresponding to the population of the sample that is promoted to the excited state via the pump pulse. It is negative because there are fewer molecules in the ground state for the excited sample as

compared to the non-excited sample[59]. Stimulated emission (SE) is another negative contribution to ΔA because a photon from the probe pulse induces the emission of a photon from the excited molecule. The stimulated emission produced photon emits in the same direction as the probe photon so both are detected causing an increase of light hitting the detector as compared to the unexcited molecule[60]. Excited state absorption (ESA) is a positive ΔA spectral feature caused by levels of higher excited states (*n*) being populated from the initial excited state (*i*) if the extinction coefficient for the excited state absorption $\varepsilon(i \rightarrow n) > \varepsilon(0 \rightarrow i)$. Product absorption may also result in a positive spectral feature. Such products may be long-lived but transient intermediate states that include triplet formation, charge-separated states, and isomerization states[57].

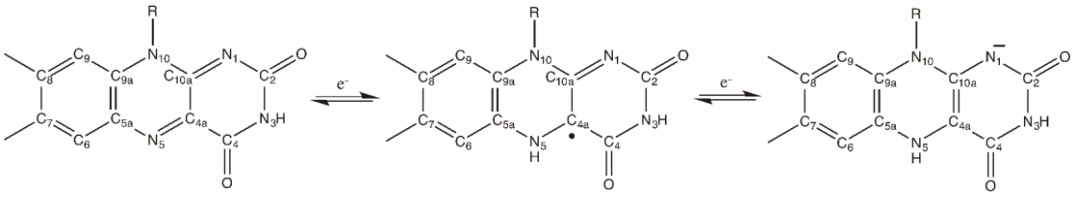

Figure 1.1: Three oxidations states of flavins (left to right): Oxidized (Fl_{OX}), semiquinone ($FlH^{\bullet}$, $1e^-$), and anionic hydroquinone (FlH^-, $2e^-$).

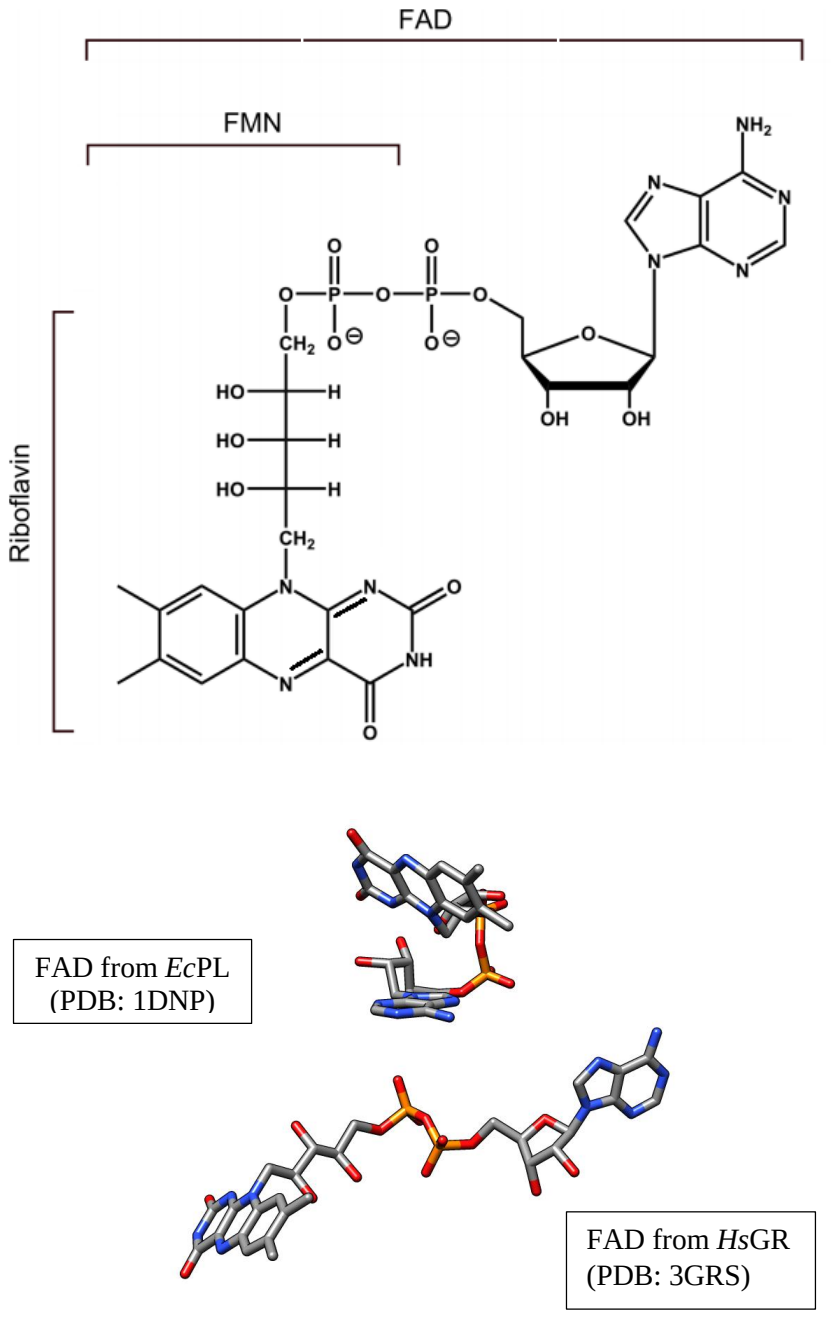

Figure 1.2: Flavin adenine dinucleotide in PL and glutathione reductase, a "normal" FAD-dependent metabolic enzyme.

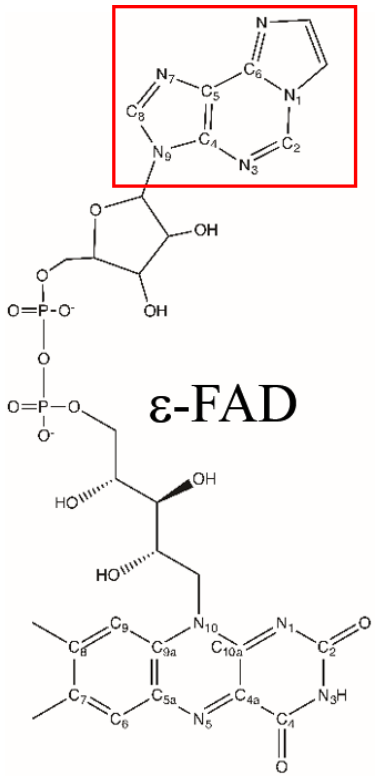

Figure 1.3. εFADox. The εAdo moiety is boxed in red

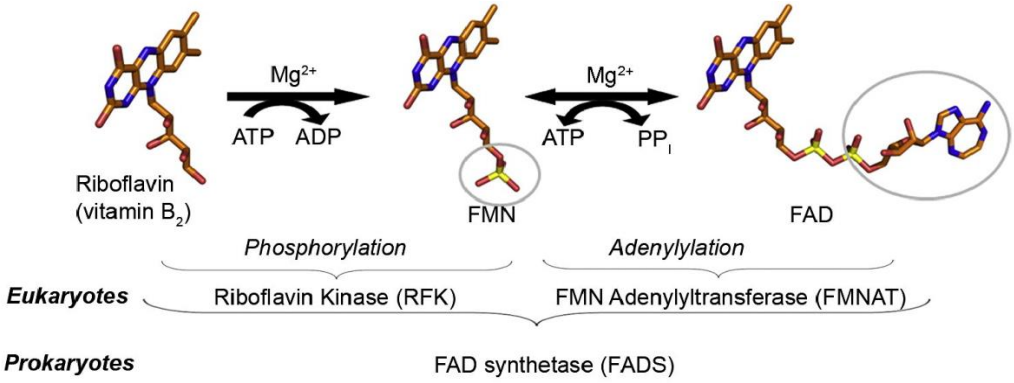

Figure 1.4. Reaction scheme of bifunctional enzyme FAD synthetase. Reverse scheme not shown[6,8].

Figure 1.5. Crystal structure of oligomeric FAD synthetase isolated from *C. ammoniagenes* PDB ID 2X0K[8].

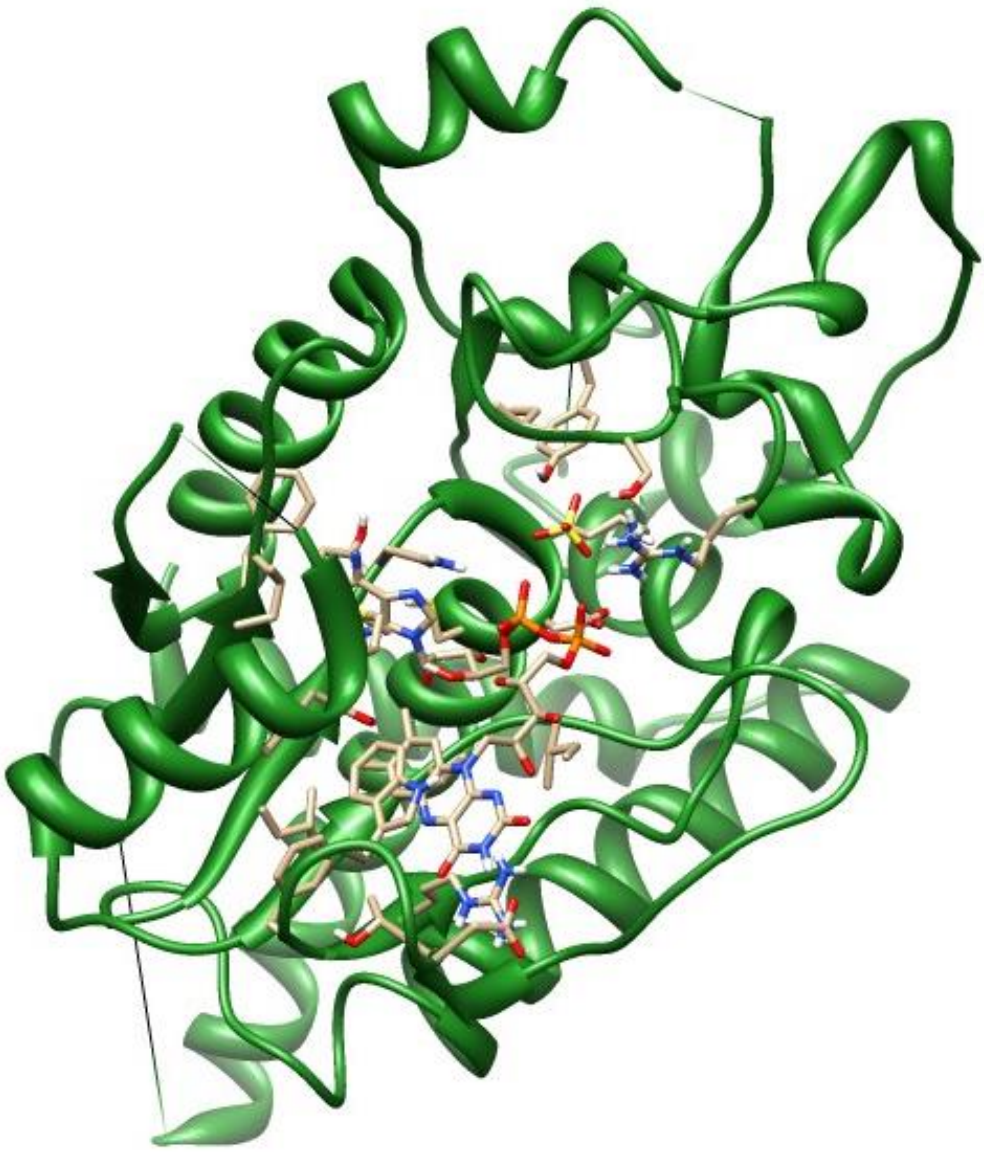

Figure 1.6. Crystal structure of FAD synthetase isolated from *S. cerevisiae* PDB ID 2WSI[61].

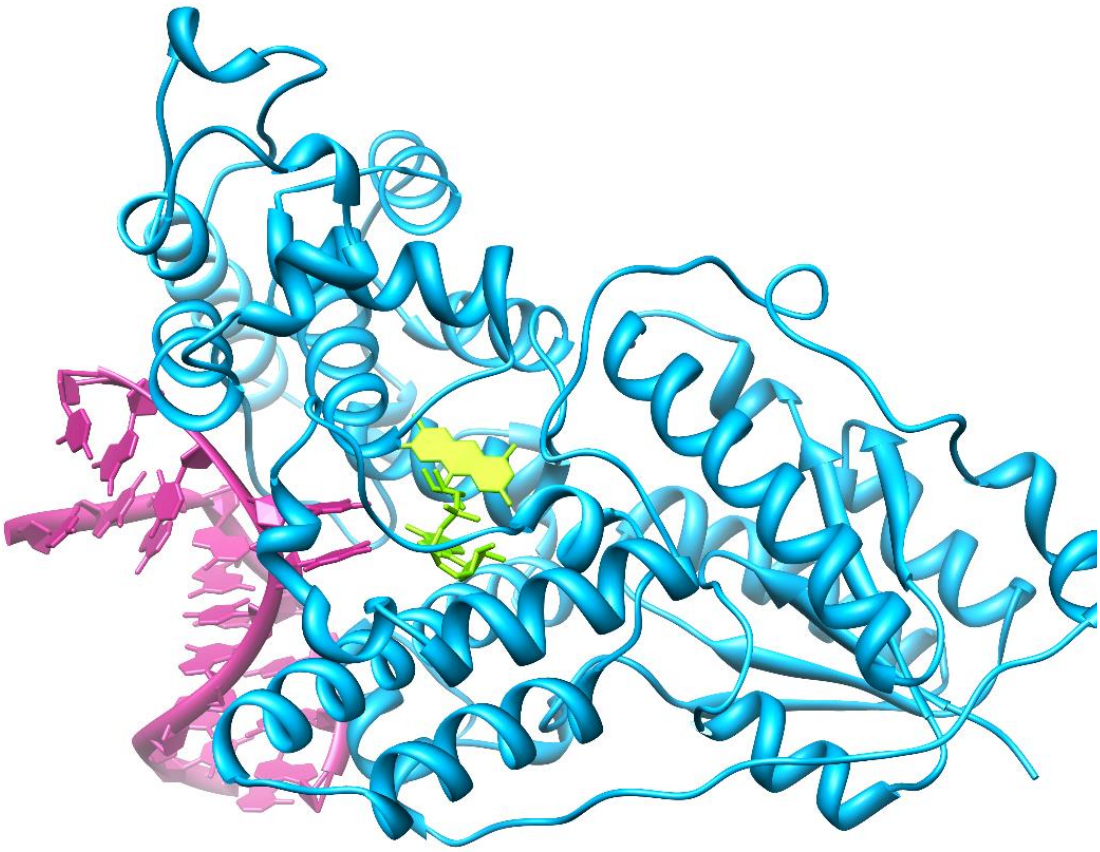

Figure 1.7. Crystal structure of *A. nidulans* DNA Photolyase PDB ID 1TEZ[62].

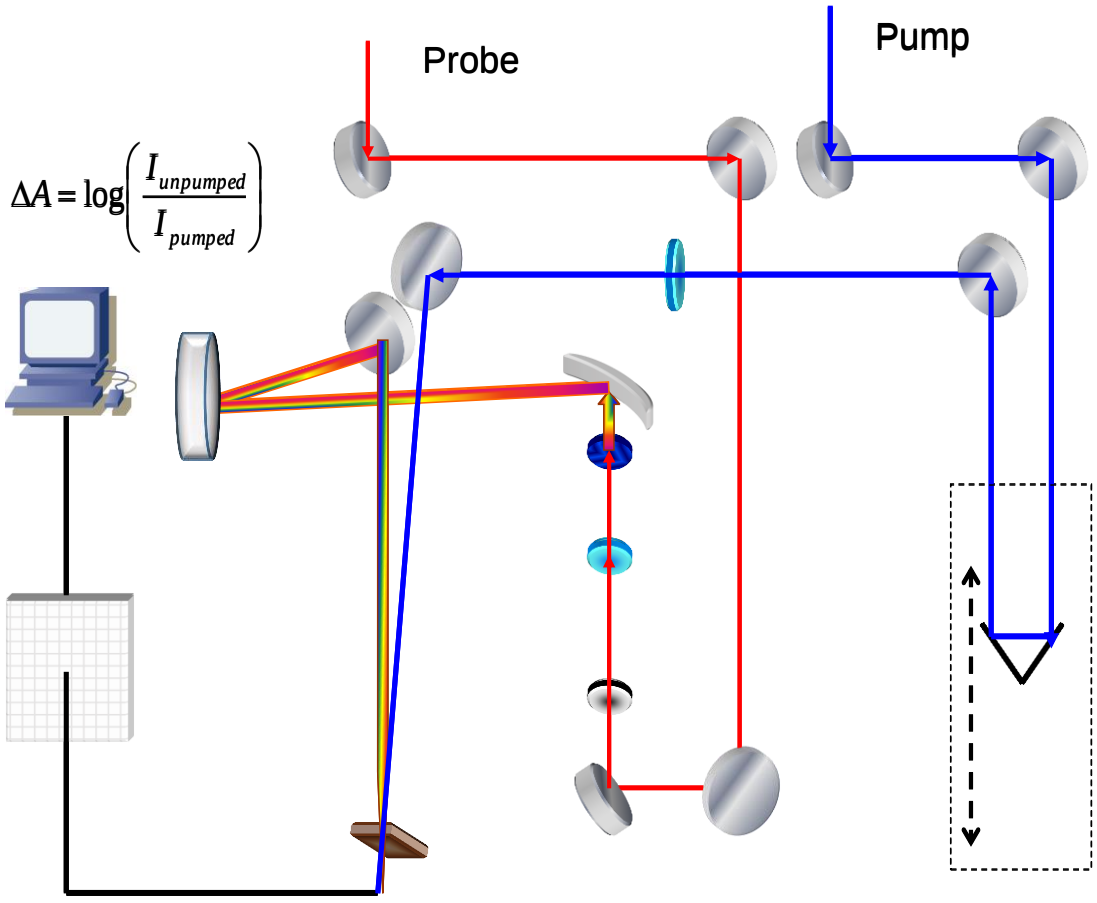

Figure 1.8. Transient absorption experimental setup[63].

1.8 References

(1) Müller, F. In *Topics in Current Chemistry*; Springer-Verlag: Berlin, 1983; Vol. 108, pp 71–107.

(2) Sancar, A. *Adv. Electron Transf. Chem* **1992**, *2*, 215–272.

(3) MacFarlane Iv, A. W.; Stanley, R. J. *Biochemistry* **2003**, *42* (28), 8558–8568.

(4) Liu, Z.; Tan, C.; Guo, X.; Kao, Y.-T.; Li, J.; Wang, L.; Sancar, A.; Zhong, D. *Proc. Natl. Acad. Sci.* **2011**.

(5) Brettel, K.; Byrdin, M. *Curr. Opin. Struct. Biol.* **2010**, *20* (6), 693–701.

(6) Efimov, I.; Kuusk, V.; Zhang, X.; McIntire, W. S. *Biochemistry* **1998**, *37* (27), 9716–9723.

(7) Frago, S.; Velazquez-Campoy, A.; Medina, M. *J. Biol. Chem.* **2009**, *284* (11), 6610–6619.

(8) 1. Herguedas, B.; Martinez-Julvez, M.; Frago, S.; Medina, M.; Hermoso, J. A. *J. Mol. Biol.* **2010**, 218–230.

(9) Bacher, A. *Chem. Biochem. Flavoenzymes* **1991**, *1*, 349–370.

(10) Galluccio, M.; Brizio, C.; Torchetti, E. M.; Ferranti, P.; Gianazza, E.; Indiveri, C.; Barile, M. *Protein Expr. Purif.* **2007**, *52* (1), 175–181.

(11) Torchetti, E. M.; Bonomi, F.; Galluccio, M.; Gianazza, E.; Giancaspero, T. A.; Iametti, S.; Indiveri, C.; Barile, M. *FEBS J.* **2011**, *278* (22), 4434–4449.

(12) Visser, A.; Ghisla, S.; Massey, V.; Muller, F.; Veeger, C. *Eur. J. Biochem.* **1979**,

101 (1), 13–21.

(13) MacHeroux, P.; Kappes, B.; Ealick, S. E. *FEBS Journal*. 2011, pp 2625–2634.

(14) Stankovich, M. T. In *Chemistry and Biochemistry of Flavoenzymes*; Müller, F., Ed.; CRC Press: Boca Raton, 1991; Vol. I.

(15) Sancar, G. B. *Mutat. Res.* **1990**, *236* (2-3), 147–160.

(16) Barile, M.; Giancaspero, T. A.; Brizio, C.; Panebianco, C.; Indiveri, C.; Galluccio, M.; Vergani, L.; Eberini, I.; Gianazza, E. *Curr. Pharm. Des.* **2013**, *19* (14), 2649–2675.

(17) Bacher, A.; Eberhardt, S.; Fischer, M.; Kis, K.; Richter, G. *Annu. Rev. Nutr.* **2000**, *20*, 153–167.

(18) Roje, S. *Phytochemistry*. 2007, pp 1904–1921.

(19) Serrano, A.; Ferreira, P.; Martínez-Júlvez, M.; Medina, M. *Curr. Pharm. Des.* **2013**, *19* (14), 2637–2648.

(20) Payne, G.; Wills, M.; Walsh, C.; Sancar, A. *Biochemistry* **1990**, *29* (24), 5706–5711.

(21) Jorns, M. S.; Wang, B.; Jordan, S. P.; Chanderkar, L. P. *Biochemistry* **1990**, *29* (2), 552–561.

(22) Pedrolli, D. B.; Nakanishi, S.; Barile, M.; Mansurova, M.; Carmona, E. C.; Lux, A.; Gärtner, W.; Mack, M. *Biochem. Pharmacol.* **2011**, *82* (12), 1853–1859.

(23) Murthy, Y. V. S. N.; Massey, V. *J. Biol. Chem.* **1998**, *273* (15), 8975–8982.

(24) Islam, S. D. M.; Susdorf, T.; Penzkofer, A.; Hegemann, P. *Chem. Phys.* **2003**, *295* (2), 137–149.

(25) Islam, S. D. M.; Penzkofer, A.; Hegemann, P. *Chem. Phys.* **2003**, *291* (1), 97–114.

(26) Brazard, J.; Usman, A.; Lacombat, F.; Ley, C.; Martin, M. M.; Plaza, P. *J. Phys. Chem. A* **2011**, *115* (15), 3251–3262.

(27) Kao, Y.-T.; Tan, C.; Song, S.-H.; Oztuerk, N.; Li, J.; Wang, L.; Sancar, A.; Zhong, D. *J. Am. Chem. Soc.* **2008**, *130* (24), 7695–7701.

(28) Stanley, R. J.; Macfarlane Iv, A. W. In *Proceedings of the 13th International Congress on Flavins and Flavoproteins*; Weber, R., Ed.

(29) Barrio, J. R.; Tolman, G. L.; Leonard, N. J.; Spencer, R. D.; Weber, G. *Proc. Natl. Acad. Sci. USA* **1973**, *70* (3), 941–943.

(30) Radoszkowicz, L.; Huppert, D.; Nachliel, E.; Gutman, M. *J. Phys. Chem. A* **2010**, *114* (2), 1017–1022.

(31) Penzer, G. R. *Eur. J. Biochem.* **1973**, *34* (2), 297–305.

(32) Harvey, R. A. In *Methods in Enzymology*; Donald B. McCormick, L. D. W., Ed.; Academic Press, 1980; Vol. Volume 66, pp 290–294.

(33) Li, G. F.; Glusac, K. D. *J. Phys. Chem. B* **2009**, *113* (27), 9059–9061.

(34) Medvedev, D.; Stuchebrukhov, A. A. *J. Theor. Biol.* **2001**, *210* (2), 237–248.

(35) Prytkova, T. R.; Beratan, D. N.; Skourtis, S. S. *Proc. Natl. Acad. Sci. U. S. A.* **2007**, *104* (3), 802–807.

(36) Acocella, A.; Jones, G. A.; Zerbetto, F. *J. Phys. Chem. B* **2010**, *114* (11), 4101–4106.

(37) Heelis, P. F.; Rowley-Williams, C. A.; Hartman, R. F.; Rose, S. D. *J. Photochem. Photobiol., B* **1994**, *23* (2-3), 155–159.

(38) Ghisla, S.; Massey, V.; Lhoste, J.-M.; Mayhew, S. G. *Biochemistry* **1974**, *13* (3), 589–597.

(39) Enescu, M.; Lindqvist, L.; Soep, B. *Photochem. Photobiol.* **1998**, *68* (2), 150–156.

(40) Kondo, M.; Nappa, J.; Ronayne, K. L.; Stelling, A. L.; Tonge, P. J.; Meech, S. R. *J. Phys. Chem. B* **2006**, *110* (41), 20107–20110.

(41) Li, G.; Sichula, V.; Glusac, K. D. *J. Phys. Chem. B* **2008**, *112* (34), 10758–10764.

(42) Visser, A. J. W. G.; Ghisla, S.; Lee, J. In *Flavins and Flavoproteins 1990*; Walter de Gruyter & Co.: Berlin, 1991.

(43) Pauszek, R.; Kodali, G.; Siddiqui, M. S.; Stanley, R. J. In *Proceedings of the 17th International Symposium on Flavins and Flavoproteins*.

(44) Siddiqui, M. S. U.; Kodali, G.; Stanley, R. J. *J. Phys. Chem. B* **2008**, *112* (1), 119–126.

(45) Liu, Z. Y.; Guo, X. M.; Tan, C.; Li, J.; Kao, Y. T.; Wang, L. J.; Sancar, A.; Zhong, D. P. *J. Am. Chem. Soc.* **2012**, *134* (19), 8104–8114.

(46) Moser, C. C.; Keske, J. M.; Warncke, K.; Farid, R. S.; Dutton, P. L. *Nature* **1992**, *355*, 796–802.

(47) Marcus, R. A. *Report* **1987**, No. AD, 717.

(48) Solovieva, I. M.; Tarasov, K. V.; Perumov, D. A. *Biochem.* **2003**, *68* (2), 177–181.

(49) Serrano, A.; Frago, S.; Herguedas, B.; Mart??nez-J??lvez, M.; Vel??zquez-Campoy, A.; Medina, M. *Cell Biochem. Biophys.* **2013**, *65* (1), 57–68.

(50) Yruela, I.; Arilla-Luna, S.; Medina, M.; Contreras-Moreira, B. *BMC Evol. Biol.* **2010**, *10* (1), 311.

(51) Torchetti, E. M.; Brizio, C.; Colella, M.; Galluccio, M.; Giancaspero, T. A.; Indiveri, C.; Roberti, M.; Barile, M. *Mitochondrion* **2010**, *10* (3), 263–273.

(52) Huerta, C.; Borek, D.; Machius, M.; Grishin, N. V.; Zhang, H. *J. Mol. Biol.* **2009**, *389* (2), 388–400.

(53) Sancar, G. B.; Sancar, A. *Trends Biochem. Sci.* **1987**, *12(7)*, 259–261.

(54) Johnson, J. L.; Hamm-Alvarez, S.; Payne, G.; Sancar, G. B.; Rajagopalan, K. V; Sancar, A. *Proc. Natl. Acad. Sci. U. S. A.* **1988**, *85* (7), 2046–2050.

(55) Thiagarajan, V.; Villette, S.; Espagne, A.; Eker, A. P. M.; Brettel, K.; Byrdin, M. *Biochemistry* **2010**, *49* (2), 297–303.

(56) Megerle, U.; Pugliesi, I.; Schriever, C.; Sailer, C. F.; Riedle, E. *Appl. Phys. B Lasers Opt.* **2009**, *96* (2-3), 215–231.

(57) Berera, R.; van Grondelle, R.; Kennis, J. T. M. *Photosynthesis Research*. 2009, pp 105–118.

(58) Walker, G. C.; Hochstrasser, R. M. *Tech. Chem.* **1995**, *Volume Dat*, 23,385–422.

(59) van Stokkum, I. H. M.; Larsen, D. S.; van Grondelle, R. *Biochim. Biophys. Acta, Bioenerg.* **2004**, *1657* (2-3), 82–104.

(60) Ruckebusch, C.; Sliwa, M.; Pernot, P.; de Juan, A.; Tauler, R. *Journal of Photochemistry and Photobiology C: Photochemistry Reviews*. 2012, pp 1–27.

(61) Leulliot, N.; Blondeau, K.; Keller, J.; Ulryck, N.; Quevillon-Cheruel, S.; van Tilbeurgh, H. *J. Mol. Biol.* **2010**, *398* (5), 641–646.

(62) Tamada, T.; Kitadokoro, K.; Higuchi, Y.; Inaka, K.; Yasui, A.; De Ruiter, P. E.; Eker, A. P. M.; Miki, K. *Nat. Struct. Biol.* **1997**, *4* (11), 887–891.

(63) Berera, R.; van Grondelle, R.; Kennis, J. T. M. *Photosynth. Res.* **2009**, *101* (2-3), 105–118.

CHAPTER 2

ULTRAFAST EXCITED STATE DYNAMICS OF FLAVIN N^1,N^6-ETHENOADENINE DINUCLEOTIDE: IMPLICATIONS FOR THE ELECTRON TRANSFER MECHANISM IN FAD-BINDING DNA PHOTOLYASE

2.1 Introduction

Flavins are vital biological redox molecules that can undergo either one- or two-electron transfer, making them much more versatile than the $2e^-$ redox cofactor nicotinamide. The simplest derivative is riboflavin, in which the isoalloxazine (or flavin) ring has a ribose group appended at N^{10} (see Figure 2.1 for numbering). This form is used to make the phosphorylated and dinucleotide derivatives flavin mononucleotide (FMN), and flavin adenine dinucleotide (FAD) respectively. These more complex derivatives (not riboflavin) are essential cofactors participating in electron transfer reactions that are fundamental to many biochemical processes such as photosynthesis, metabolic pathway signaling, and DNA repair[1–3].

One example of DNA repair in *E.coli* is facilitated by photoinduced electron transfer (PET) between photoexcited hydroquinone anion $^*FADH^-$ and the cyclobutane pyrimidine dimer (CPD)[4–6]. *E.coli* DNA photolyase (PL), a monomeric flavoenzyme, uses flavin adenine dinucleotide (Figure 2.2) as a coenzyme to repair UV damaged DNA. This repair reaction is facilitated by the transfer of an electron. Although the kinetics of CPD repair have been elucidated by our group and others, the role of adenine in the electron transfer pathway is still unclear[7–13].

The spectroscopic evidence, to date, does not clearly answer whether or not the electron is transferred directly from the isoalloxazine moiety to the dimer or whether the electron hops from the isoalloxazine moiety to the adenine moiety to the dimer. A sequential hopping mechanism should exhibit ground state absorption features for the flavosemiquinone and bands corresponding to the adenine radical anion. If superexchange is operative, there would be no $Ade^{\bullet-}$.

Transient absorption studies by MacFarlane and Stanley[7], and Liu *et al.* [14] have been performed, but no single study has been definitive. Working with PL_{OX}, MacFarlane *et al.* ascribed a long-lived excited state absorption band in the far red to a charge transfer complex between photoexcited oxidized flavin ($*Fl_{OX}$) and the adenine (Ade) moiety (or possibly a tryptophan). Liu *et al.* suggest that Ade is a virtual intermediate in a superexchange mechanism $*FADH^-$ and the CPD substrate. A different experimental approach, eliminating the adenine moiety from FAD, would be very enlightening. However, the reconstitution of apo-PL with riboflavin or flavin mononucleotide has been unsuccessful[15].

It is widely assumed that the photoinduced intramolecular electron transfer occurs in the $*FAD_{OX}$ in large part because the dinucleotide adopts a stacked geometry, reminiscent of its structure in PL. A large number of time-resolved studies[16–19] have been performed on both $*FAD_{OX}$ and $*FADH^-$, but the identification of any radical Ado species has been wanting. The thermodynamics of the process has been debated as well, but reliable estimates of the reduction potentials of flavin and adenine are still subjects of debate.

We have addressed the role of the adenine in DNA repair by reconstituting apo-PL with a FAD in which the adenosine group (Ado, upper back box, Fig. 2) was bridged chemically to yield a modified adenosine, 1,N^6 - ethenoadenosine (εAdo, see red box of Figure 2.2). This modified FAD was first synthesized by Barrio and Leonard[20–22]. εAdo is more highly conjugated and extended than Ado and thus has a red-shifted UVB absorption band centered around 305 nm. This band, serendipitously, lies in a spectral "valley" between the $S_0 \rightarrow S_2$ (~370 nm) and $S_0 \rightarrow S_3$ (~265 nm) transitions of Fl_{OX}, with an extinction maximum of about ε~3,200 $M^{-1}cm^{-1}$ compared to about ε~1200 $M^{-1}\,cm^{-1}$ for Fl_{OX} at this wavelength. We hypothesized that the resulting dinucleotide, ε-FAD, would have an altered thermodynamic driving force for PET between the FlH^- and ε-Ado by lowering the energy gap between the excited state flavin donor and the bridging adenosine molecule[20–23]. *E. coli* apo-PL accepted this ε-FAD with a ~15% increase in the overall repair rate (manuscript submitted).

In this work, we present the photophysical characterization of the ε-FAD cofactor by a comparative transient absorption study of the excited state dynamics of FMN, FAD, and ε-FAD in oxidized and two electron reduced states in aqueous solution to ascertain whether PET is occurring between the stacked ε-Ado and $*Fl_{OX}$ or $*FlH^-$. Previous spectroscopic studies of FAD in solution do not definitely retrieve features of an adenine radical anion intermediate species[19]. Although both the flavosemiquinone and flavohydroquinone anion have a moderately strong excited state absorption bands in the near UV/vis, the relatively weak equivalent absorption features of the adenine radical anion have not yet been observed in the ultrafast transient kinetic fits. Our species associated spectra show evidence of ε-Ado radical anion formation and semiquinone

formation at early times for the reduced ε-FADH anion.

2.2 Materials and Methods

2.2.1 Sample Preparation and Photoreduction

Flavin adenine dinucleotide was purchased from TCI, Japan (>95% purity). The sample purity was checked by reversed-phase C_{18} high pressure liquid chromatography (HPLC) and used as received. For synthesis of ε-FAD we followed the procedure of Barrio *et al.* [21]. Approximately 50 mg of FAD was stirred gently in 20 mL of 1.5 M chloroactealdehyde (Sigma-Aldrich, ~50 wt.% in water) for 72 hours. The reaction was carried out at room temperature in a light-protected round-bottom flask. To further confim the product identification we have shown, as was demonstrated by Barrio *et al.*, that the addition of phosphodiesterase to a solution of εFAD results in a dramatic increase in *εAdo emission (data not shown). This was explained as the loss of energy transfer in the stacked nucleotide upon enzymatic hydrolysis of the phosphodiester bond[21].

Purification of εFAD was accomplished in two steps as described by Walsh *et al.*[24]. The reaction mixture was first purified on a weak anion exchange resin, DEAE Sephadex A-25 (Sigma Aldrich), using 100 mM potassium phosphate buffer, pH 6.8, for loading and elution. The eluate was dried under vacuum and then further purified using reversed-phase HPLC on an Agilent 1100 separations module fitted with a YMC-ODS-AQ 250 mm x 10 mm column. An isocratic method was applied using 25% methanol in 5 mM ammonium acetate, pH 6.0. Purity and fidelity of the εFAD was assessed by steady-state fluorescence and UV-vis absorption spectra. The yield of the purified product was typically ~40%. The purified sample was vacuum-dried and stored at -20°C as smaller aliquots. An aliquot was then resuspended in the appropriate buffer system.

All Fl_{OX} were studied in 50 mM Tris HCl, pH 7.0 buffer. All FlH^- samples were photoreduced using freshly prepared sample solutions of 175-350 μM (concentrations confirmed by UV-vis absorption). After deoxygenation in an anoxic glove box, the sample was irradiated for ~15 min. with a blue-light 450 nm LED array (GoLITE HF3332, Philips) at 1mW power. 5 mM EDTA was used as the reducing agent in 50 mM Tris HCl buffer at pH 7-9. Photoreduction was deemed complete by examination of the absorbance and fluorescence spectra. Care was taken not to overexpose the samples [25] as lumichrome (Lc) and lumazine (Lz) form readily, as determined by C_{18} HPLC analysis of the post-irradiation samples. Both Lc and Lz are very fluorescent compared with FAD or $FADH^-$. Under the above conditions photoreduction took only about 3 min. of illumination before $FMNH^-$ photodegradation was observed. FAD and εFAD were photoreduced for ~30 minutes.

2.2.2 Steady-State Spectroscopy

All linear absorption measurements were carried out on Hewlett Packard 8452A Diode Array Spectrophotometer. Steady-state fluorescence studies were carried out on a PTI Quantamaster 3 single photon-counting fluorimeter (Birmingham, NJ). Relative emission quantum yields were made using quinine sulfate in 0.1 N HCl as a standard.

2.2.3 Transient Absorption Spectroscopy

A Ti:Sapphire laser (KLM, ~80 MHz, 780 nm) was amplified using a regenerative amplifier to produce ~ 300 μJ, 120 fs pulses at ~250 Hz. This was split into two beams. A white-light continuum probe beam (WLC, 350-710 nm) was generated by focusing a few microjoules (NA ~ 0.04) into a slowly translating CaF_2 crystal. The majority of the 780

nm fundamental was used to generate the pump beam at the second-harmonic, 390 nm, using a 2 mm type-I BBO crystal.

The pump beam was focused using a 40 cm quartz lens, while the WLC was focused using an off-axis 90° aluminum paraboloid with a focal length of 10 cm. The angle between the focused pump and the probe beams at the sample was ~ 2°. Their relative polarization was set to magic angle (54.7°) using a half-wave plate in the pump beam. A CMOS camera with 25 μm square pixels was placed at the focus to measure the diameters of the focused beams. This is a crucial operation as the pump beam must be no smaller than the probe beam to ensure homogeneous pumping of the sample volume. In addition, the optical alignment of the delay stage (pump beam) was checked to ensure overlap over the full 3 ns range. Typical pump and probe beam diameters were 264 and 126 μm. Care was taken to attenuate the near-IR fundamental remaining in the WLC by using a Schott BG39 filter. The pump power was measured before and after the completed scans by reflecting the pump pulse before the cuvette onto a calibrated silicon joulemeter (Molectron J3-S10), which was read by a 400 MHz digital oscilloscope.

The pump-probe delay is set using a motorized delay rail that adjusted the path-length of the pump beam to provide a delay range of up to 4 ns with a resolution of ~10 fs. To build the difference absorption spectra, the sample was pumped at ~125 Hz and the WLC transmittance measured on a cooled CCD detector (Andor, 1024x32 pixels) at ~250 Hz. The single-shot transmittance spectra were transferred to a computer for construction of the ΔA spectra and averaging using in-house developed LabView software. Analysis of the data is performed using Origin 9, MATLAB (2015b), and the global fitting analysis tool Glotaran [26].

The sample was held in a 2 mm path length fused silica cuvette that was fitted with an air-tight septum. This cuvette was maintained at a constant temperature using a thermostatted cuvette holder (QNW FLASH 300). The thermostatted sample was continuously stirred with an 8 mm diameter by 0.6 mm thick magnetic stir disc. The beams overlapped about 2-4 mm above the stir disc.

For the chirp correction and fitting of the instrument response function (IRF), the cuvette sample solution was replaced with water or buffer. The high intensity pump beam induces an optical Kerr effect in the solution that refracts a fraction of the probe beam away from the detector. Data was taken in 0.2 ps steps to obtain the cross correlation between the pump and WLC. The experimentally obtained IRF was fitted using Glotaran. This IRF was very nearly identical to that obtained when Glotaran uses only the sample data to estimate the IRF. In subsequent analyses Glotaran was used in this fashion to model the IRF.

2.2.4 Computational Methods

The ground-state geometries of 9-methyl-εAde radical anion and cation were optimized using the DFT package in Gaussian 09 at the UB3LYP/6-311+G(d,p) level of theory. B3YLP/6-311+G(d,p) was used for the neutral $9CH_3$-ε-Ade. The solvent was modeled using the polarizable continuum model (PCM) developed by Mennucci *et al*[27]. Minimum energy structures were confirmed by vibrational frequency calculations at the same level of theory. Simulated absorption spectra were calculated using TD-DFT calculations at the same level of theory on the optimized geometry. Transition energies from the TD-DFT calculations were used to generate absorption spectra assuming a Gaussian line shape with a 5 nm full width half maximum for the ν=0 vibronic band of

only the optically bright transitions. These calculations were carried out by Dr. Madhavan Narayanan.

2.3 Results

2.3.1 Steady-State Spectroscopy of FMN_{OX}, FAD_{OX}, and εFAD_{OX}

The solution state spectra of FMN_{OX} and FAD_{OX} have been studied exhaustively[17–19,28–34]. εFAD and other ε-dinucleotides have been characterized by Barrio *et al* and others[20,21,23,35,36]. The room temperature absorption spectra of these flavins and nucleosides are plotted in Figure 2.3, with the singlet $S_0 \rightarrow S_n$ transitions (n=1-4, S_{0n}) indicated. Significant spectral features between the chemically modified εFAD and FAD are the differences in extinction at 222 nm and 310 nm. The increased extinction at 310 nm led us to choose this analogue because of the change in LUMO-LUMO gaps between the nucleoside acceptor and the isoalloxaine moiety. It also affords for the selective excitation or probing of the εAdo moiety. The overlapping spectral features in the visible region of the spectrum (>340 nm) confirm that the ground state electronic interaction between the two chromophoric moieties is negligible and the absorption spectrum of the ε-FAD can be treated as a linear combination of ε-Ado and the flavin moiety. The steady-state fluorescent properties of ε-FAD_{OX} were identical with previous measurements[20–23] (data not shown).

2.3.2 Steady-State Spectroscopy of $FMNH^-$, $FADH^-$, and $\varepsilon FADH^-$

The absorption and fluorescence spectra of reduced flavins are still a subject of some debate. The difficulty lies in obtaining purely $2e^-$ reduced samples without significant photodegradation[19,25]. This is especially true for FMN, which is degraded

easily to lumichrome and lumazine under quite modest light intensities, even in the presence of a sacrificial electron donor like EDTA or oxalate. To this end, photodegradation was carefully monitored using HPLC.

The absorption spectra of $FMNH^-$, $FADH^-$, and $\varepsilon FADH^-$ are shown in Figure 2.4 The $S_0 \rightarrow S_n$ transitions (n=1-4, S_{0n}) of $FMNH^-$ have maxima as indicated. $\varepsilon FADH^-$ has greater extinction around S_{03} and 225 nm because of the εAdo. In their reduced forms $FADH^-$ and $\varepsilon FADH^-$ are well fitted by a linear combination of the $FMNH^-$ and Ado or εAdo spectra (analysis not shown), indicating that there is little ground state coupling between the flavin and adenosine moieties.

It was found that complete photoreduction of $FMN_{OX} \rightarrow FMNH^-$ was attained in 180 sec. using only 1 mW/cm^2 of 445 nm light (c.f. Fig. 2.3 and Fig. 2.4, green). At greater exposure times Lc was observed with Lz forming subsequently (data not shown). The mechanism for flavin photodegradation is thought to center on the nanosecond lifetime of *FMN. The singlet lives long enough that ^{3}FMN forms with good quantum yield[37,38], which is photochemically active. FAD and εFAD required significantly larger photon fluxes because their singlet lifetimes are orders of magnitude shorter, but eventually photodegrade as well.

The steady-state fluorescence of the reduced flavins is shown in Figure 2.5. The excitation slits were kept at 5 nm band pass because larger slit widths led to photodegradation, as determined by nonstoichiometric increases in fluorescence and HPLC analysis (data not shown). The emission spectrum of the $\varepsilon FADH^-$ has a maximum at ~475

nm when excited at 370 nm. The quantum yield (relative to quinine sulfate) of *εFADH$^-$ is Φ_f=0.005 while Φ_f= 0.0015 for *FADH$^-$.

We attribute the differences in Φ_f to the amount of stacked versus unstacked conformers. In the oxidized form of εFAD, the orbital overlap of the εAdo group with the isoalloxazine ring is better than that of stacked FAD resulting in higher FRET efficiency and a lower quantum yield [21,39]. However, εFADH$^-$ appears to display the opposite trend. This may be due to the changes in the ratio of stacked to unstacked dinucleotide caused by butterfly bending conformational motions of the N^5-N^{10} axis in the reduced isoalloxazine ring described by Ghisla [40]. *Fl_{OX} is known to be planar in both ground and excited singlet states rather than bent.

The fluorescence excitation spectra for *FADH$^-$ and *εFADH$^-$ monitoring emission at 525 nm[17,30] are shown in Fig. 2.5. The *FADH$^-$ spectrum illustrates the exisitence of two electronic transitions (S_{01}, S_{02}) for reduced flavins with maxima at 415 nm and 350 nm[31,41]. The increased intensity near 305 nm of the *εFADH$^-$ spectrum indicates that energy transfer occurs between *εAdo and FlH$^-$. This in turn suggests that a significant population of the reduced dinucleotide retains the stacked conformation in spite of the structural differences between εAde and Ade. This nice result validates the use of ε-FADH$^-$ as a FADH$^-$ analogue for probing FAD-dependent cofactor dynamics of Ade/reduced flavin dynamics in real time by selective excitation of the εAde moiety.

2.3.3 Ultrafast Transient Absorption Spectroscopy of Oxidized Flavins

It has been widely accepted that the fluorescence of oxidized FAD as well as the excited state of the reduced anionic FAD (*FlH$^-$) are quenched due to stacking with the

adenine moiety[16,19,21,39,42,43]. In order to investigate the role of adenine in the non-radiative decay pathway of FAD, and to provide a reference point for comparison to FAD, flavin mononucleotide transient measurements were made to model the unstacked population kinetics of the *Fl molecule.

Data for FMN and the other flavins were obtained at a variety of pump pulse energies from 0.05 to 0.5 μJ/pulse and at two different temperatures, 4°C and 20°C. A typical data set consists of ~320-620 nm spectral range and ~3 ns of time delay. Each scan of the delay line includes 800 laser shots per delay setting, amounting to 400 single-shot spectra. These spectra were averaged and the delay stage moved to the next time setting. Five complete scans were taken to improve the signal to noise and to obtain estimates of the standard deviation of the data. The raw data are processed in MATLAB to take out artifacts and to baseline correct the data by averaging at least 5 pre-zero spectra and subtracting these from the data set. In the raw spectra scattered pump light appears as a very large negative ΔA. If left in the data set it would swamp the fitting algorithm. This narrow spike was removed by deleting the data from, for example, 390-405 nm. A typical FMN_{OX} data set taken at 20°C is shown in the top panel of Fig. 2.6. Noise around 400 nm is remaining scattered pump light. The excitation energy was 0.131 μJ. Using the measured beam diameter of 264 μm the pump fluence is 0.02 $\mu J/cm^2$. A knowledge of the beam intensity is particularly important when looking at $*FMN_{OX}$ because of its proclivity to undergo a multiphoton photoreduction to the flavosemiquinone. Based on the work of Plaza an upper limit for the laser fluence is 0.66 $\mu J/cm^2$ [19].

Using the global analysis tool Glotaran, two evolution associated spectra (EAS) with lifetimes 1.1 ps and > 5 ns were extracted from a two state sequential model. We attribute the 1.1 ps lifetime to internal conversion from the $S_2 \rightarrow S_1$ state. This is reasonable because both states have approximately the same extinction at λ_{EX}=398 nm. Thus roughly half of the excited population is in S_2 and relaxes to S_1 in picoseconds. The longer component is attributed to radiative (fluorescence) decay from $S_1 \rightarrow S_0$. See Figure 2.6 for fits and associated spectra. These results are in good agreement with previously reported results[7,18,19,38], with one difference (see Table 2.1). These measurements, done in both Tris and phosphate buffers, are notably absent in the ^{3}FMN species. Islam *et al.*[38] determined that the quantum yield for riboflavin intersystem crossing, Φ_{ISC}~0.36. The triplet spectrum has a rather broad ground state absorption from about 500 to beyond 700 nm with an extinction coefficient at 600 nm of about 6,000 $M^{-1}cm^{-1}$[37]. With Φ_{ISC}~0.36 we would expect to see its contribution in the long component since ISC proceeds from the long-lived singlet. In addition, at 600 nm there is a zero-crossing in the transient absorption spectrum making it easier to observe ^{3}FMN in this wavelength region. However, both components are nearly identical, ruling out the presence of more than a few percent of ^{3}FMN. We do not yet have an adequate explanation for this result.

Using this as a reference, we assigned the oxidized FMN kinetic parameters as the representation for the 20% unstacked population of oxidized FAD at 20°C[16,21,39,42,43]. FAD_{OX} was fitted to a model containing three states. Two states correspond to the sequential mechanism for FMN_{OX} (20% population) with a single state to model the decay of the stacked FAD population (80%). In this case the fitted model spectra are called “Species Associated Spectra” (SAS) as they are the spectra associated with a

particular unique molecular species as opposed to the evolution of one species (EAS). It should be noted that the addition of an additional state or rate constant engendered oscillatory SAS which could not be physically justified. This model is also unique in this particular buffer system, as only two SAS were extracted from the species in phosphate buffer (discussed in Chapter 4). In general, the simplest model that fit the data was considered the best model (Occam's Razor).

The data were taken under similar conditions as those for FMN (200 μM, identical excitation fluences and wavelength (390 nm) at 20ºC). Fig. 2.7 shows a typical data set, SAS, and the fastest fitted component at 7 ps. The 7 ps relaxation of the stacked population to the ground state is assigned to a conical intersection indicating charge transfer between the adenine moiety and $*Fl_{OX}$. This result agrees well with Zhong *et al.*[7,34]. The unstacked kinetics result in lifetimes of 1 ns and long. This result is quite different from the kinetics of FMN. There are two possible explanations for this. One explanation is that the flavin triplet species is forming at long times. Penzkofer *et al.* reports that the lifetime for intersystem crossing to the triplet state is on the order of 1 ns with positive features in the red edge of the spectrum[38]. Another possible explanation is that an aqueous electron is forming[19,34]. The formation of an aqueous electron is less likely because we do not observe this behavior under the same experimental fluence conditions for the FMN system.

Oxidized εFAD (εFAD_{OX}) fit well to a two state parallel model. The starting population for the stacked versus unstacked species were set to agree with the results of Barrio *et al.* obtained from a fluorimetric analysis of static and dynamic quenching[21]. The unstacked population was set to a starting population of 10% and the stacked population

was to a starting population of 90%. The lifetimes associated with the model employed are 3.9 ps and long. We attribute the 3.9 ps lifetime to a conical intersection transient of the εAdo moiety and the $*Fl_{OX}$. The long components are representative of the small unstacked population which undergoes a different relaxation pathway than the FMN_{OX}. The 3.9 ps SAS component revealed positive spectral features that are indicative of a charge separated species (black line of Figure 2.8). The amplitude of the stacked associated spectra is much lower than that of the associated spectra of the unstacked because the extinction of the contributing charge separated species in the stacked conformation is only 22% of the excited state unstacked flavin extinction.

2.3.4 Ultrafast Transient Absorption Spectroscopy of Reduced Flavins

Excited state kinetics have been measured for $FMNH^-$ and $FADH^-$ by several groups. These results are summarized in Table 2.2. Our current measurements of $FMNH^-$ results agree with a two state sequential model as was done for FMN_{OX}. The shorter lifetime is 39 ps with the 2nd component having a lifetime longer than our delay stage allows us to measure accurately, see Figure 2.9. The two state sequential model is justified because we excite the molecule at 390nm therefore populating S2 and S1 electronic states[41].

The kinetic results from our $FADH^-$ fits yielded two lifetimes that correspond to a simple sequential two state model similar to $FMNH^-$. The lifetime for the faster component is 18 ps, which may correspond to a conical intersection decay pathway and then the longer lived component corresponds to relaxation from the S1 state. This proposed model agrees well with computational results calculated by Matsika *et al.* (manuscript submitted). Additional model states did not improve the fit and extracted

associated spectra did not show significant spectral signal. The buildup of the 580nm spectral feature in the long time, see Figure 2.10 red line, is a multiphoton, power dependent feature.

The kinetics of the εFADH$^-$ system were much more complicated than FADH$^-$ and FMNH$^-$ as to be expected. The driving force for electron transfer was altered by incorporating the modified nucleoside and therefore a three state model was utilized. The fastest component is attributed to internal conversion at 1.6 ps. The 27 ps component is attributed to photoinduced electron transfer because the shoulder of the associated spectra is indicative of semiquinone formation overlapping with etheno radical anion formation, see Figure 2.11 and Figure 2.12. The long component is attributed to recombination to the ground state. This is a very exciting result as it is the first reported measurement, to our knowledge, of the reduced excited state properties of ε-FADH$^-$ system. By altering the driving force for electron transfer, we have made another decay pathway available to the system that is a bright state rather than a dark state (conical intersection). Spectral evidence supports the presence of a charge separated state that is emissive.

2.4 Discussion

To examine the role of the Ade in the PL catalytic cofactor FAD we hypothesize that by tuning the free energy of the donor-acceptor (*FlH$^-$/Ade) pair in the electron transport pathway, the rate of electron transfer would be altered. To attain this goal, the Ade group was modified to εAde. εPL was shown to repair CPD DNA with a slight increase in rate (Narayanan *et al.*, manuscript submitted). Here we have presented the excited-state dynamics of εFAD and εFADH$^-$ with subpicosecond resolution. The motivation for doing so was to serve as a set of control experiments on the modified

cofactor in the absence of protein to test whether PET occurs and whether the kinetics are affected between the *Fl (*FlH^-) and εAdo and compare these results with the dynamics of *FAD and *$FADH^-$.

Liu *et al.* used the Dutton-Moser electron transfer approximation to compute the electron transfer rate constant. This approximation requires accurate distance measurements between the donor and acceptor, r_{DA}. Liu *et al.* used the distance from position N10 on the isoalloxazine moiety to the acceptor (Figure 2.2). Based on a number of pre-existing experimental and computational results this seems to be an odd choice. These earlier studies concur that the electron density of the excited state reduced anionic flavin resides on the xylene ring C8 thus implicating that donor in the electron transfer reaction would be localized around C8 [10,44–46]. Since the ET rate constant depends exponentially on r_{DA}, a small error in this parameter can invalidate the results. Further, proteins are not rigid, crystalline materials but have motions over a wide range of time scales that can gate the ET reaction (i.e., the pathway model of Onuchic, Beratan, and Gray[47]). Needless to say, this same caveat, to perhaps an even greater extent, applies to modified cofactors. It is important to keep this in mind when measuring the excited state dynamics of flavins in all redox forms to assign the electron transfer mechanism in adenylated flavins.

2.5 Conclusions

In this paper, we presented our initial findings on subpicosecond optical broadband transient absorption measurements of flavin 1, N^6-ethenoadenine dinucleotide and made a direct comparison to its parent analogue – flavin adenine dinucleotide. Complementing the results with steady-state and time-resolved fluorescence studies, our

initial investigations suggest that in their oxidized and reduced forms in free solution, ε-FAD and FAD display different charge transfer and deactivation dynamics. The ε-FADH- with a stronger intramolecular aromatic stacking interaction, exhibits unique electron transfer and recombination rates. Our studies further indicate that ε-FAD could be a very useful molecule in unraveling the pathway and mechanism of electron transfer in FAD-binding flavoproteins. Ultrafast measurements should provide more insight on the role played by played by adenine within the enzyme DNA photolyase for repair of CPD by electron transfer.

	FMN_{OX}	FAD_{OX}
This work	1.1 ps, long	7 ps , 1 ns, long
Zhong, '08 λ_{EX} = 400 nm	N/A	1.4 ps, 7.8 ps, 1.8 ns
Plaza, '11 λ_{EX} = 470 nm	2.5 ps, 4.6 ns.	1.0 ps, 5.5 ps, 31 ps, 3.0 ns

Table 2.1. Ultrafast lifetimes of FMN_{OX} and FAD_{OX} [19,34,42]

	FMNH-	FADH-
This work	39 ps, long	18 ps, long
Rose, '93		100ps
Lindquist, '98	60 ps ,1.5 ps	17 ps, 1.5 ps
Stanley, '03	41 ps, 843ps	4 ps, 121 ps
Glusac, '08	40 ps, 529 ps, long	23 ps, 401 ps, long
Zhong, '08	5.8 ps, 35 ps, 1.5 ns	5 ps, 31 ps, 2 ns
Plaza, '11		1ps, 5.5ps, 32ps, 5ns
Meech, '11		5.3ps, 29ps

Table 2.2. Ultrafast lifetimes of $FMNH^-$ and $FADH^-$[7,13,19,33,48–50]

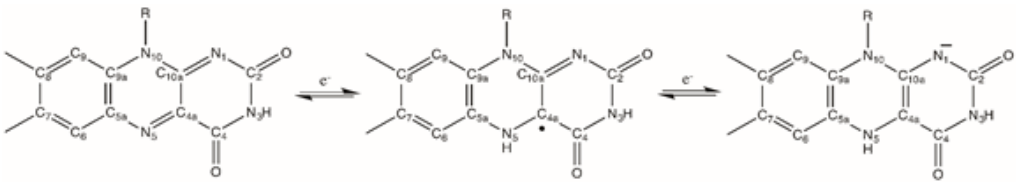

Figure 2.1: Three oxidation states of flavins (left to right): Oxidized (Fl_{OX}), semiquinone ($FlH^{\bullet}$, $1e^-$), and anionic hydroquinone (FlH^-, $2e^-$).

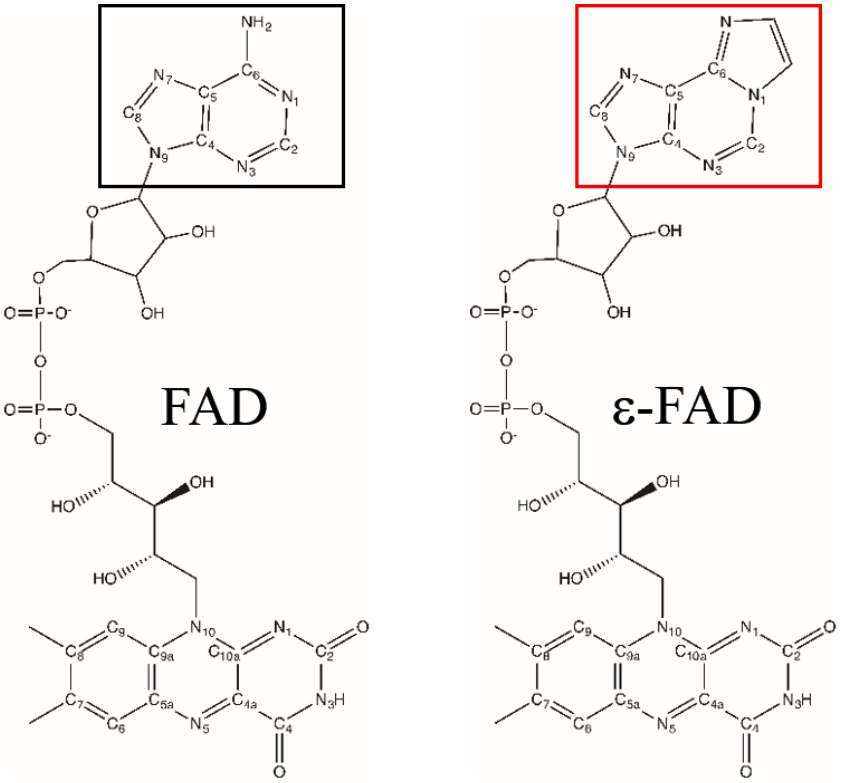

Figure 2.2: Flavin adenine dinucleotide (FAD) and Flavin N1,N6 ethenoadenine dinucleotide.(εFAD). The isoalloxazine moiety is indicated by the large black box with the adenine moiety above it in a smaller box. The etheno bridge modification is indicated by a red box.

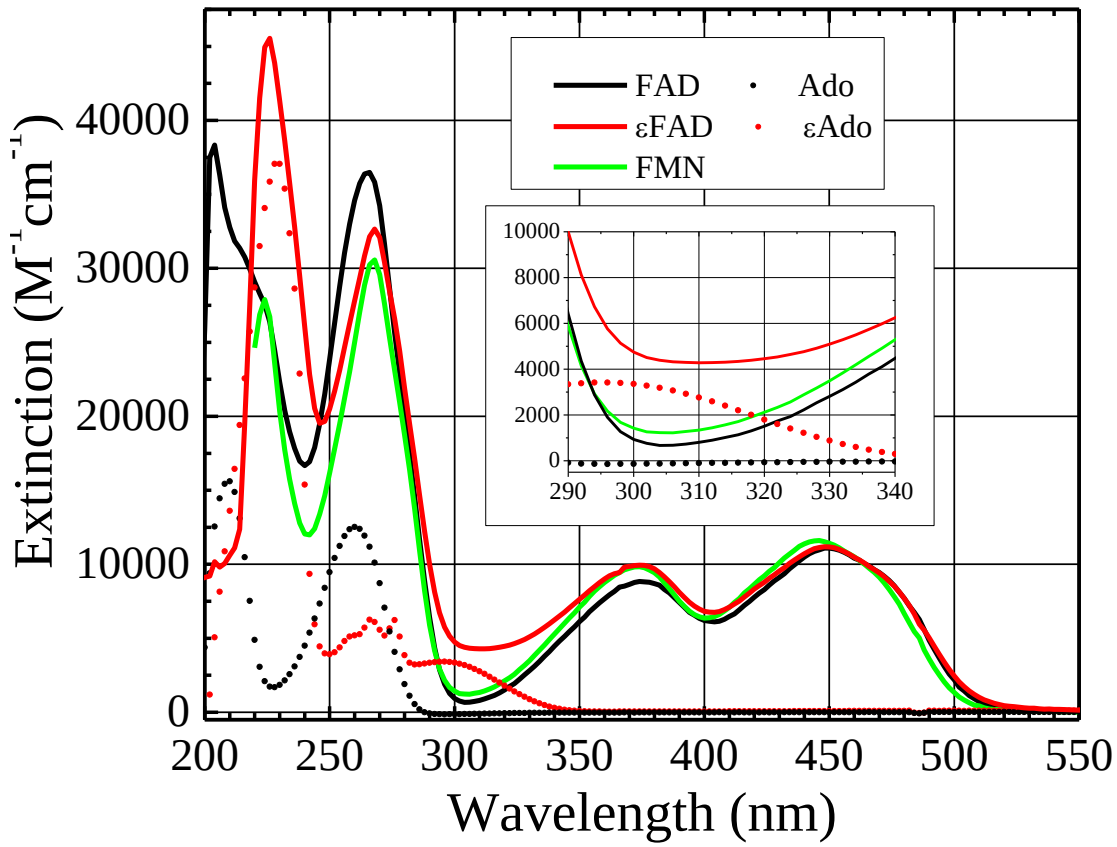

Figure 2.3: Room temperature absorption spectra of FAD, εFAD, FMN, Ado, and εAdo in 50mM Tris Buffer pH 7.0. The red-shifted absorption of the εAdo as compared to the adenosine molecule increases the extinction in the 300 nm region of the εFAD. The inset plot highlights this significant difference.

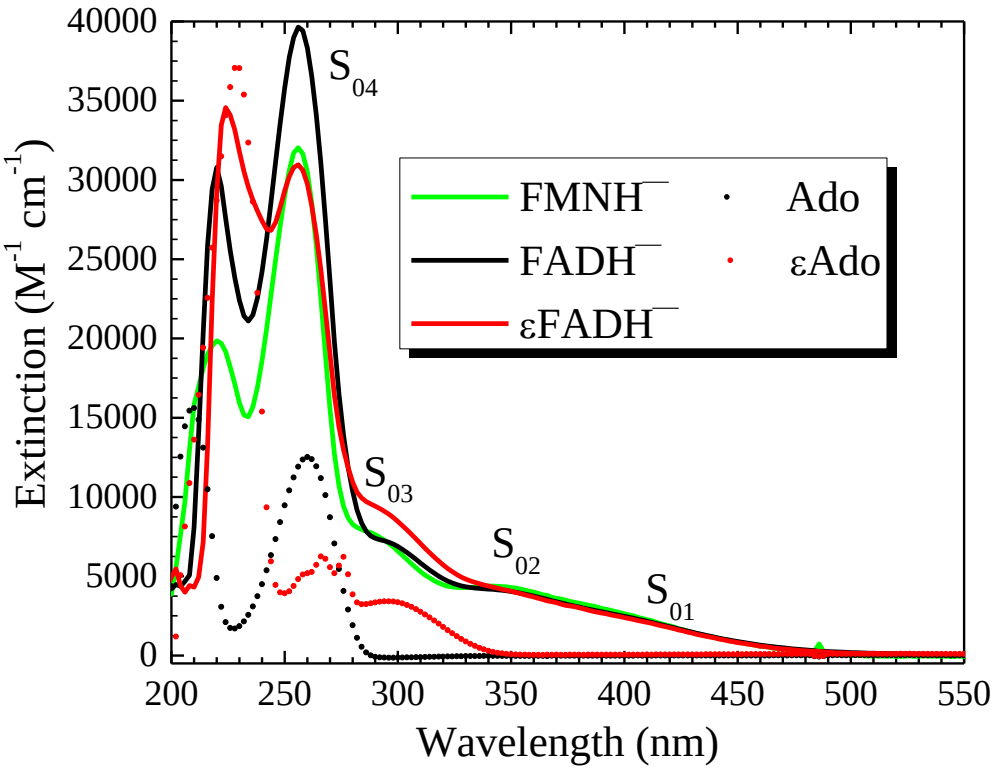

Figure 2.4 : Absorption spectra of $FMNH^-$, $FADH^-$, and $\varepsilon FADH^-$.

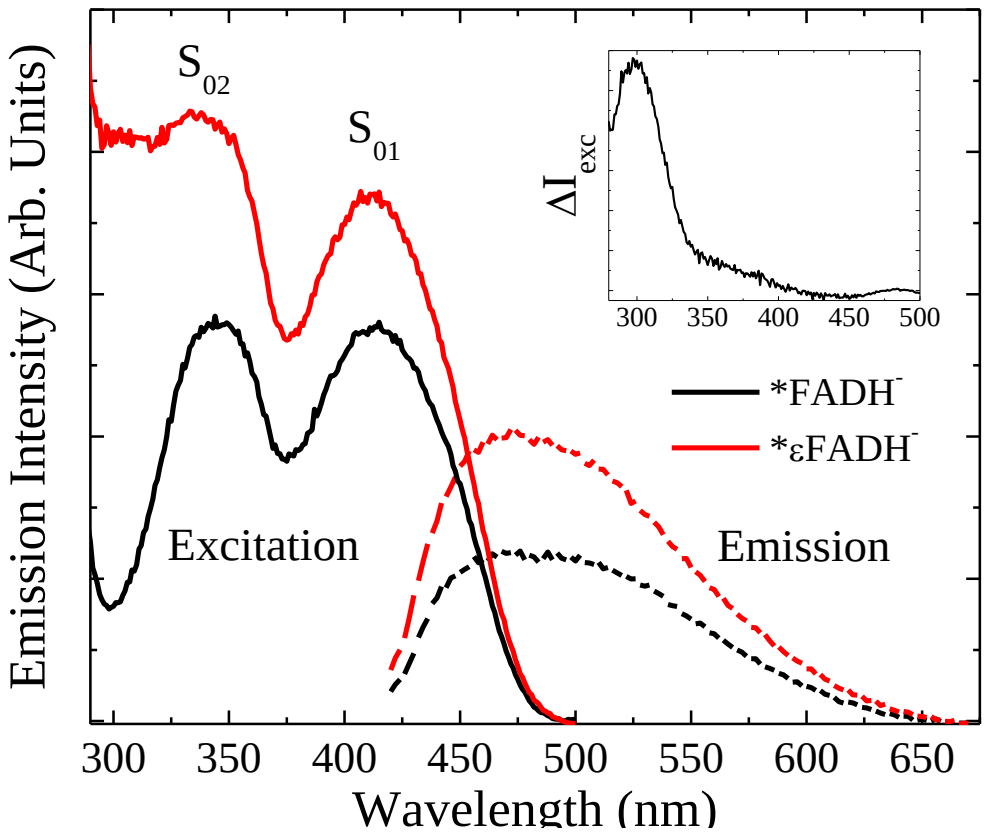

Figure 2.5: Excitation and emission spectra of $FADH^-$ and ε-$FADH^-$ in 50 mM Tris, 50mM sodium oxalate, pH 9.0. For excitation, emission was monitored at 525 nm. For emission excitation was set to 370 nm.

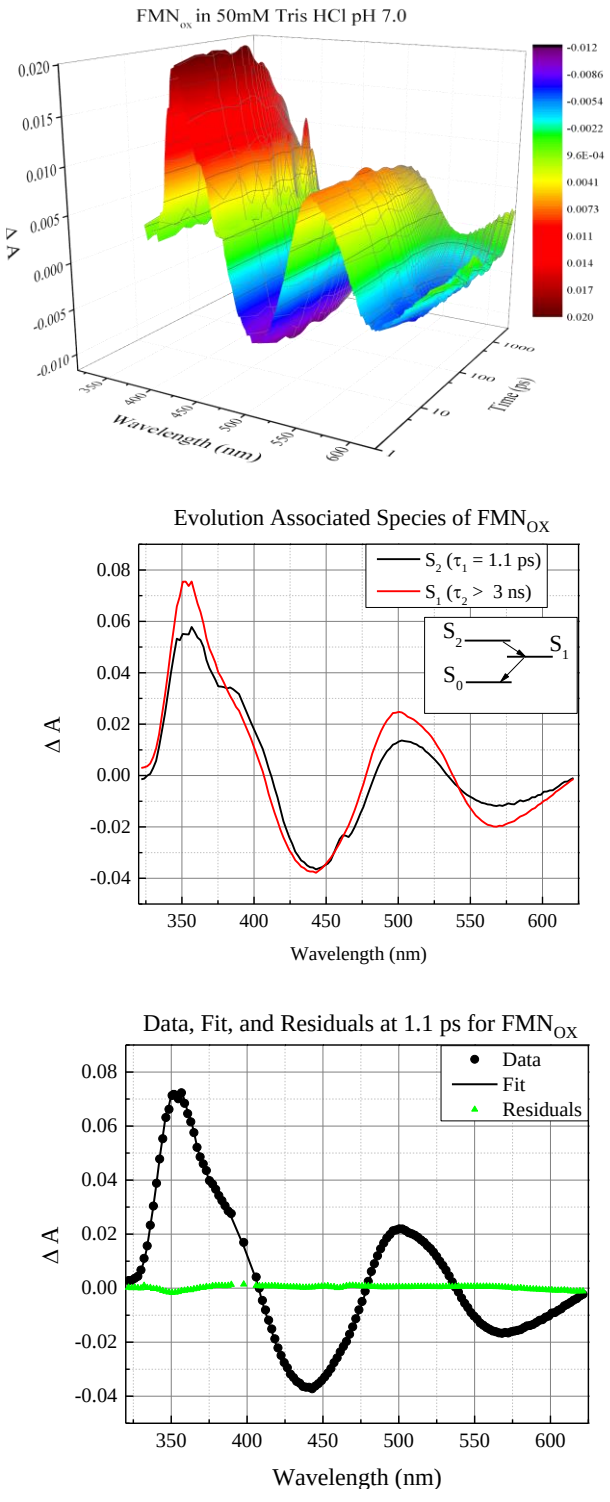

Figure 2.6 Transient absorption spectra of FMN$_{OX}$ in 50 mM Tris-HCl pH 7.0

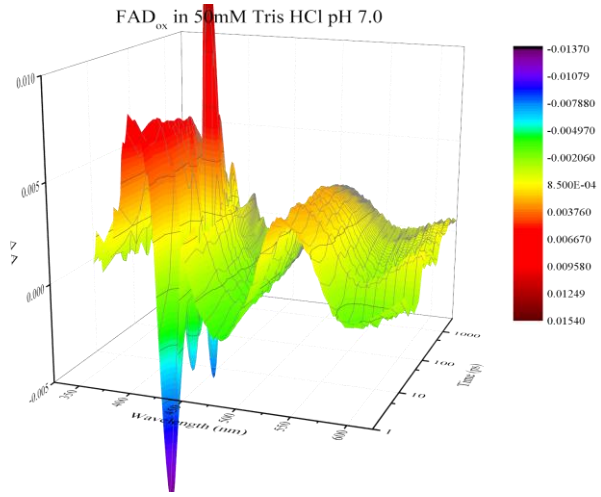

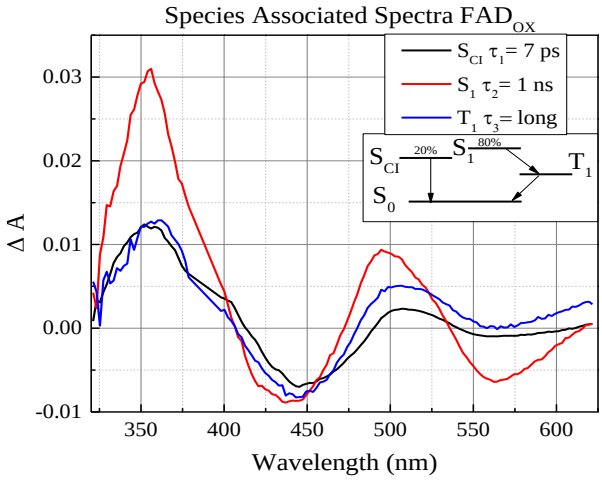

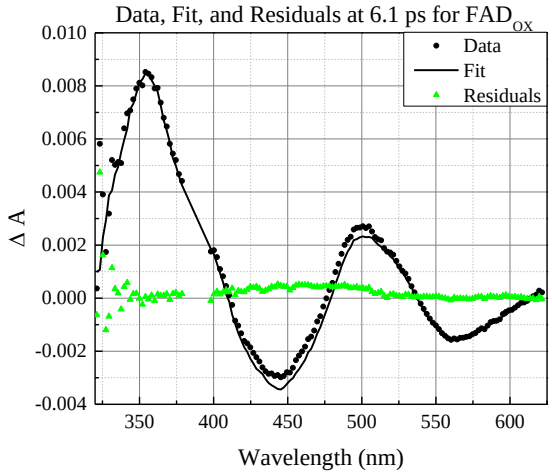

Figure 2.7. Transient absorption spectra of FAD$_{OX}$ in 50 mM Tris-HCl pH 7.0

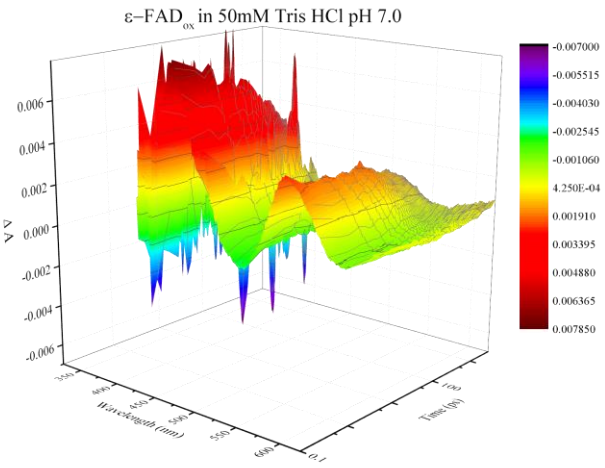

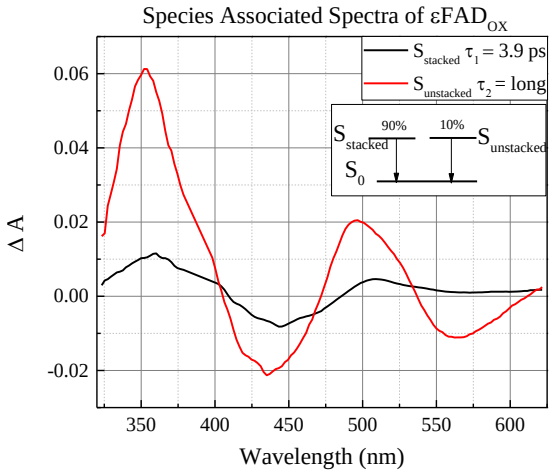

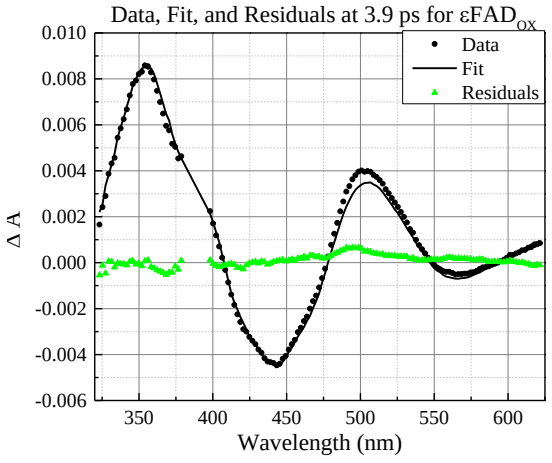

Figure 2.8 Transient absorption spectra of εFAD$_{OX}$ in 50 mM Tris-HCl pH 7.0

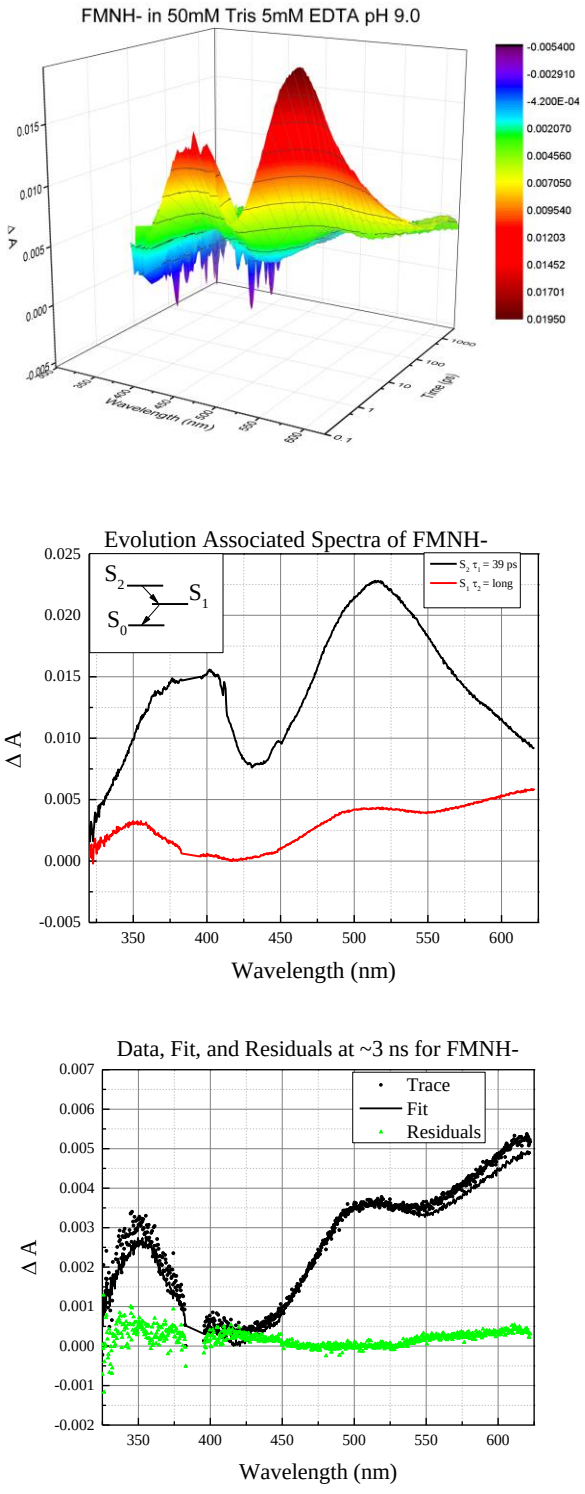

Figure 2.9: Transient absorption spectra of $FMNH^-$ in 50 mM Tris 5 mM EDTA pH 9.0

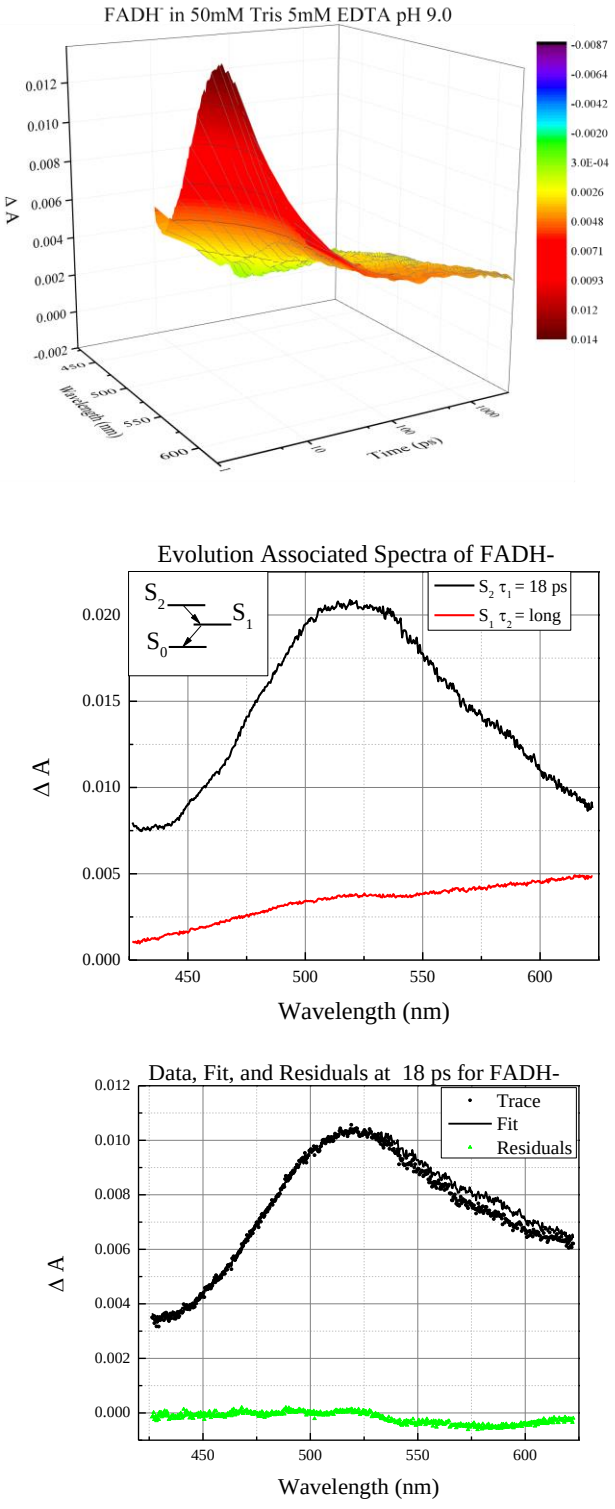

Figure 2.10: Transient absorption spectra of FADH- in 50 mM Tris 5 mM EDTA pH 9.0.

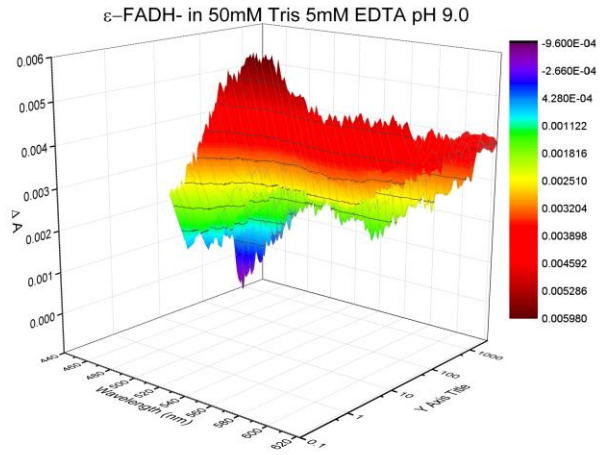

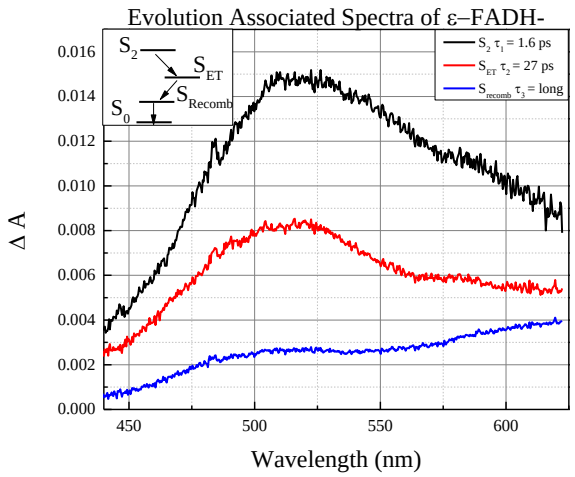

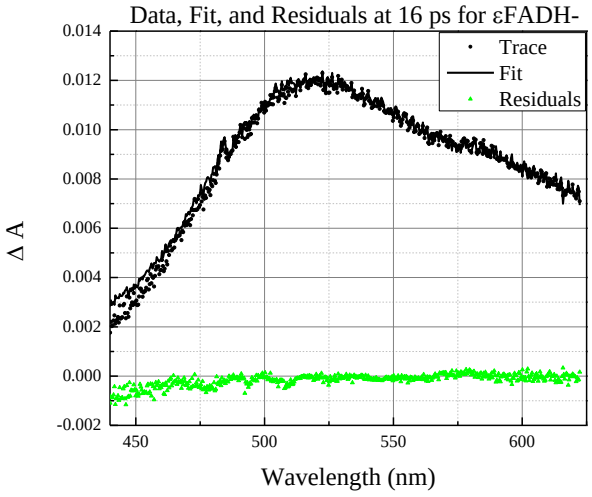

Figure 2.11: Transient absorption spectra of ε-FADH- in 50 mM Tris 5 mM EDTA pH 9.0

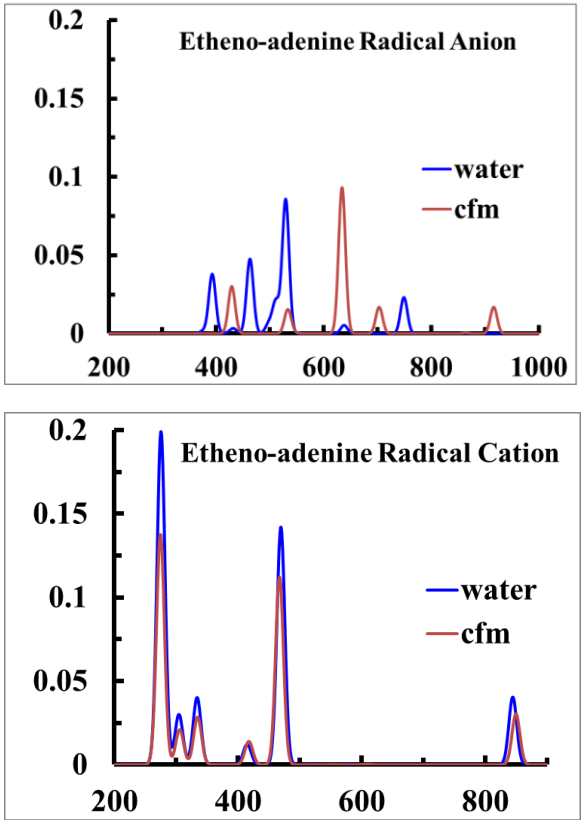

Figure 2.12. DFT calculated spectra of etheno-radical protonation states in chloroform (cfm) and water performed by Dr. Madhavan Narayanan.

2.6 References

(1) Müller, F. In *Topics in Current Chemistry*; Springer-Verlag: Berlin, 1983; Vol. 108, pp 71–107.

(2) Stankovich, M. T. In *Chemistry and Biochemistry of Flavoenzymes*; Müller, F., Ed.; CRC Press: Boca Raton, 1991; Vol. I.

(3) Ghisla, S.; Massey, V. *Eur. J. Biochem.* **1989**, *181*, 1–17.

(4) Sancar, G. B. *Mutat. Res.* **1990**, *236* (2-3), 147–160.

(5) Payne, G.; Heelis, P. F.; Rohrs, B. R.; Sancar, A. *Biochemistry* **1987**, *26* (22), 7121–7127.

(6) Sancar, A. *Adv. Electron Transf. Chem* **1992**, *2*, 215–272.

(7) MacFarlane IV, A. W.; Stanley, R. J. *Biochemistry* **2003**, *42* (28), 8558–8568.

(8) Kao, Y.-T.; Saxena, C.; Wang, L.; Sancar, A.; Zhong, D. *Proc. Natl. Acad. Sci. U. S. A.* **2005**, *102* (45), 16128–16132.

(9) Thiagarajan, V.; Byrdin, M.; Eker, A. P. M.; Muller, P.; Brettel, K. *Proc. Natl. Acad. Sci. U. S. A.* **2011**, *108* (23), 9402–9407.

(10) Medvedev, D.; Stuchebrukhov, A. A. *J. Theor. Biol.* **2001**, *210* (2), 237–248.

(11) Acocella, A.; Jones, G. A.; Zerbetto, F. *J. Phys. Chem. B* **2010**, *114* (11), 4101–4106.

(12) Rigden, D. J.; Jedrzejas, M. J.; de Mello, L. V. *FEBS Lett* **2003**, *544* (1-3), 103–111.

(13) Li, G.; Sichula, V.; Glusac, K. D. *J. Phys. Chem. B* **2008**, *112* (34), 10758–10764.

(14) Liu, Z. Y.; Guo, X. M.; Tan, C.; Li, J.; Kao, Y. T.; Wang, L. J.; Sancar, A.; Zhong, D. P. *J. Am. Chem. Soc.* **2012**, *134* (19), 8104–8114.

(15) Jorns, M. S.; Wang, B.; Jordan, S. P.; Chanderkar, L. P. *Biochemistry* **1990**, *29* (2),

552–561.

(16) Visser, A. J. W. G. *Photchem. Photobio.* **1984**, *40* (6), 703–706.

(17) Ghisla, S.; Massey, V.; Lhoste, J.-M.; Mayhew, S. G. *Biochemistry* **1974**, *13* (3), 589–597.

(18) Li, G. F.; Glusac, K. D. *J. Phys. Chem. B* **2009**, *113* (27), 9059–9061.

(19) Brazard, J.; Usman, A.; Lacombat, F.; Ley, C.; Martin, M. M.; Plaza, P. *J. Phys. Chem. A* **2011**, *115* (15), 3251–3262.

(20) Secrist, J. A.; Weber, G.; Leonard, N. J.; Barrio, J. R. *Biochemistry* **1972**, *11* (19), 3499 – &.

(21) Barrio, J. R.; Tolman, G. L.; Leonard, N. J.; Spencer, R. D.; Weber, G. *Proc. Natl. Acad. Sci. USA* **1973**, *70* (3), 941–943.

(22) Harvey, R. A. In *Methods in Enzymology*; Donald B. McCormick, L. D. W., Ed.; Academic Press, 1980; Vol. Volume 66, pp 290–294.

(23) Harvey, R. A.; Damle, S. *FEBS Lett.* **1972**, *26* (1-2), 341–343.

(24) Light, D. R.; Walsh, C.; Marletta, M. A. *Anal. Biochem.* **1980**, *109* (1), 87–93.

(25) Holzer, W.; Shirdel, J.; Zirak, P.; Penzkofer, A.; Hegemann, P.; Deutzmann, R.; Hochmuth, E. *Chem. Phys.* **2005**, *308* (1-2), 69–78.

(26) van Stokkum, I. H. M.; Larsen, D. S.; van Grondelle, R. *Biochim. Biophys. Acta, Bioenerg.* **2004**, *1657* (2-3), 82–104.

(27) Mennucci, B.; Tomasi, J. *J. Chem. Phys.* **1997**, *106* (12), 5151–5158.

(28) Stanley, R. J.; MacFarlane, A. W. I. V. *B. Abstr. 218th ACS Natl. Meet. New Orleans, Aug. 22-26* **1999**, HYS – 362.

(29) Stanley, R. J.; Macfarlane Iv, A. W. In *Proceedings of the 13th International*

Congress on Flavins and Flavoproteins; Weber, R., Ed.

(30) Visser, A. J. W. G.; Ghisla, S.; Lee, J. In *Flavins and Flavoproteins 1990*; Walter de Gruyter & Co.: Berlin, 1991.

(31) Visser, A.; Ghisla, S.; Massey, V.; Muller, F.; Veeger, C. *Eur. J. Biochem.* **1979**, *101* (1), 13–21.

(32) El Hanine-Lmoumene, C.; Lindqvist, L. *Photochem. Photobiol.* **1997**, *66* (5), 591–595.

(33) Enescu, M.; Lindqvist, L.; Soep, B. *Photochem. Photobiol.* **1998**, *68* (2), 150–156.

(34) Kao, Y.-T.; Saxena, C.; He, T.-F.; Guo, L.; Wang, L.; Sancar, A.; Zhong, D. *J. Am. Chem. Soc.* **2008**, *130* (39), 13132–13139.

(35) Penzer, G. R. *Eur. J. Biochem.* **1973**, *34* (2), 297–305.

(36) Imakubo, K. *Nucleic Acids Res.* **1978**, *1* (suppl 2), s357–s362.

(37) Li, H.; Melo, T. B.; Naqvi, K. R. *J. Photochem. Photobiol. B-Biology* **2012**, *106*, 34–39.

(38) Islam, S. D. M.; Penzkofer, A.; Hegemann, P. *Chem. Phys.* **2003**, *291* (1), 97–114.

(39) Islam, S. D. M.; Susdorf, T.; Penzkofer, A.; Hegemann, P. *Chem. Phys.* **2003**, *295* (2), 137–149.

(40) Massey, V.; Ghisla, S. *Ann. N. Y. Acad. Sci.* **1974**, *227*, 446–465.

(41) Siddiqui, M. S. U.; Kodali, G.; Stanley, R. J. *J. Phys. Chem. B* **2008**, *112* (1), 119–126.

(42) Stanley, R. J.; MacFarlane Iv, A. W. *J. Phys. Chem. A* **2000**, *104* (30), 6899–6906.

(43) Karen, A.; Ikeda, N.; Mataga, N.; Tanaka, F. *Photochem. Photobiol.* **1983**, *37* (5), 495–502.

(44) Pauszek, R.; Kodali, G.; Siddiqui, M. S.; Stanley, R. J. In *Proceedings of the 17th International Symposium on Flavins and Flavoproteins*.

(45) Kodali, G.; Siddiqui, S. U.; Stanley, R. J. *J. Am. Chem. Soc.* **2009**, *131* (13), 4795–4807.

(46) Prytkova, T. R.; Beratan, D. N.; Skourtis, S. S. *Proc. Natl. Acad. Sci. U. S. A.* **2007**, *104* (3), 802–807.

(47) Beratan, D. N.; Onuchic, J. N.; Winkler, J. R.; Gray, H. B. *Science (80-.).* **1992**, *258*, 1740–1741.

(48) Heelis, P. F.; Hartman, R. F.; Rose, S. D. *Photochem. Photobiol.* **1993**, *57* (6), 1053–1055.

(49) Kao, Y.-T.; Tan, C.; Song, S.-H.; Oztuerk, N.; Li, J.; Wang, L.; Sancar, A.; Zhong, D. *J. Am. Chem. Soc.* **2008**, *130* (24), 7695–7701.

(50) Zhao, R. K.; Lukacs, A.; Haigney, A.; Brust, R.; Greetham, G. M.; Towrie, M.; Tonge, P. J.; Meech, S. R. *Phys. Chem. Chem. Phys.* **2011**, *13* (39), 17642–17648.

CHAPTER 3

CHARACTERIZATION OF PROMISCUITY IN ADENYL TRANSFERASE ACTIVE SITES OF FAD SYNTHETASES

3.1 Introduction

FAD Synthetase (FADS) is a ubiquitous enzyme responsible for the production of the essential cofactor flavin adenine dinucleotide (FAD) via an adenylation reaction of flavin mononucleotide (FMN) from adenosine triphosphate (ATP)[1]. In bacteria, this enzyme is bifunctional, also producing FMN via the phosphorylation of riboflavin[2,3]. Plants and many bacteria have the ability to synthesize riboflavin, the precursor to FMN and FAD, *de novo*[4,5]. Mammals are restricted to dietary uptake of riboflavin[6]. Unlike bacteria, mammals require two separate enzymes for flavin biosynthesis. Riboflavin kinase synthesizes FMN from ATP and riboflavin in a Mg^{2+} dependent reaction. This product is then shuttled to FAD synthetase to adenylate FMN in a sequential Mg^{2+} dependent reaction using ATP and FMN, see Figure 3.1 for scheme [1,6,7]. The evolutionary development of different flavin biosynthesis pathways in bacteria and humans implicates that targeting the pathway in bacteria may be a selective drug target.

FAD synthetase in humans, also named as FAD synthase, is a 57kDa monofunctional enzyme found in two isoforms[8,9]. Each isoform is localized to a different compartment of the cell, isoform 1 (hFADS1) is found in the mitochondria and isoform 2 (hFADS2) is localized to the cytosol[10,11]. All work in this dissertation corresponds to hFADS2 only. The hFADS2 enzyme folds into two domains, a phosphoadenosine

phosphosulfate reductase at the C-terminus and a molybdo-pterin-binding domain at the N-terminus[6,9]. To date, the crystal structure of hFADS2 remains unsolved; the FAD synthetase crystal structure from eurkaryotic yeast is shown in Figure 3.2 [12]. However, the order of binding and product release follows the same behavior of bacterial and other mammalian FAD synthetases, an ordered bi-bi mechanism in which the ATP binds before FMN and pyrophosphate (PPi) releases before FAD[11]. It has been suggested that the redox state of the flavin and the presence of other apo-flavoproteins significantly affects the product release and ultimately the overall rate of catalysis[13,14]. Promiscuity of the flavin binding pocket has been tested with deazaflavins and roseflavin antibiotics; however, the promiscuity of the ATP binding pocket has not been tested, to our knowledge, with modified fluorescent based analogues[13]. It would be advantageous to examine the promiscuity of this active site and compare it to that of a bacterial FAD synthetase to see if there was yet another degree of drug target selectivity between species.

FAD synthetase isolated from *C. ammoniagenes* is a 38 kDa bifunctional enzyme that binds its substrates and releases its products in an ordered bi-bi mechanism[3,15]. It has been shown that ATP binds first, followed by FMN, once catalysis occurs, pyrophosphate is released and then FAD is the rate limiting step. There are two independent ATP binding sites and two independent flavin binding sites in each of the functional domains; see Figure 3.1. for the crystal structure of the oligomeric assembly [15–17]. While FADS isolated from *C. ammoniagenes* does not accept all triphosphate nucleosides, it has been demonstrated that bacterial FADS will accept the fluorescent base analogue aminopurine-2'-deoxyriboside-5'-triphosphate (2ApTP) for the production of F-2Ap-D[3,18]. Preliminary

experiments indicate the monofunctional human FADS (hFADS) is not similarly promiscuous. These results raise questions about the differences in substrate specificity of bacterial and hFADS. Understanding these enzymes may lead to new drug therapies, bioimaging techniques, and structure function relationships in the FMNAT family.

3.2 Materials and Methods

3.2.1 Overexpression and Purification of caFADS

The *Corynebacterium ammoniagenes* FAD synthetase (caFADS) plasmid was generously provided by Prof. M. Medina. The pET28a-(+) vector was transformed into BL-21 DE3 competent cells. These cells were grown at 30^{o}Cin LB media and overexpressed using 1mM IPTG after the cells had reached an O.D. of 0.6 (~3 hours) at 600 nm. The cells were then spun down after 5 hours of additional growth, homogenized in disruption buffer (50mM Tris, 12mM beta-mercaptoethanol/BME, incubated with 1mg/mL of lysozyme (FisherSci), and then sonicated (Sonetek) with ¼" tip for 8 minutes at 30 seconds on and 30 seconds off on level 4. After pelleting the cell debris at 15000xg for 30 minutes the volume of the supernatant was measured and ammonium sulfate was added to a final percentage of 35% (w/v). A 5mL Hi-Trap phenyl sepharose column was used as a first round of purification of caFADS. The protein mixture was loaded onto the column, washed with 20 mL of Buffer B (50mM Tris, 20% ammonium sulfate 5mM $MgCl_2$ pH 8.0), and then eluted using a linear gradient of 25 mL Buffer B to Buffer C (50mM Tris, 5mM $MgCl_2$ pH 8.0) sulfate over 20 minutes. The collected fractions were then combined and buffer exchanged into cFS Activity Buffer (50mM Tris 5mM $MgCl_2$ pH 8.0) and loaded onto a 30mL DEAE Sephadex column A-25. This column was washed with 60 mL Buffer dsB (50mM Tris, 5mM $MgCl_2$, 100mM NaCl pH 8.0), and the

caFADS was eluted using a gradient from Buffer ds B to 100 % Buffer dsC (50mM Tris, 5mM $MgCl_2$, 500mM NaCl pH 8.0) over 20 minutes at a flow rate of 1.5 mL per min[16]. The protein was then buffer exchanged into cFS Activity Buffer and stored in -20ºC. Typical yields of purified protein were 2-5mg/g of wet cell weight.

3.2.2 Overexpression and Purification of hFADS2

The human isoform 2 FAD synthetase plasmid was generously provided by Dr. M. Barile. The plasmid bearing the recombinant His-tagged protein gene was transformed into Rosetta DE3 component cells. These cells were grown in LB media to $O.D._{600}$ = 0.6 and overexpressed using 1mM IPTG at 37ºC. The cells were then spun down (~15g/L), homogenized in buffer hA (50mM HEPES, 100mM NaCl, 10% sucrose, 10mM BME, 10mM imidazole pH 7.4) incubated with 1mg/mL of lysozyme (FisherSci), and then sonicated (Sonetek) with ¼" tip for 8 minutes 30 second on and 30 seconds off on level 3. The protein can be isolated successfully from the soluble fraction but we have found that resuspension of the insoluble fraction did not yield significant amounts of protein. Therefore, the insoluble fraction was discarded. It has been reported that the insoluble fraction may contain 75% of the expressed protein[6]. After pelleting the cell debris at 15000xg for 30 minutes the supernatant was filtered and loaded onto a preequilibrated 5mL Hi-Trap Ni^{2+} sepharose column. The column was washed with 20 mL of Buffer hB (50mM HEPES, 100mM NaCl, 10% sucrose, 10mM BME, 500mM imidazole pH 7.4) and then the protein was then eluted with 30 mL of Buffer hC (50mM HEPES, 100mM NaCl, 10% sucrose, 10mM BME, 500mM imidazole pH 7.4). The collected fractions were then combined and buffer exchanged into hFS Activity Buffer

50mM Tris 5mM $MgCl_2$ pH 7.4 and stored at 4°C. Typical yields of purified protein were 0.78mg/g of wet cell weight.

3.2.3 Activity Assay of caFADS and hFADS2

In a 1.0 mL reaction volume, 1 µM caFADS or hFADS2 was incubated at 37°C with 100µM 2ApTP (BioLog) or ATP and 100 µM 98% pure FMN (Sigma) for two hours in their respective Activity Buffers. Pseudo-first order reactions were performed using 100nM caFADS/hFADS2, 1mM 2ApTP or ATP, and 10 µM of FMN. The reaction was quenched by heating the samples to 100°C for 5 min. The sample was centrifuged at 15,000xg to remove the caFADS/hFADS2 from solution before purification on a 250x4.6mm Beta Basic HPLC column. The isocratic method consisted of 100% 5mM Ammonium Acetate pH 6.0 doped with 20% HPLC grade methanol. Peaks were integrated and corresponding areas were converted to concentrations from a calibration curve. An isolated peak corresponding to F2ApD was collected, freeze dried, and stored in -20°C until used for further analysis.

3.3 Results

3.3.1 Control Experiments

Activity assays were monitored using steady-state fluorescence and HPLC. Control reactions were run using ATP and FMN to ensure the enzyme was active; see Figure 3.3 for standards. The decrease in fluorescence (see Figure 3.4) corresponds to the production of FAD because FAD has a lower quantum yield in the oxidized state compared to FMN[19,20]. The reported kinetic constants for caFADS FMNAT activity are k_{cat} =17 min^{-1}, K_M^{ATP} = 36µM, and K_M^{FMN} = 1.2µM[3,21,22]. These K_M values are average

Michaelis constants since it was not possible to determine the constant for each specific independent binding site[17]. The k_{cat} is a k_{cat}^{eff} because it is not possible to isolate the protein from oligomeric mixtures (i.e. hexamer, trimers, and monomers)[16]. For our experimental conditions we report an average k_{cat}^{eff} of 13 min^{-1} for the reactions associated with Figure 3.4. See equation 1.

$$\frac{V_{max}}{[E]_T} = k_{cat}^{eff}$$

Equation 1.

Equation 1. was used because under all experimental conditions one of the substrates was held in a 10 fold excess of the binding constant (see section 3.2 for concentrations). This allowed one to assume that the enzyme substrate complex behaved under steady-state kinetics.

For the hFADS2 reactions, the reported constants are k_{cat} = 4.14 min^{-1}, K_M^{FMN} = 350 nM and K_M^{eff} =15.3µM [6]. Researchers report that there is a decrease in activity of up to 40% upon converting the holo-protein to apo-form[6,9]. For all experiments presented here, the enzymes were washed with excess ATP to allow for the removal of endogenous substrate or product still bound after purification, confirmed by a lack of absorption at 450 nm corresponding to flavin. Therefore, all of the protein that was used for promiscuity experiments were in the apo-form initially. Our measured k_{cat}^{eff} is 1.34 min^{-1} based on the experiments shown in Figure 3.5.

3.3.2 Promiscuity Experiments

The enzymatic reactions were assembled in the same way that the control reactions were run. Two experiments were designed so that the concentration of the

2ApTP was in a high excess of the binding constant reported for ATP so that binding would not be the limiting step of catalysis (67 fold excess for hFADS2 and 28 fold excess for caFADS). Interestingly the bacterial enzyme showed activity while the human isoform 2 did not, for two different concentrations of 2ApTP, see Figures 3.6 and 3.7. We report an effective $k_{cat} = 4.68\ min^{-1}$ for the 2ApTP reaction of caFADS.

3.3.3 F2ApD

The novel product named F2ApD was isolated and characterized using UV-vis absorption, steady-state fluorescence, and ultrafast transient absorption. These results are discussed in Chapter 4.

3.4 Discussion

The promiscuity of the adenylation active site seems to be selectively for the bacterial enzyme. However, these results are still preliminary due to the fact that the hFADS2 isoform displays a significant loss of activity even with the native substrates. It is important that the K_D and K_M for 2ApTP are accurately determined. Experiments to date attempted to calculate the K_D using a fluorimetric competitive binding assay. However, when plotting the fraction bound versus the ATP concentration added to the solution, the data did not display sigmoidal behavior typical of competitive binding curves. This may be due to: a mixture of oligomeric states of caFADS, 2ApTP base stacking quenching effects, and multiple binding sites for ATP.

The FADS adenylation reaction is expected to occur via a nucleophilic attack by the 5' phosphate of the FMN on the α- phosphate of ATP without the direct involvement of residues in the active site[17]. Yet, the effect catalytic rate constants are different by a factor of 3 for the caFADS. Medina *et al*. modeled FMN and ATP using crystal structures

of FAD synthetases co crystallized with substrate. The authors suggest that the α,β phosphates are situated within interacting distance of the neighboring His residues. The adenine is located at the bottom of the cavity making hydrogen bonding contacts to the backbone of hydrophobic residues[16]. It seems as if the displacement of the amino group on adenine did not perturb the contacts with the α,β phosphates, but may have induced some repulsive interactions with residue Arg161 thus affecting the binding or release of the 2Ap group.

For the human isoform 2, it is more difficult to make structural conclusions because the crystal structure has not yet been solved. However, comparing the hFADS2 sequence with that of *S. cerevisiae* (60% identity and 34% similarity of the PAPS reductase domain) one may argue that the increased interaction between the residues and the adenine moiety is a clear indicator as to why the displacement of the amino group caused inactivation of the enzyme. In *S. cerevisiae* Fad1p the adenine base plane is perpendicular to the isoalloxazine ring. The ring is tightly surrounded by side chains of the totally conserved P-loop. The N6 is hydrogen bonded to the carbonyl group of Ile107. By moving this group to the C2 position this interaction is completely lost, the 2-aminopurine may not bind at all in the human isoform 2[12,23]. It has been proposed that the increase number in interactions and the tight binding of the bent FAD product may act as a regulatory role in eukaryotic cellular FAD homestasis[11].

3.5 Conclusions

Here we present the promiscuity of adenyltransferase active sites between a bacterial FAD synthetase and a human isoform 2 FAD synthetase. This interesting result leaves open questions about the evolutionary divergence of FAD synthetases. Bacterial

systems may not need a tight regulation on flavin homeostasis because they do not possess mitochondria. Flavins are found in many mitochondrial proteins and are involved in metabolic processes for higher lifeforms. Due to the lack of interactions with the adenine moiety, caFADS is able to turnover 2ApTP and form F2ApD. Although the turnover is at a much lower rate, this provides mechanistic insight to the catalytic activity of the protein. The new enzymatically produced F2ApD may prove to be a useful flavin derivative for imaging experiments or mechanistic studies requiring modifications to the adenine.

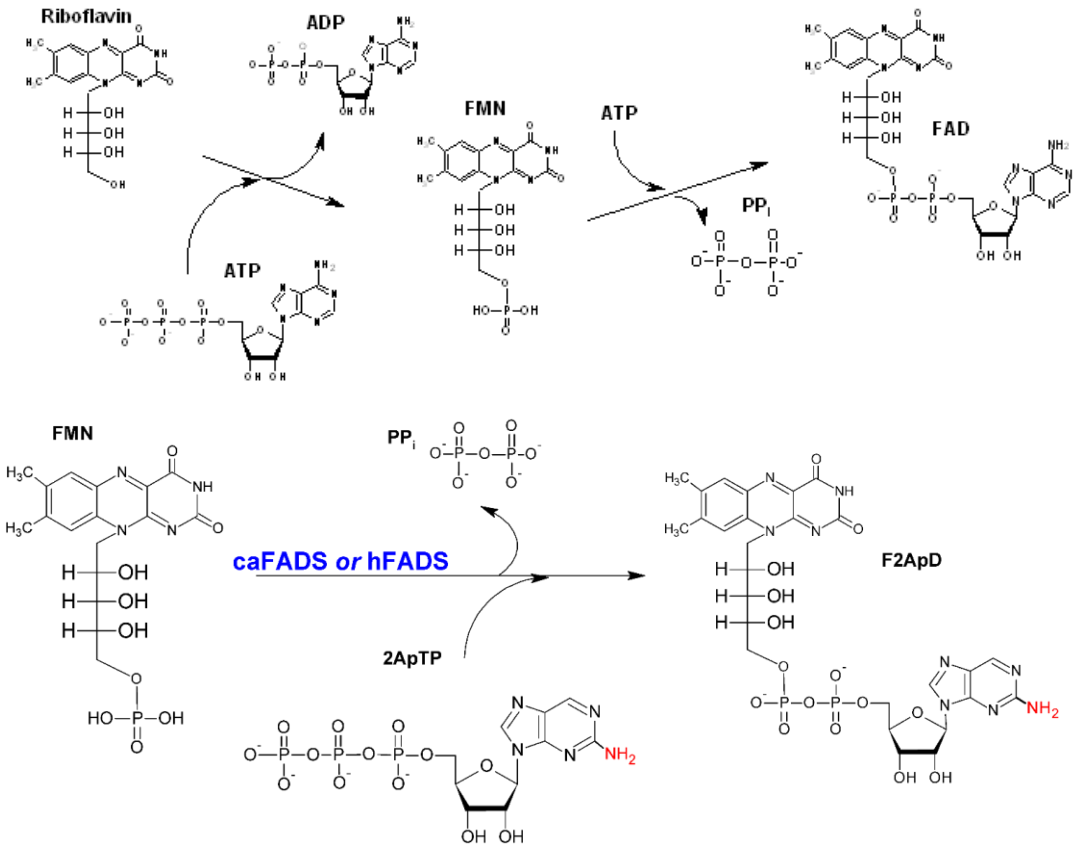

Figure 3.1. Reaction scheme for bacterial FAD synthetase is shown on top. The bottom panel shows a reaction scheme for F2ApD production.

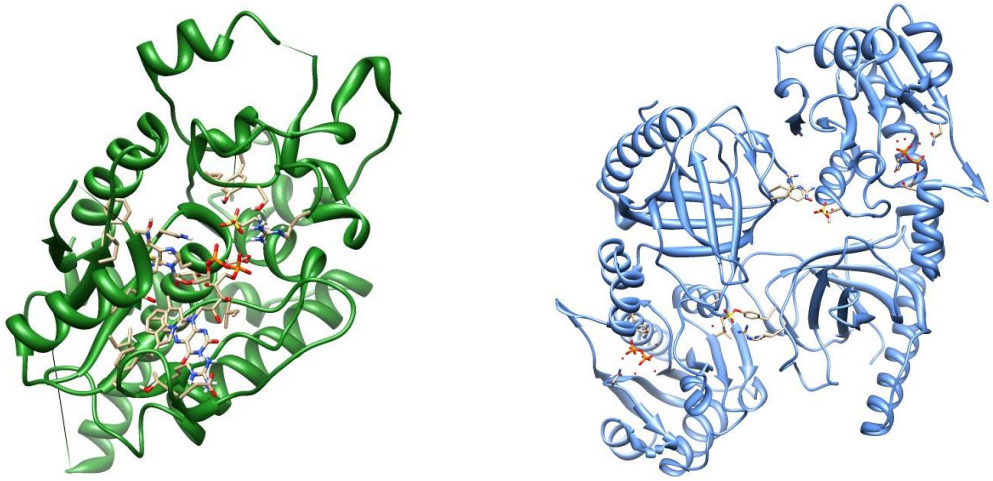

Figure 3.2. Crystal structure of FAD synthetase isolated from *S. cerevisiae* PDB ID 2WSI[24] (left). Crystal structure of hexameric FAD synthetase isolated from *C. ammoniagenes* PDB ID 2X0K (right)[16].

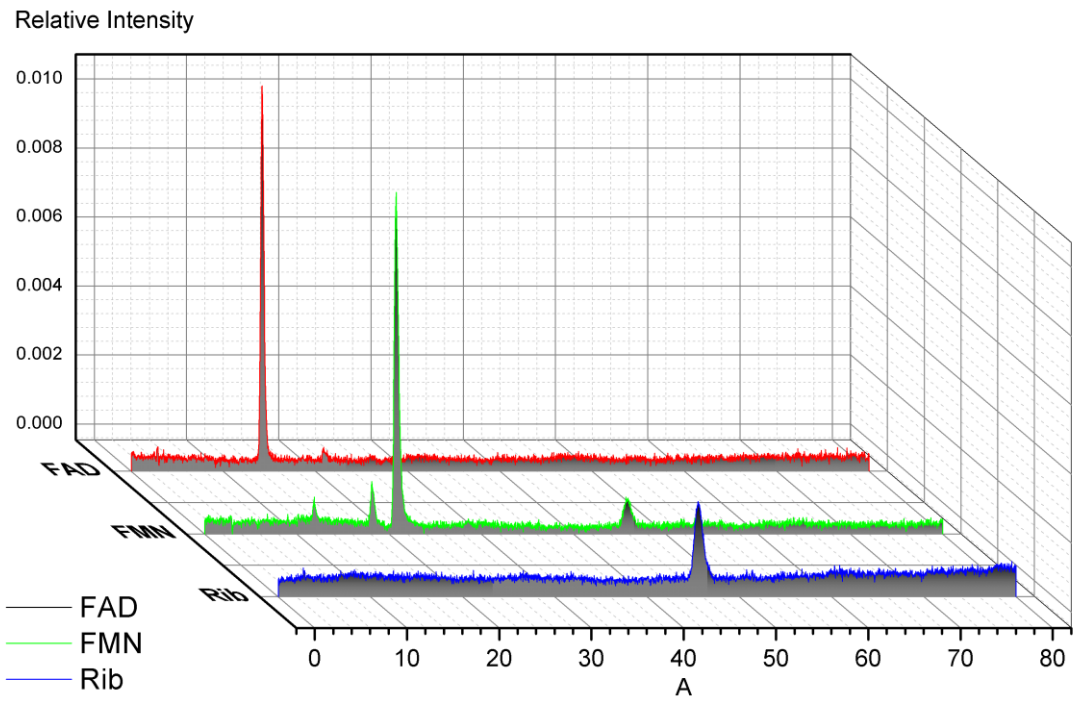

Figure 3.3. HPLC standards of 10 µM flavins on 250 mm x 4.6 mm Beta Basic column

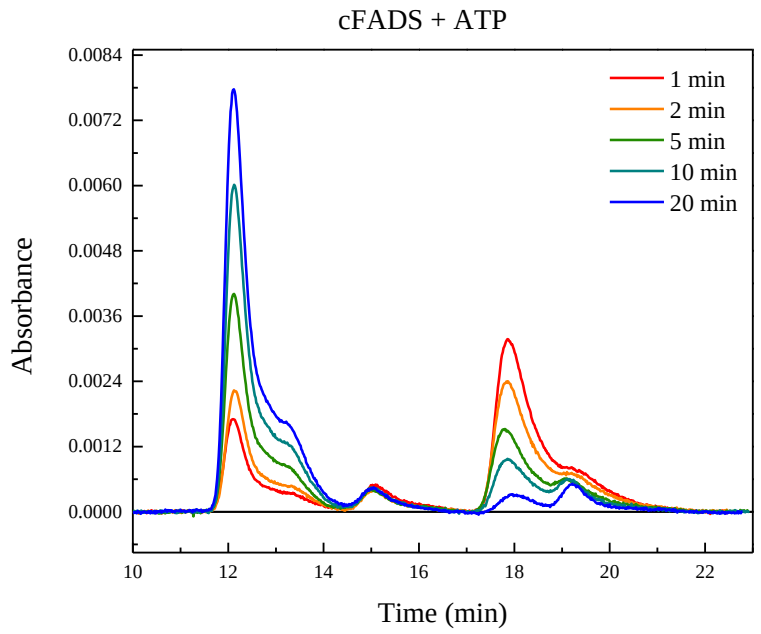

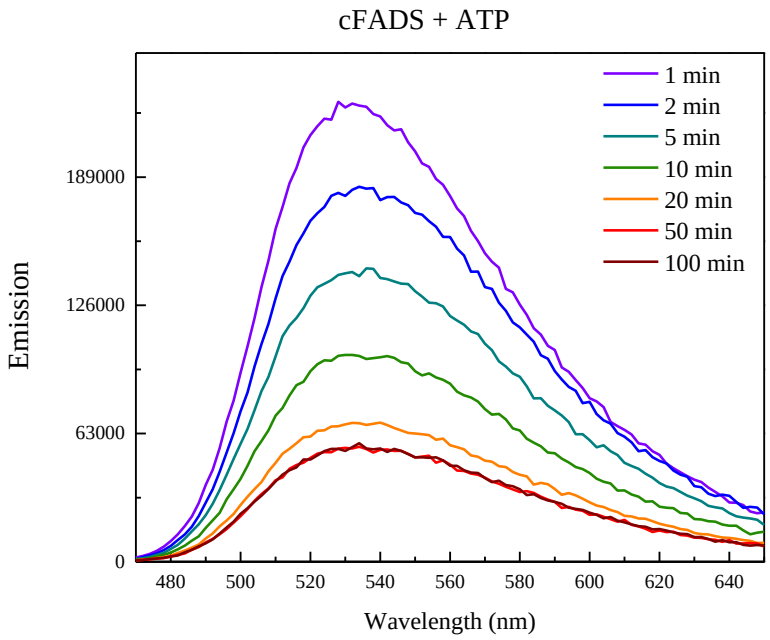

Figure 3.4. Control reaction of caFADS using 100 µM ATP and 10 µM FMN at 37°C pH 8.0 in 50 mM Tris 5 mM $MgCl_2$

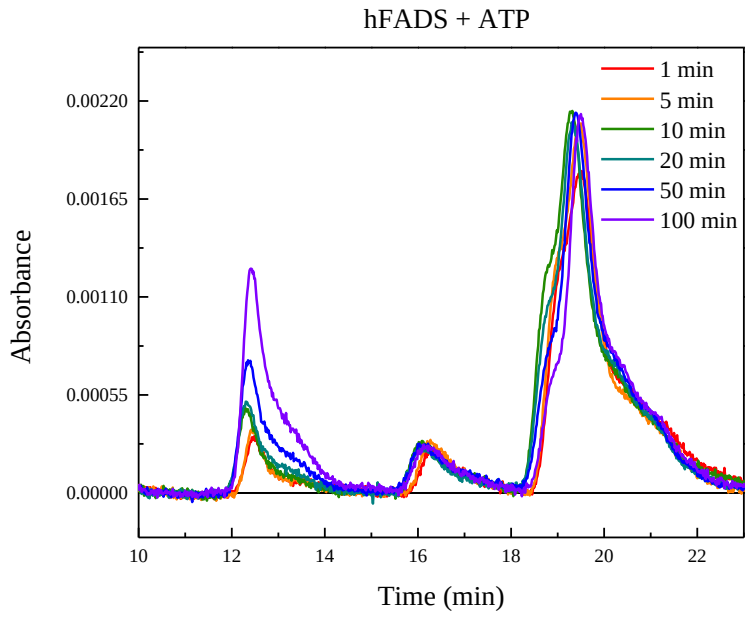

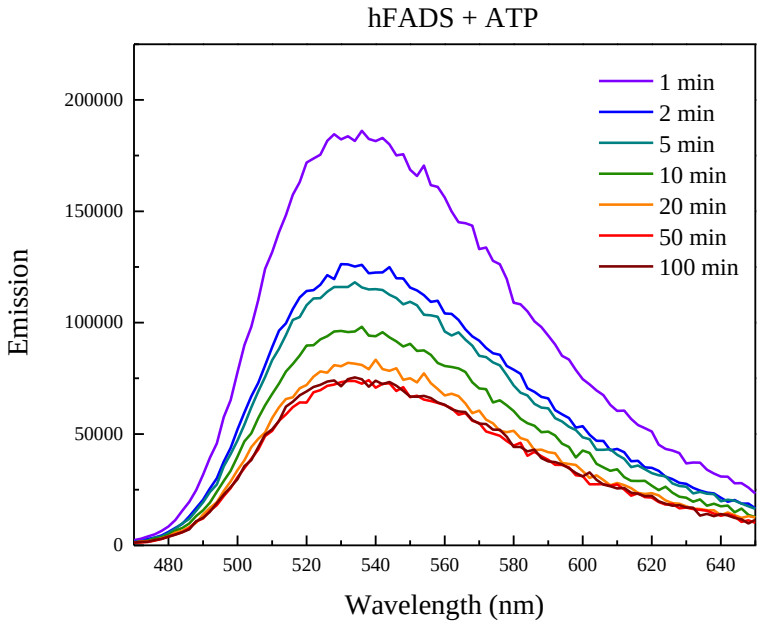

Figure 3.5. Control reaction of hFADS2 with 100 µM ATP and 10 µM FMN at 37°C pH 7.4 in 50 mM Tris 5 mM $MgCl_2$

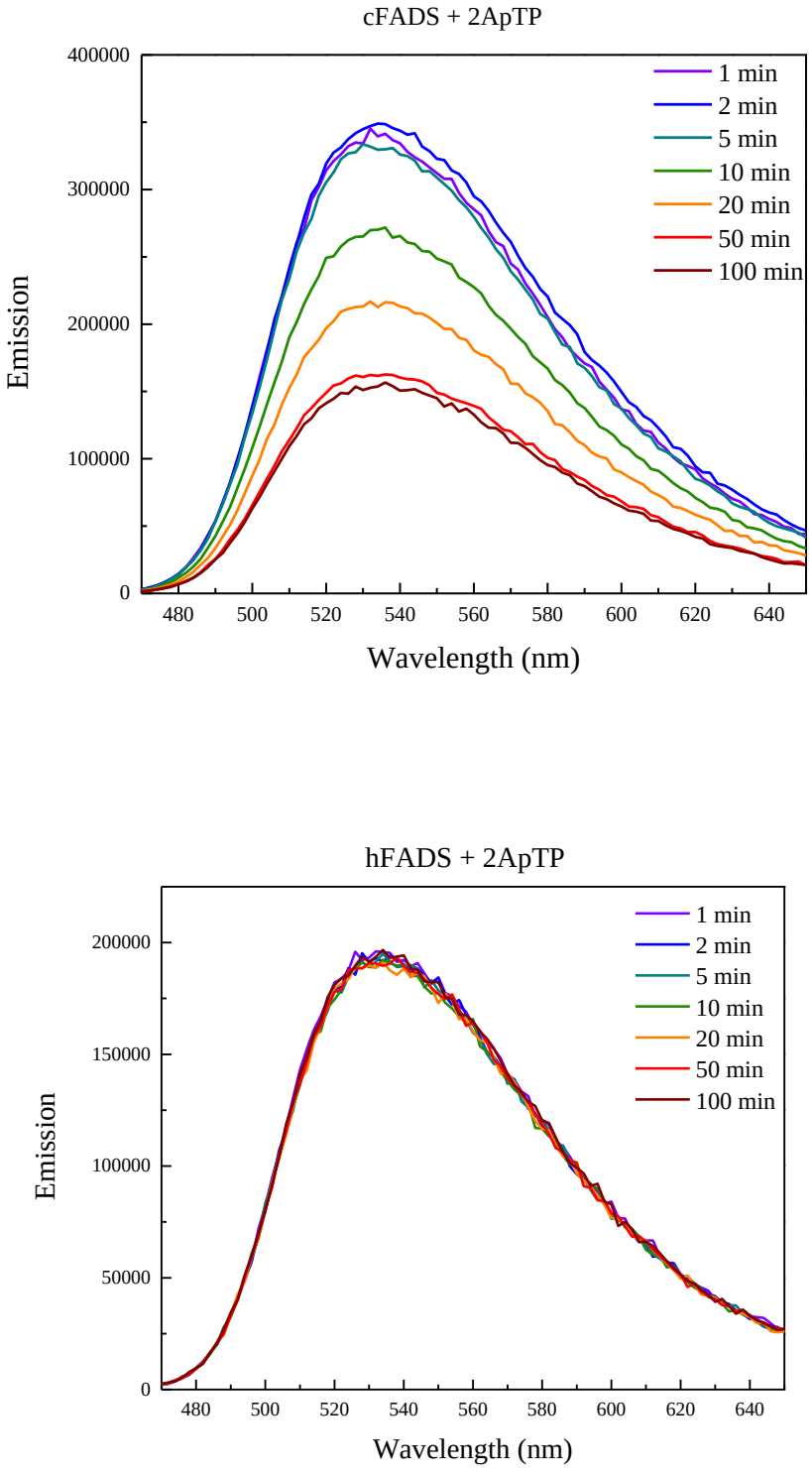

Figure 3.6. Reaction of caFADS/hFADS2 with 100 µM 2ApTP and 10 µM FMN at 37°C pH 8.0/7.4 in 50 mM Tris 5 mM $MgCl_2$

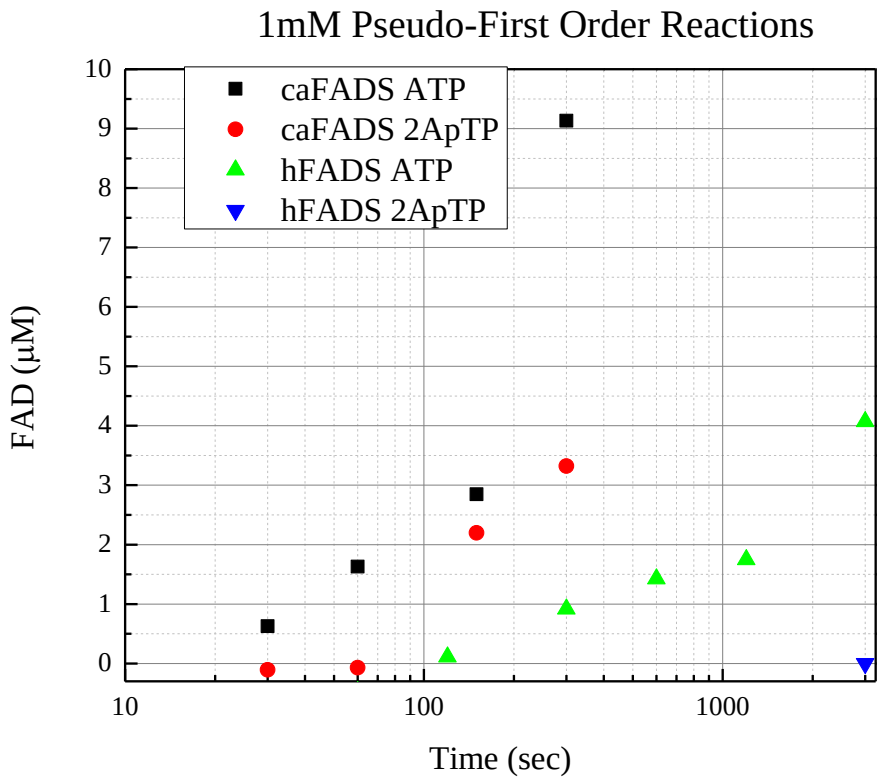

Figure 3.7. Pseudo-first order reactions of caFADS and hFADS2 using 1mM ATP or 2ApTP, 0.010 mM FMN in Activity Buffer (pH 8.0 and 7.4 respectively). All reactions were run at 37ºC.

3.6 References

(1) Bacher, A. *Chem. Biochem. Flavoenzymes* **1991**, *1*, 349–370.

(2) Krupa, A.; Sandhya, K.; Srinivasan, N.; Jonnalagadda, S. *Trends Biochem. Sci.* **2003**, *28* (1), 9–12.

(3) Efimov, I.; Kuusk, V.; Zhang, X.; McIntire, W. S. *Biochemistry* **1998**, *37* (27), 9716–9723.

(4) Roje, S. *Phytochemistry*. 2007, pp 1904–1921.

(5) Bacher, A.; Eberhardt, S.; Fischer, M.; Kis, K.; Richter, G. *Annu. Rev. Nutr.* **2000**, *20*, 153–167.

(6) Torchetti, E. M.; Bonomi, F.; Galluccio, M.; Gianazza, E.; Giancaspero, T. A.; Iametti, S.; Indiveri, C.; Barile, M. *FEBS J.* **2011**, *278* (22), 4434–4449.

(7) Yamada, Y.; Merrill, A. H.; McCormick, D. B. *Arch. Biochem. Biophys.* **1990**, *278* (1), 125–130.

(8) Torchetti, E. M.; Brizio, C.; Colella, M.; Galluccio, M.; Giancaspero, T. A.; Indiveri, C.; Roberti, M.; Barile, M. *Mitochondrion* **2010**, *10* (3), 263–273.

(9) Galluccio, M.; Brizio, C.; Torchetti, E. M.; Ferranti, P.; Gianazza, E.; Indiveri, C.; Barile, M. *Protein Expr. Purif.* **2007**, *52* (1), 175–181.

(10) Barile, M.; Passarella, S.; Bertoldi, A.; Quagliariello, E. *Arch. Biochem. Biophys.* **1993**, *305* (2), 442–447.

(11) Barile, M.; Giancaspero, T. A.; Brizio, C.; Panebianco, C.; Indiveri, C.; Galluccio, M.; Vergani, L.; Eberini, I.; Gianazza, E. *Curr. Pharm. Des.* **2013**, *19* (14), 2649–2675.

(12) Leulliot, N.; Blondeau, K.; Keller, J.; Ulryck, N.; Quevillon-Cheruel, S.; van Tilbeurgh, H. *J. Mol. Biol.* **2010**, *398* (5), 641–646.

(13) Pedrolli, D. B.; Nakanishi, S.; Barile, M.; Mansurova, M.; Carmona, E. C.; Lux, A.; Gärtner, W.; Mack, M. *Biochem. Pharmacol.* **2011**, *82* (12), 1853–1859.

(14) Ye, H.; Rouault, T. A. *Biochemistry*. 2010, pp 4945–4956.

(15) Frago, S.; Velazquez-Campoy, A.; Medina, M. *J. Biol. Chem.* **2009**, *284* (11), 6610–6619.

(16) 1. Herguedas, B.; Martinez-Julvez, M.; Frago, S.; Medina, M.; Hermoso, J. A. *J. Mol. Biol.* **2010**, 218–230.

(17) Serrano, A.; Frago, S.; Velázquez-Campoy, A.; Medina, M. *Int. J. Mol. Sci.* **2012**, *13* (12), 14492–14517.

(18) Murthy, Y. V. S. N.; Massey, V. *J. Biol. Chem.* **1998**, *273* (15), 8975–8982.

(19) Visser, A. J. W. G. *Photchem. Photobio.* **1984**, *40* (6), 703–706.

(20) Islam, S. D. M.; Susdorf, T.; Penzkofer, A.; Hegemann, P. *Chem. Phys.* **2003**, *295* (2), 137–149.

(21) Serrano, A.; Ferreira, P.; Martínez-Júlvez, M.; Medina, M. *Curr. Pharm. Des.* **2013**, *19* (14), 2637–2648.

(22) Serrano, A.; Frago, S.; Herguedas, B.; Martinez-Julvez, M.; Velazquez-Campoy, A.; Medina, M. *Cell Biochem. Biophys.* **2013**, *65* (1), 57–68.

(23) Huerta, C.; Borek, D.; Machius, M.; Grishin, N. V.; Zhang, H. *J. Mol. Biol.* **2009**, *389* (2), 388–400.

(24) Leulliot, N.; Blondeau, K.; Keller, J.; Ulryck, N.; Quevillon-Cheruel, S.; van Tilbeurgh, H. *J. Mol. Biol.* **2010**, *398* (5), 641–646.

CHAPTER 4

PHOTOPHYSICAL CHARACTERIZATION OF AN ENZYMATICALLY-SYNTHESIZED DUALLY FLUORESCENT FAD COFACTOR

4.1 Introduction

Flavin adenine dinucleotide (FAD) participates as a redox cofactor in many mitochondrial flavoproteins, in which flavin can transfer either one or two electrons. Such pathways are prime targets for biomarkers because regulatory processes include apoptosis, oxidative stress response, and free radical generation[1,2]. FAD has been exploited as a biomarker and endogenous reporter of metabolic imaging because each of the redox states of the flavin exhibits unique spectroscopic characteristics. Flavin cofactors have been studied using two photon microscopy because of its intrinsic low autofluorescence and high spatial resolution[1,3]. Although the flavin ring system is emissive, the quantum yield of FAD is quite low (0.03)[4]. The ideal dually fluorescent imaging FAD or "iFAD" would enhance the emission of the flavin ring system while achieving efficient selective excitation of the donor chromophore, further eliminating background fluorescence.

By exploiting *Corynebacterium ammoniagenes* FAD synthetase adenylation promiscuity (manuscript in progress), we have enzymatically synthesized and purified a novel dually fluorescent flavin dinucleotide analog (DF-FD). FAD synthetase efficiently adenylates flavin mononucleotide using ATP. By substituting 2-aminopurine riboside triphosphate (2ApTP), a new FAD analog, flavin 2-aminopurine (2Ap) dinucleotide (F2ApD), was isolated, see Figure 4.1 for structural comparison. This new DF-FD can be

selectively excited through the 2Ap molecule at λ_{max} = 310 nm, a wavelength at which flavins have very low extinction. Free 2Ap emits with high quantum yield at 370 nm, which overlaps almost perfectly with the 370 nm transition of flavin ($S_0 \rightarrow S_1$). This overlap is a prerequisite for resonance energy transfer from *2Ap:Fl→2Ap:*Fl with resulting emission from *Fl at 520 nm[5–10]. Here we report the synthesis, purification, and photophysical characterization of F2ApD using steady-state absorption and fluorescence spectroscopies as well as its excited state photodynamics at the femtosecond timescale.

4.2 Materials and Methods

4.2.1 Protein Purification

The *Corynebacterium ammoniagenes* FAD synthetase (*Ca*FADS) plasmid was generously provided by Prof. M. Medina. The pET28a-(+) vector was transformed into BL-21(DE3) competent cells. These cells were grown in LB media and overexpressed using 1 mM IPTG after the cells had reached an O.D. of 0.6 at 600 nm. The cells were then spun down, homogenized in disruption buffer (50 mM Tris, 12 mM βME), incubated with 1 mg/mL of lysozyme (FisherSci), and then sonicated (Sonetek) with a ¼" tip for 8 minutes, 30 second on and 30 seconds off, at level 4. After pelleting the cell debris at 15000 xg for 30 minutes, ammonium sulfate ($AmSO_4$) was added to a final concentration of 35% (w/v). A 5 mL Hi-Trap phenyl sepharose column was used as a first round of purification of *Ca*FADS. The protein mixture was loaded onto the column, washed with Buffer B (50 mM Tris, 20% $AmSO_4$, 5 mM $MgCl_2$, pH 8.0), and then eluted using a linear gradient of Buffer B to Buffer C (Buffer B with no $AmSO_4$) over 20 minutes. The collected fractions were then combined and buffer exchanged into Activity

-Buffer (50 mM Tris, 5 mM $MgCl_2$, pH 8.0) and loaded onto a DEAE Sephadex A-25 column. The column was washed with Buffer dsB (50 mM Tris, 5 mM $MgCl_2$, 100 mM NaCl, pH 8.0), and the *Ca*FADS was eluted using Buffer dsC (Buffer dsB with 500 mM NaCl)50mM Tris, 5mM MgCl2, 500mM NaCl pH 8.0)[11]. The protein was buffer-exchanged into Activity Buffer and stored in -20° C.

4.2.2 CaFADS iFAD Reaction Conditions

In a 1.0 mL reaction volume 1 µM *Ca*FADS was incubated at 37°C with 100 µM 2ApTP (BioLog) and 100 µM FMN (Sigma) for two hours. Control reactions were ran with FMN and ATP, see Chapter 3. The reaction was stopped by heating the samples to 100° C for 5 min. The sample was centrifuged at 15,000 xg to remove the *Ca*FADS from solution before purification on a 250x4.6 mm Beta Basic HPLC column by an isocratic method consisting of 100% 5 mM Ammonium Acetate pH 6.0 doped with 20% HPLC grade methanol. A peak corresponding to F2ApD was collected, freeze dried, and stored in -20° C until used for further analysis.

4.2.3 Steady-State Absorption and Fluorescence Spectroscopy

All linear absorption measurements were carried out on Hewlett Packard 8452A Diode Array Spectrophotometer. Steady-state studies were carried out on a PTI fluorimeter (Birmingham, NJ). Excitation slits were kept at 2 nm to prevent photodegradation of the flavin and emission slits were kept at 3 nm to optimize the signal to noise ratio. The F2ApD samples were then resuspended in a 50 mM Tris, 100 mM phosphate buffer, or 50 mM HEPES buffers, pH 7.0. F2ApD in Tris buffer led to photoproducts/adducts when using 310 nm excitation, while 50 mM HEPES buffer

undergoes photo-oxidation at this wavelength. Therefore, all redox states of the flavin were studied in 100 mM phosphate buffer pH 7.0.

Phosphodiesterase assays were performed using 2 µL of a 1 mg stock solution at 23^{o}C in 100 mM phosphate buffer pH 7.0. The phosphodiesterase *C. durissus (*Boehringer Mannheim Gmbh) was generously donated from Dr. Richard Waring.

4.2.4 Transient Absorption Spectroscopy

A seed beam at 780 nm from a Ti:Sapphire laser (KLM, ~80 MHz) is amplified using a regenerative amplifier to produce a 1.5 µJ, 120 fs fundamental output at 250 Hz. This is then split to generate the white-light continuum (400-710 nm) probe beam by focusing (NA ~ 0.04) one part of the fundamental onto a slowly translating CaF_2 crystal and the other part produces a pump beam at second-harmonic of the fundamental, 390 nm, using a 2 mm type-I BBO crystal. While the angle between the pump and the probe beams focused at the sample is ~ 2°, their relative polarization is held at magic angle (54.7°). The pump-probe delay is set using a motorized delay rail that adjusted the path-length of the pump beam to provide a delay range of up to 4 ns with a resolution of ~10 fs. To build the difference absorption spectra, the sample is pumped at 50 Hz while data acquisition from a water cooled CCD detector (Andor, 256 X 1024 pixels) is performed at 100 Hz. Data is then transferred onto the computer using in-house developed LabView software. Analysis of the data is performed using Origin 9, MATLAB, and global fitting analysis tool Glotaran[12].

For the chirp correction and fitting of the instrument response function (IRF), the cuvette sample solution is replaced with water. The high intensity pump beam induces an optical kerr effect (OKE) in the solution that refracts a fraction of the probe beam onto

the detector. Using the delay rail, the pump beam is made to sample the entire probe spectrum to enable building the cross correlation. This correction correlates well with the Glotaran software IRF fitting tool.

4.3 Results and Discussion

4.3.1 Absorption and Steady-State Fluorescence Spectra

It is known that FAD synthetase will uptake flavin derivatives, however it will not turnover with other nucleotide triphosphates (CTP, GTP, TTP)[11,13]. We have used the fluorescent ATP analog 2-aminopurine triphosphate (2ApTP), hypothesizing that small changes to the adenine ring would be tolerated by FADS. The promiscuity of the adenylation active site proved sufficient to incorporate 2ApTP and adenylate FMN to make F2ApD. This is somewhat surprising because several hydrogen bonding contacts are removed upon the 2Ap substitution when compared to adenine binding in the crystal structure[11,14]. Nonetheless, this represents, to our knowledge, the first time FADS has been shown to take up a modified base nucleotide of any kind, and represents the first enzymatically-synthesized dually fluorescent FAD analog.

The absorption spectra of F2ApD, FAD, and FMN are shown in Fig. 1. For sake of comparison the spectra have been normalized to ε_{450} = 11,200 $M^{-1}cm^{-1}$. The most singular feature is the remarkably strong and well-defined extinction of F2ApD at about 310 nm, which about 3-fold higher than the chemically-synthesized εFAD and about 7-fold higher than FMN for the same wavelength. Nevertheless, the $S_0 \rightarrow S_1$ (S_{01}) and S_{02} transitions at *ca.* 450 and 370 nm, respectively, have comparable extinctions. Not surprisingly, the Ade UV absorption at ~265 nm is missing in the F2ApD spectrum.

Another significant difference in the UV occurs at ~225 nm, where the Ade analog confers about twice the extinction of either FMN or FAD.

Clearly the unique spectroscopic differences between the F2ApD and FAD allow for exploitation of the 2Ap moiety, particularly in fluorescence as suggested above. (see Figure 4.2a-b). The excitation spectra have been normalized at 446 nm for comparison.

The relative intensities of the emission spectra (Fig. 2b) suggest that F2ApD stacking interactions are significantly different compared to FAD. To validate that the 2Ap moiety is stacked with the isoalloxazine moiety a phosphodiesterase digestion was performed using a small aliquot of enzyme added to 1μM F2ApD or FAD. Figure 4.3 illustrates that the 2Ap fluorescence increases upon cleavage of the phosphodiester bond. As a control, FAD digestion was performed and shows the expected emission increase at 520 nm. The assay was completed over the course of 2.5 hours.

Control experiments were conducted to calculate the degree of quenching using free FMN in simple solvent as a secondary emission standard. Solutions containing 1 μM FMN + 1 μM 2ApTP showed no signs of fluorescence quenching due to intermolecular stacking, as evidenced by the high emission intensity of the *2Ap chromophore. Compare this to *FMN or *FAD emission with λ_{ex} = 310 nm. The emission intensity is negligible, in good agreement with previously reported quantum yields of oxidized flavin fluorescence[15–17]. Contrary to expectations, there is no evidence of strong energy transfer in F*2ApD. Excitation at 310 nm shows quenching of *2Ap emission by more than a factor of five, but there is no compensating *Fl emission at 520 nm. In fact, the emission intensity of *(F2ApD) at 520 nm is just slightly more than that of FMN itself. A possible quenching mechanism of stacked *F2ApD is photoinduced electron transfer between the

*2Ap moiety and the isoalloxazine ring system, $Fl\cdots{}^*2Ap \rightarrow Fl^{\bullet-}\cdots 2Ap^{\bullet+} \rightarrow Fl\cdots{}^*2Ap$. Another possibility is that energy transfer occurs but PET follows immediately with $Fl\cdots{}^*2Ap \rightarrow {}^*Fl\cdots 2Ap \rightarrow Fl^{\bullet-}\cdots 2Ap^{\bullet+}$. Indeed, it is also possible that interactions between Fl and 2Ap engender the formation of a conical intersection with subsequent ultrafast population relaxation from $S_n \rightarrow S_0$ (n = 1,2). It was necessary to perform ultrafast transient absorption measurements of the F2ApD molecule to ascertain the quenching mechanism.

Stacking in FAD and F2ApD were computed as follows. The count intensity of the centered around 525 nm for F2ApD is indicative of a 40% stacked population, see equation 1. Taking the ratios of the 450 nm intensity when monitoring emission at 530 nm yields 80% stacked FAD and 40% stacked F2ApD when compared to FMN emission. It is important to note that the equation and calculation described assumes that the quantum yields for the stacked and unstacked population of F2ApD are equivalent to the quantum yields for the FAD stacked and unstacked populations relative to FMN. This is a preliminary assumption and future experimentation is required to calculate a relative quantum yield to quinine sulfate (a well characterized chromophore typically used in quantum yield calculations[18]).

$$Stacked_{\%} = \frac{Fl\ Intensity_{530\ nm}}{Fl\ Intensity_{FMN\ 530\ nm}}$$

Equation 1. Calculating the percentage of stacked versus unstacked flavin populations.

To examine the temperature dependence of stacking, the fluorescence emission spectra were measured at both 4°C and 20°C. The data shows that there is a collisional thermal quenching effect on fluorescence. We had expected to see an increase in fluorescence as stacking decreased with increasing temperatures. Our data shows that fluorescence decreases as temperature increases.

4.3.2 Time-Resolved Ultrafast Transient Absorption

To further examine the evolution of *F2ApD, we measured its ultrafast dynamics using transient absorption (TA) spectroscopy. As a reference, TA data of 200 µM FMN in 100 mM phosphate buffer pH 7.0 was obtained at a pump wavelength of ~390 nm. The surface plot in Fig. 4 shows the smooth, slow decay of $*FMN_{OX}$. Of note, as they appear in subsequent decays, are the characteristic *FMN ground state bleach (GSB) at 450 nm with a $\sim\Delta A = -0.01$ persisting throughout the 3 ns scan range. Equally prominent are excited state absorptions (ESA) at ~350 and 505 nm. These ESAs are the result of transitions from $S_1 \rightarrow S_{2,3,4,5\ldots}$ giving ESA features at 2000 (not observed), 675, 450, and 350 nm.

The data were fitted to a two state sequential model, the simplest possible model that yielded a good fit. The lifetimes of the two states were $\tau_1 = 5.4 \pm 0.39$ ps and $\tau_2 > 3$ ns (described as "long"). The 5.4 ps component is attributed to internal conversion of the S_2 to S_1 state while the long component is attributed to radiative decay from the S_1 state, see Figure 4.4.

The FAD_{OX} excited state kinetics were fit to a two state parallel model where the starting populations were set to represent 80% stacked and 20% unstacked

conformations. The lifetimes assigned to each state were 6 ± 0.14 ps for the stacked conformation and > 3 ns for the unstacked conformation. The quenching mechanism of the stacked conformation has long been associated with photoinduced electron transfer. If this were the case, then the spectrum of the radical adenine intermediate (cation or anion[19,20]) should appear in the TA data. No evidence for this species is seen in our data (see Figure 4.5), suggesting that a more likely explanation is an ultrafast transit through a conical intersection for the stacked populations. This result agrees well with the conclusion of Zhong *et al* [21]. We have also found this to be the case for εFAD_{OX} (see Chapter 2).

The *F2ApD TA data was fit to a two state parallel model like the *FAD kinetic model. One exponential decay was assigned to a 60 % unstacked conformation yielding a long lifetime. The other 40 % (stacked) population gave a fast 1.8 ± 0.018 ps lifetime. The 1.8 ps lifetime reveals what may be the charge transfer state between the 2Ap and flavin moiety, see Figure 4.6[22–24]. In Figure 4.6, one can clearly see a shift in the excited state absorption maxima and a positive broad absorption band at ~560 nm. It has been proposed that DNA base stacked *2Ap can decay via an exciplex dependent dark state, conical intersection, or a bright state, radiative decay[24]. The kinetic model for the work presented here represents a stacked and unstacked conformation system of *F2ApD; therefore, we propose that the stacked population follows a relaxation pathway similar to the base stacked population of *2Ap leading to a conical intersection yielding a charge transfer state. The long component associated spectra resembles that of an unstacked flavin (FMN_{OX} **).**

4.4 Conclusions

The photophysical properties of a new dually fluorescent flavin adenine analog dinucleotide, F2ApD, in the oxidized form have been reported here. Characteristic and significant absorption of 2Ap at 310 nm affords for selective excitation of this potential energy transfer donor. However, steady-state fluorescence spectroscopy shows quenching of the *2Ap moiety and a very small increase in emission from the isoalloxazine ring. Ultrafast transient absorption studies revealed two relaxation pathways similar to that of the *FAD kinetic model. The unique feature of the *F2ApD fast component is the broad spectroscopic feature around 560 nm indicating charge transfer. We attribute the quenching of the *2Ap emission to a dark state conical intersection decay pathway yielding a charge transfer state. Regrettably, F2ApD may not hold much promise as an iFAD in photolyase because the 2Ap group is so quenched upon stacking interactions. However, the F2ApD may live up to this role in FAD-dependent proteins where the 2Ap and flavin are no longer stacked. This promise remains to be realized.

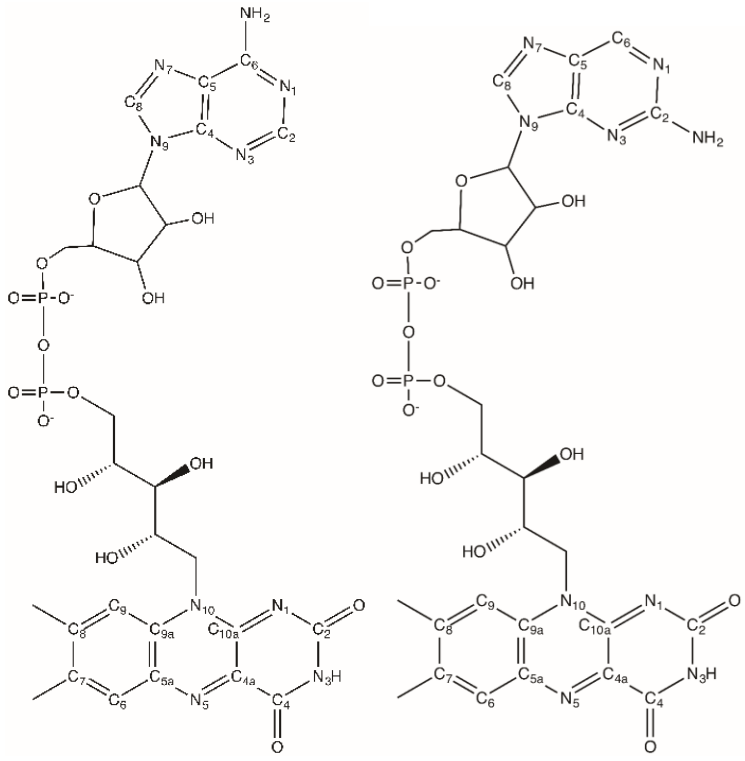

FAD F2ApD

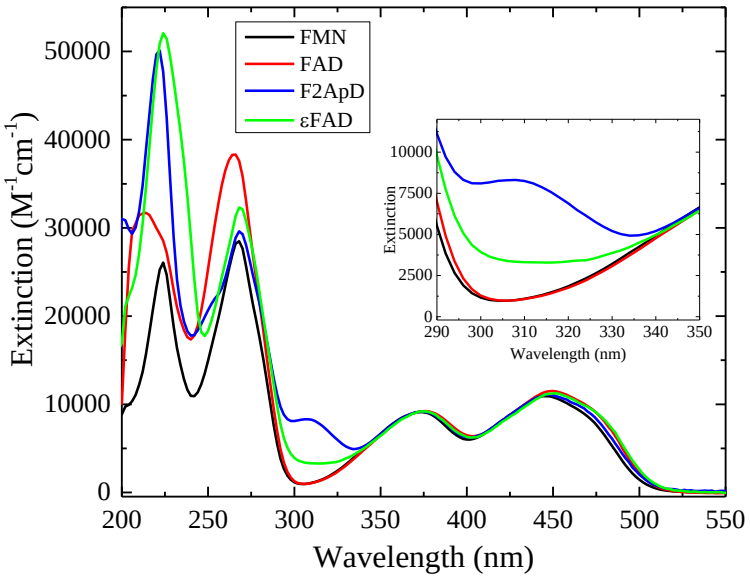

Figure 4.1. Flavin Adenine Dinucleotide. Room temperature absorption spectra of flavin mononucleotide, flavin adenine dinucleotide, flavin 2-aminopurine dinucleotide, and flavin ethenoadenine dinucleotide in phosphate buffer. The extinction at 307 nm and 310 nm is significantly higher for the modified flavins than that of the naturally occurring flavins. The isoalloxazine absorbance features are nearly identical for all four flavins.

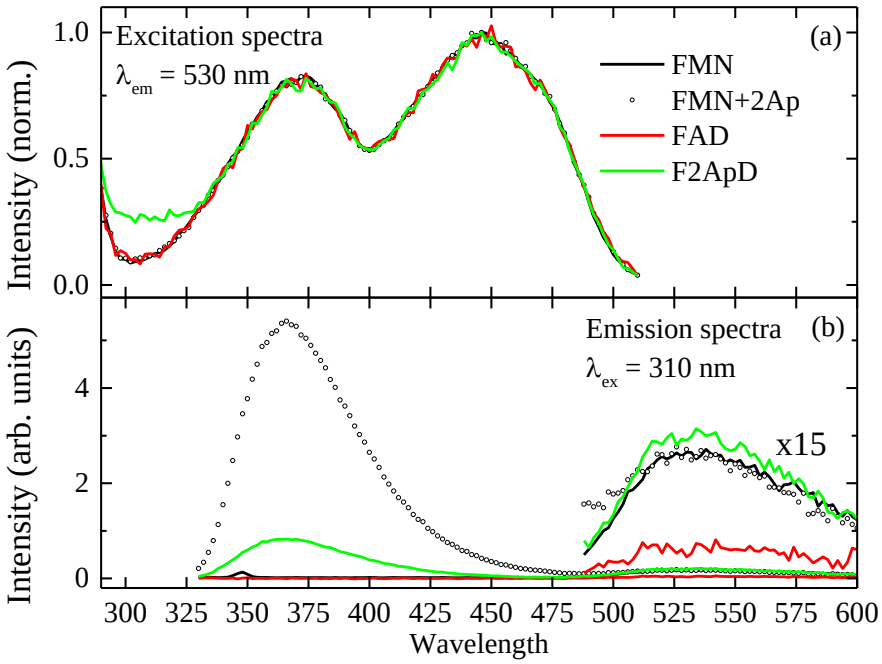

Figure 4.2. Excitation and emission spectra of FMN, FMN+2ApTP, FAD, and F2ApD in the oxidized form. The buffer system for all samples was 100 mM phosphate pH 7.0. Emission spectra were measured using an excitation wavelength of 310 nm. Excitation spectra were measured monitoring emission from the flavin ring system at 530 nm. All spectra plotted were collected at 4°C to avoid collisional quenching exhibited at 20°C.

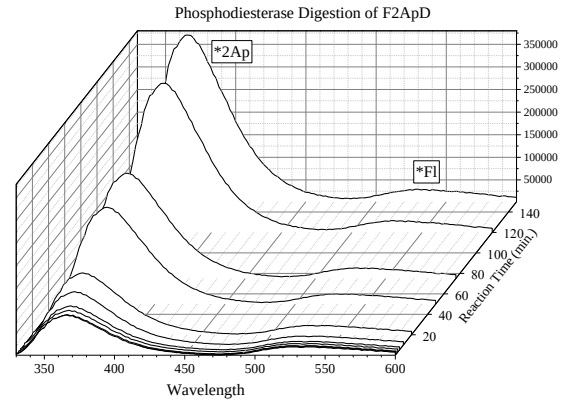

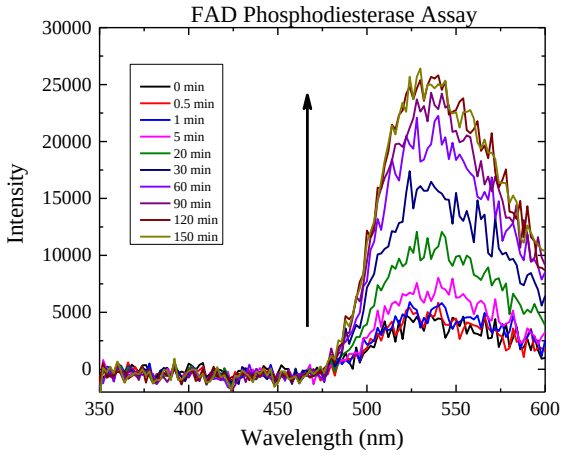

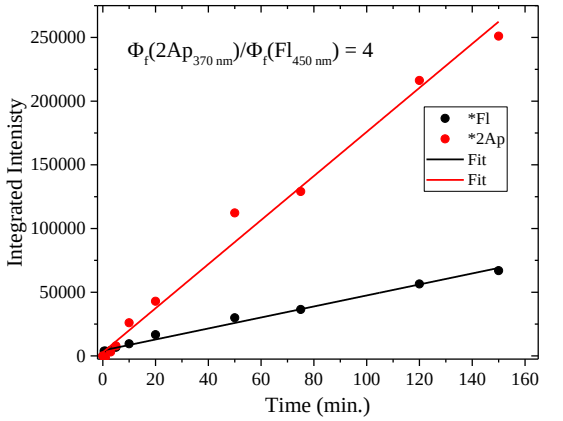

Figure 4.3. Phosphodiesterase digestion of F2ApD (top) and FAD (middle) monitored by steady-state emission. After 2.5 hours there was no additional increase in emission intensity. The bottom graph shows that emission at various digestion times for each molecule.

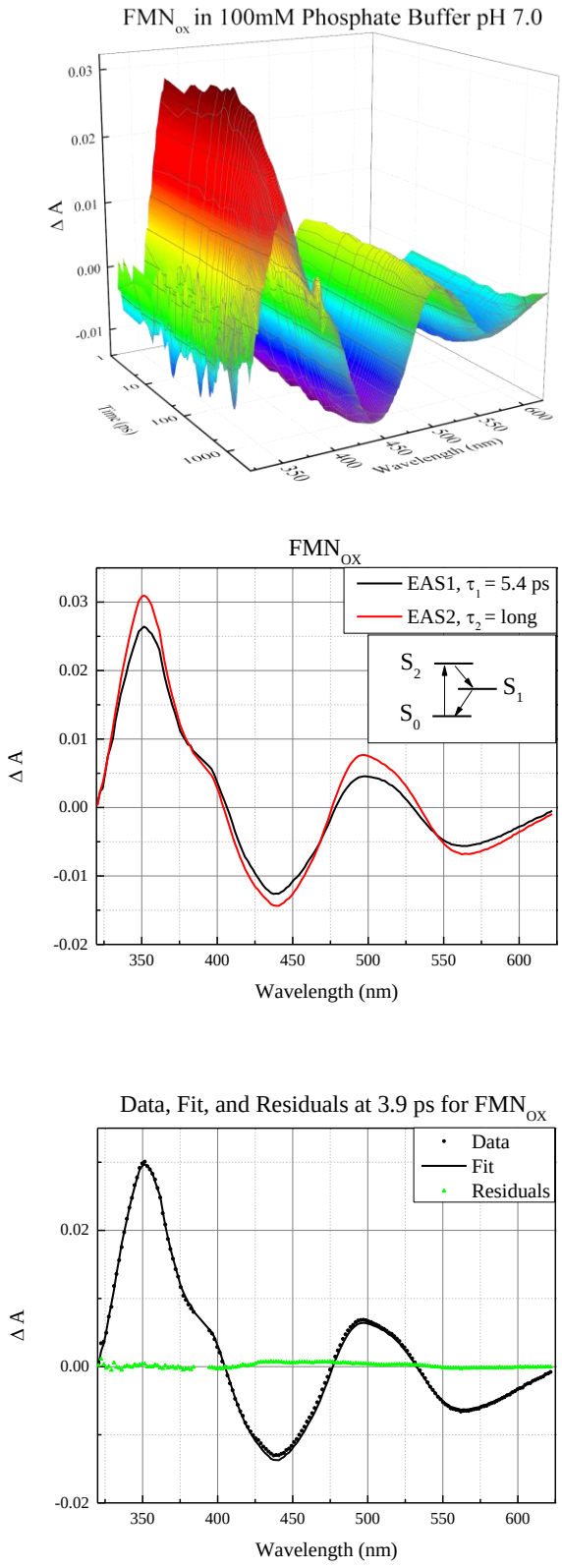

Figure 4.4. Transient absorption data of 200 µM FMNox in 100 mM phosphate buffer

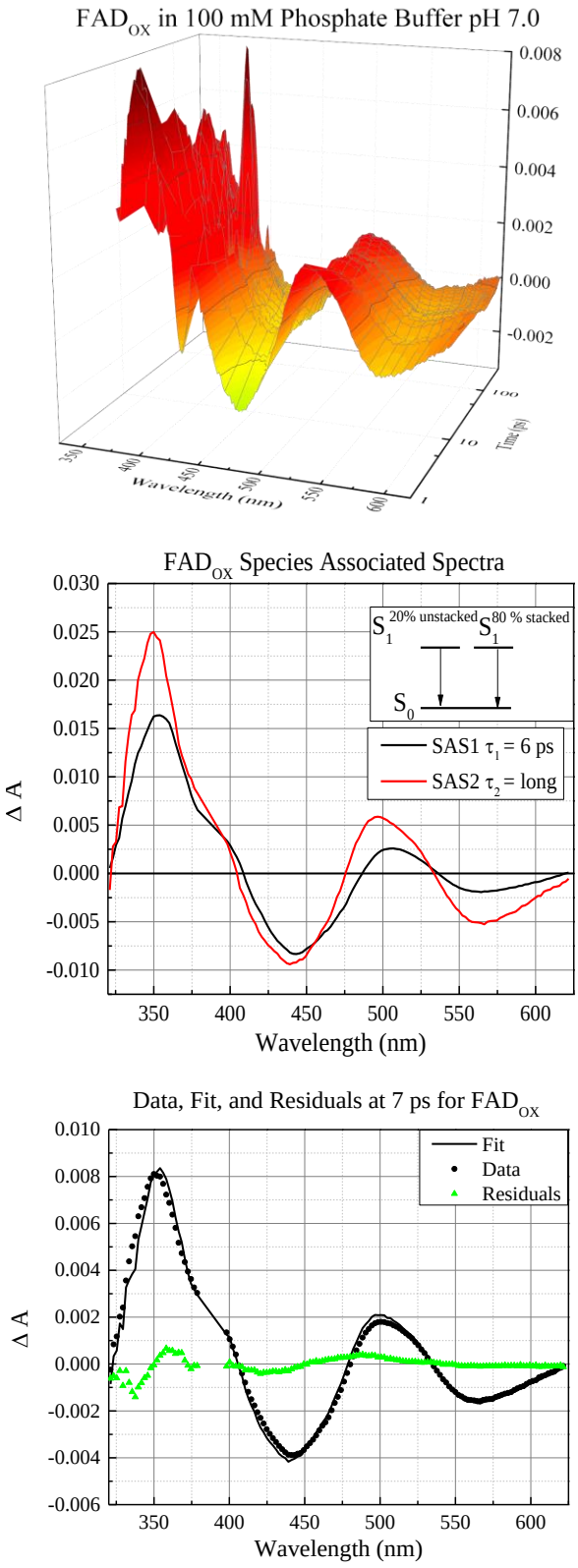

Figure 4.5. Transient absorption data of 200 µM FAD in 100 mM phosphate pH 7.0

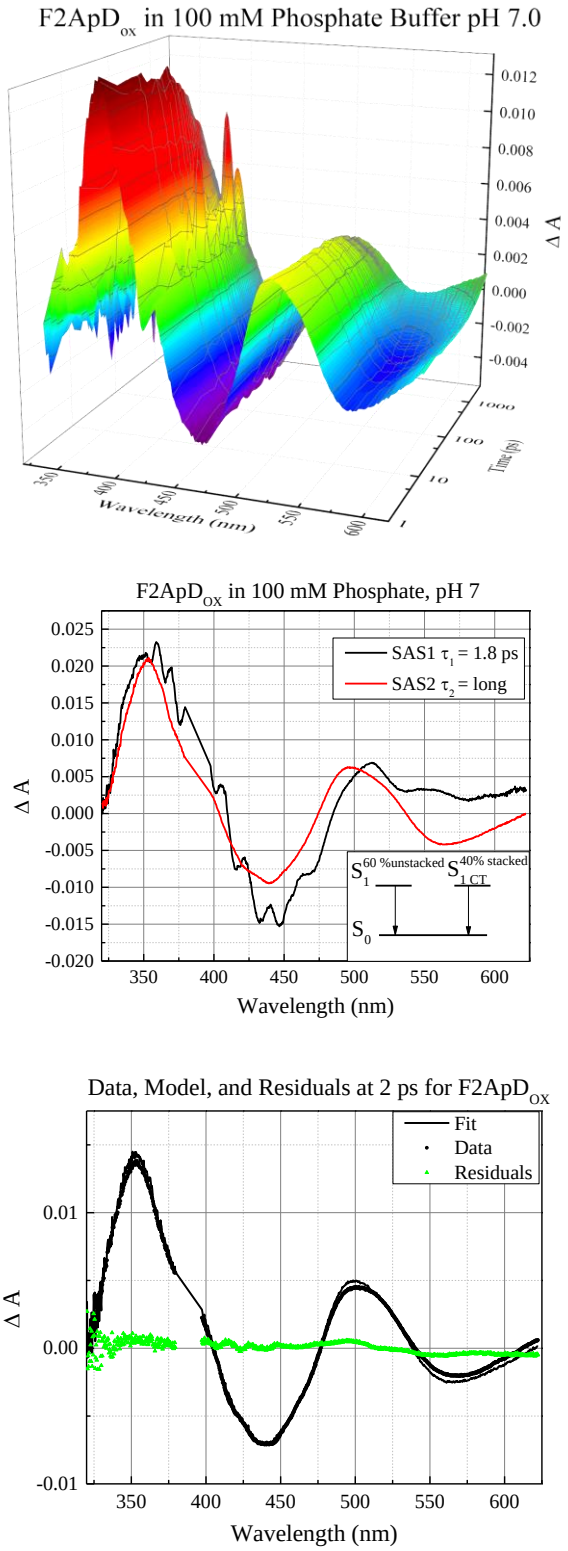

Figure 4.6. Transient spectra of 100 µM F2ApD in 100 mM phosphate pH 7.0

4.5 References

(1) Heikal, A. A. *Biomark. Med.* **2010**, *4* (2), 241–263.

(2) Ghisla, S.; Massey, V. *Eur. J. Biochem.* **1989**, *181*, 1–17.

(3) Huang, S.; Heikal, A. A.; Webb, W. W. *Biophys. J.* **2002**, *82* (5), 2811–2825.

(4) Benson, R. C.; Meyer, R. A.; Zaruba, M. E.; McKhann, G. M. *J. Histochem. Cytochem.* **1979**, *27* (1), 44–48.

(5) Rachofsky, E. L.; Ross, J. B. A.; Krauss, M.; Osman, R. *Acta Phys. Pol., A* **1998**, *94* (5-6), 735–748.

(6) Evans, K.; Xu, D.; Kim, Y.; Nordlund, T. M. *J. Fluoresc.* **1992**, *2* (4), 209–216.

(7) Frey, M. W.; Sowers, L. C.; Millar, D. P.; Benkovic, S. J. *Biochemistry* **1995**, *34* (28), 9185–9192.

(8) Wang, Q.; Raytchev, M.; Fiebig, T. *Photochem. Photobiol.* **2007**, *83* (3), 637–641.

(9) Larsen, O. F. A.; van Stokkum, I. H. M.; de Weerd, F. L.; Vengris, M.; Aravindakumar, C. T.; van Grondelle, R.; Geacintov, N. E.; van Amerongen, H. *Phys. Chem. Chem. Phys.* **2004**, *6* (1), 154–160.

(10) Massey, V.; Hemmerich, P. *Biochem. Soc. Trans.* **1980**, *8*, 246–257.

(11) 1. Herguedas, B.; Martinez-Julvez, M.; Frago, S.; Medina, M.; Hermoso, J. A. *J. Mol. Biol.* **2010**, 218–230.

(12) van Stokkum, I. H. M.; Larsen, D. S.; van Grondelle, R. *Biochim. Biophys. Acta, Bioenerg.* **2004**, *1657* (2-3), 82–104.

(13) Efimov, I.; Kuusk, V.; Zhang, X.; McIntire, W. S. *Biochemistry* **1998**, *37* (27), 9716–9723.

(14) Serrano, A.; Frago, S.; Velázquez-Campoy, A.; Medina, M. .

(15) Weber, G. *Biochem. J.* **1950**, *47*, 114–121.

(16) Barrio, J. R.; Tolman, G. L.; Leonard, N. J.; Spencer, R. D.; Weber, G. *Proc. Natl. Acad. Sci. USA* **1973**, *70* (3), 941–943.

(17) Visser, A. J. W. G. *Photchem. Photobio.* **1984**, *40* (6), 703–706.

(18) Lackowicz, J. R. In *Principles of Fluorescence Spectroscopy*; 2006; pp 353–382.

(19) Steenken, S. *Chem. Rev.* **1989**, *89* (3), 503–520.

(20) Li, G. F.; Glusac, K. D. *J. Phys. Chem. B* **2009**, *113* (27), 9059–9061.

(21) Kao, Y.-T.; Saxena, C.; He, T.-F.; Guo, L.; Wang, L.; Sancar, A.; Zhong, D. *J.*

Am. Chem. Soc. **2008**, *130* (39), 13132–13139.

(22) Shafirovich, V.; Dourandin, A.; Luneva, N. P.; Geacintov, N. E. *Perkin 2* **2000**, No. 2, 271–275.

(23) Liang, J. X.; Matsika, S. *J. Am. Chem. Soc.* **2011**, *133* (17), 6799–6808.

(24) Liang, J.; Nguyen, Q. L.; Matsika, S. *Photochem. Photobiol. Sci.* **2013**, *12* (8), 1387–1400.

CHAPTER 5

RECONSTITUTING AN iFAD INTO A FLAVOPROTEIN: MECHANISTIC INSIGHT FOR THE ROLE OF ADENINE IN DNA REPAIR

5.1 Introduction

E. coli DNA photolyase is a 54 kDa monomeric DNA repair flavoprotein (Figure 5.1 a crystal structure of *A. nidulans* photolyase co-crystallized with substrate bound). This enzyme is responsible for repairing UV-damaged DNA lesions called cyclobutylpyrimidine dimers (CPDs, or T<>T when both pyrimidines are thymidines). These T<>T dimers are bound as substrate to the enzyme and then repaired via a photoinduced electron transfer mechanism catalyzed by a fully reduced anionic flavin, $FADH^-$. *Ec*PL also contains an antenna cofactor methenyltetrahydrofolate (MTHF) that is not essential for catalysis but can improve the efficiency of repair under light limiting conditions[1,2]. Although the catalytic cycle for this enzyme has been solved the reaction intermediates are still highly debated[3–5]. Computational studies indicate that the FAD adenine mediates the electron transfer process via a virtual intermediate[6–8].

Reconstitution studies with its native chromophore FAD and non-native εFAD have been successfully performed in our laboratory earlier. This is the first report of a catalytically competent reconstituted apo-PL using an enzymatically-synthesized iFAD, F2ApD, to make a new photolyase, ApPL.

5.2 Materials and Methods

5.2.1 Preparation of Apo-Photolyase

E.coli DNA photolyase was overexpressed in MS09 cells purchased from the Yale University Cell Bank. The holo-protein was overexpressed and purified according to Gindt *et al.*[10]. Fifty mgs of purified *Ec*PL was processed to make chromophore-free apoPL following the procedure of Jorns *et al.*[11,12] with a yield of about 40%. Apo-protein should be used right away for best reconstitution yields. If experimentation with apo-PL is not performed immediately after production of apo-PL, then the enzyme should be stored in a 1:1 molar ratio of FAD and Calf Thymus DNA at -80^{o}C. This procedure preserves apo-photolyase for up to 4 years.

5.2.2 Reconstitution of Apo-Photolyase

The reconstitution of apo-photolyase was carried out at 4^{o}C in 50 mM phosphate, 10 mM βME, 50% ethylene glycol, pH 7.0. The modified cofactor F2ApD was added in a 1:1 molar ratio of flavin to apo-protein (~20 μM). This solution was left to incubate for 16 hours followed by purification on a 5 mL High Trap Blue Sepharose column following Gindt *et al.*[10]. The reconstituted protein, ApPL, was concentrated and buffer exchanged into Gindt Buffer A (50 mM HEPES, 50 mM NaCl, 10 mM βME, 10% glycerol, pH 7.0). Freshly concentrated ApPL**,** up to 5 μM, was used immediately for CPD repair assays or other characterization experiments.

5.2.3 Repair Assay

The repair assay was conducted in repair buffer: 25 mM HEPES, 25 mM NaCl, 5 mM βME, and 5% glycerol. The concentration of ApPL was 2.5 μM and the

concentration of CPD was 32 µM, greater than 10 times the 1 µM K_M for holo-photolyase[13], to provide pseudo-first order kinetics. Under these conditions the enzyme would be operating at $V_{max,}$ however this is based on the assumption that K_M would not vary much from holo- or FAD-reconstituted photolyase (r-PL). It is important to note that this assumption has already been tested with chemically-synthesized εFAD/apo-PL system, and that K_D, K_M, and k_{CAT} were not significantly modulated[9]. However, due to time constraints it was not possible to measure the K_D for ApPL at this time.

$$k_{cat} = \frac{V_{max}}{[E_T]}$$

Equation 1. Turnover kinetics under steady-state approximation.

The sample was purged with nitrogen gas for 30 minutes and then irradiated with 365 nm light (10.5 mW) in a 2 mm path length quartz cuvette in an ice bath for 15 minutes. Purged, reconstituted CPD was added (see next section for CPD generation and purification) to the irradiated ApPL and absorption spectra were taken at various irradiation time intervals to monitor repair at 266 nm. The extinction difference of CPD to repaired parent for the sequence used was ~19,000 $M^{-1}cm^{-1}$ (Integrated DNA Technologies), see equation 2 for fraction repaired calculation.

$$\Delta A = \Delta\varepsilon\Delta c l$$

$$\Delta A_{266nm} = \log(\frac{I_0^{266nm}}{I^{266nm}})$$

Equation 2. Calculating fraction of CPD repaired[5].

5.2.4 CPD generation and purification

The ssDNA used for the assay was 5'-CGTTGC-3' ("6mer", IDT, Inc.). A 240 µM aliquot was irradiated with a 150 W Xe-arc lamp for 20 minutes in a 2 mm quartz cuvette containing 15% (v/v) acetone to generate the CPD. The cuvette was placed in an ice water bath in a Pyrex beaker which was then placed in a secondary Pyrex container. This mixture of parent and CPD was then purified using an Intersil ODS-2 reverse phase 150 x 4.6 mm HPLC column. Solvent A of the mobile phase consisted of 100 mM triethylammonium acetate doped with 8% acetonitrile pH 7.0. Solvent B was 100% acetonitrile. The separation method is an isocratic flow of 1mL/min 100% solvent A for 15 minutes, then a linear gradient to 80% Solvent A over 5 minutes.

5.2.5 Spectroscopic Methods

All linear absorption measurements were carried out on Hewlett Packard 8452A Diode Array Spectrophotometer. Steady-state studies were carried out on a PTI fluorimeter (Birmingham, NJ). Excitation slits were kept at 2 nm to prevent photodegradation of the flavin and emission slits were kept at 3 nm to optimize the signal to noise ratio. The ApPLsamples were measured in a 50 mM HEPES, 50mM NaCl, 10mM BME, 10% glycerol buffer at pH 7.0. A wavelength of 310 nm excitation was used for emission scans, as excitation at 450 nm yielded no fluorescence. All excitation scans were obtained monitoring emission at 370 nm because there was no appreciable emission around 530 nm (flavin). It was later discovered that HEPES buffers undergo photo-oxidation at this wavelength. Therefore, it is important to repeat these experiments in phosphate buffers. The steady-state CPD repair assay was carried out in repair buffer: 25 mM HEPES, 25 mM NaCl, 5 mM βME 5% glycerol.

5.3 Results and Discussion

F2ApD was successfully reconstituted into *E.coli* apo-photolyase. This flavoprotein in its wild-type conformation contains a methynltetrahydrofolate (MTHF) antenna and catalytic FAD cofactors[14,3,15]. These natural chromophores were removed following established protocol by Jorns *et al.* and the apo-protein was reconstituted with F2ApD in a 1:1 molar ratio[16]. This "mutant" PL was nicknamed "ApPL",

To assess reconstitution under these conditions, the UV/vis baseline-corrected absorption spectrum of ApPL is shown in Figure 5.2. The F2ApD cofactor has a maximum at 450 nm with A_{450}~0.056. This corresponds to 25 μM ApPL. The absorbance of the protein was higher, A_{274} ~1.8 due to 14 Trp residues. ApoPL has an ε_{274}~10^5 $M^{-1}cm^{-1}$. From our earlier work, F2ApD has an ε_{274} = 30,000 $M^{-1}cm^{-1}$. For pure ApPL (i.e. no apo-protein), $\varepsilon_{274}/\varepsilon_{450}$ = 130,000/11,200 = 11.6. This preparation has A_{274}/A_{450} = 32, which indicates that there was about 87 μM apo-PL remaining. We do not know whether this is due to the loss of F2ApD from the ApPL or whether this represents the true reconstitution yield (~29%). Corroborating this estimate is the appearance of the spectrum in the 450 nm region. As was shown earlier, FAD_{OX} in solution has weak vibronic structure, but in rPL the vibronic structure sharpens considerably, indicating tight binding between the apo-PL and the FAD. The vibronic structure of the F2ApD-reconstituted apo-PL was more modest but sharper than the FAD_{aq} case. A 29% reconstitution yield is quite promising because typically reconstitution yields for the FAD/apo-PL system range from 10%-50% but require a 20-fold FAD molar excess.

ApPL was then assayed for CPD repair. 2.5 μM of ApPL was made anoxic and photoreduced using 365 nm light for 15 minutes. Substrate 6mer CPD was added using an air-tight syringe. The enzyme:substrate mixture was irradiated at 365 nm over 4 minutes while monitoring any absorption increase at 266 nm, indicative of CPD repair. The parent strand extinction at 266 nm is 51,000 $M^{-1}cm^{-1}$ while the CPD has an extinction of approximately 32,000 $M^{-1}cm^{-1}$. The k_{CAT} for ApPL is 3.1 min^{-1}. This was calculated by taking the total fraction of repaired CPD and dividing this value by the time at which the amount of CPD was repaired. This was taken as V_{max} because the substrate is in excess of the enzyme, therefore saturating the enzyme substrate complex. Vmax is then divided by the enzyme concentration, see Equation 1. The fraction repaired was determined by monitoring the increase in 266 nm absorption and confirmed by HPLC analysis, see Figure 5.3. The rate constant and rate of repair is consistent with previously measured r-PL, k_{CAT} *is* 4 min^{-1} [9]. Even though this is a steady-state assay of the overall repair yield and rate, it appears that substitution of 2Ap for Ade does not affect the overall turnover number. Nonetheless, the effect, if any, on k_{ET}, of this cofactor analog awaits ultrafast measurements. It is extremely important to note that the use of HEPES buffers should NOT be used for irradiation studies. The peak broadening seen in the HPLC trace of Figure 5.3, indicates that HEPES generates photooxidation[17] products and can affect the retention times of CPD and parent peaks. Future measurements should be conducted in phosphate buffer. Tris buffer controls have been shown to affect the 2Ap emission (perhaps reactivity with the buffer amines).

The steady state fluorescence spectra taken at 4° and 20°C seem to indicate that ApPL has very different photophysical compared to F2ApD in solution. In ApPL, the

flavin emission is completely quenched and the 2Ap emission very much attenuated (Figure 5.4). This flavin fluorescence quenching could be caused by photoinduced electron transfer from the *2Ap moiety. One might assume that this would imply that the rate of electron transfer should be affected. However, F2ApD$_{OX}$ is not the catalytic redox state of photolyase. We are in the process of performing fluorescence studies on *F2ApDH^{-} to see if this quenching pattern persists in the reduced form.

5.4 Conclusions

Here we have shown that F2ApD has successfully incorporated into *Ec* DNA photolyase apo-protein and that it is catalytically active. This will be a promising FAD analogue to deeply explore the role of adenine in DNA repair (photolyases) and blue-light signal transduction (cryptochromes).

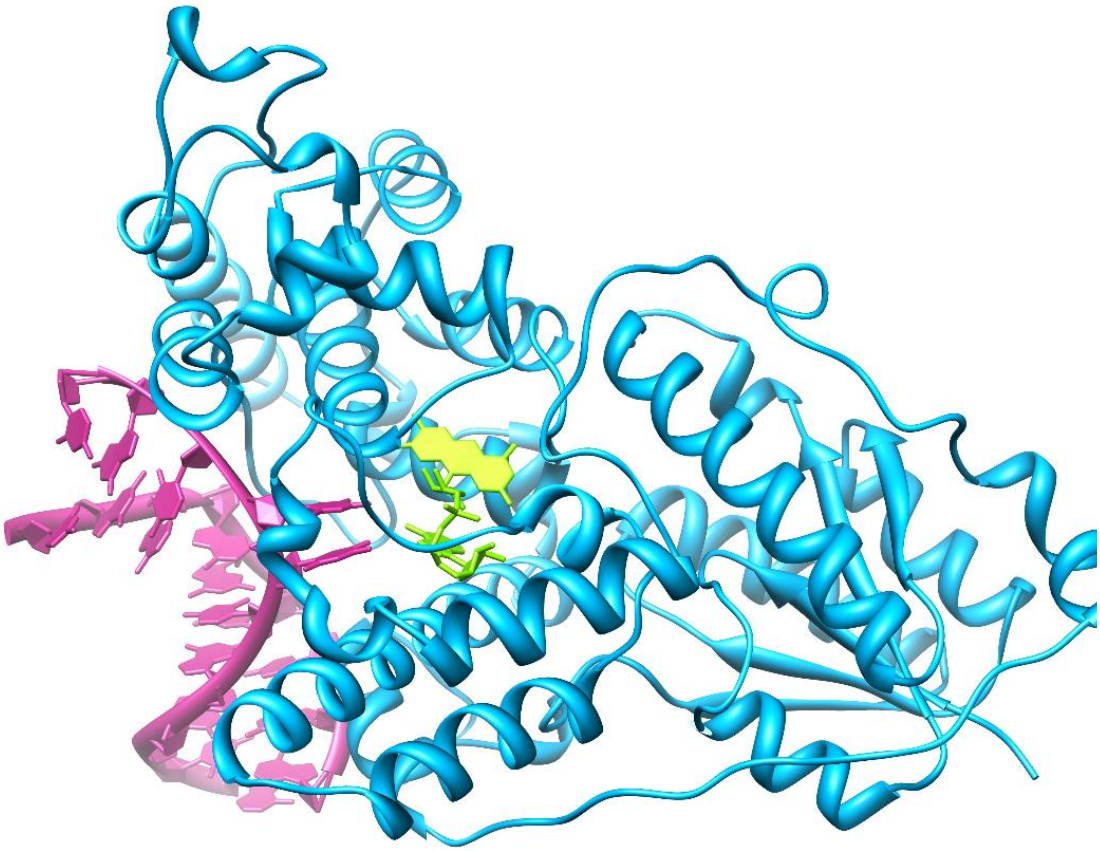

Figure 5.1. Crystal structure of *A. nidulans* DNA Photolyase (PDB ID 1TEZ[18]) with FAD cofactor shown in yellow and CPD substrate analogue, shown in pink.

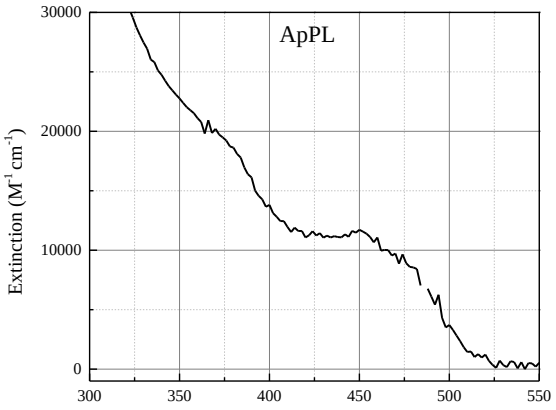

Figure 5.2. Absorption spectra of 5 µM ApPL

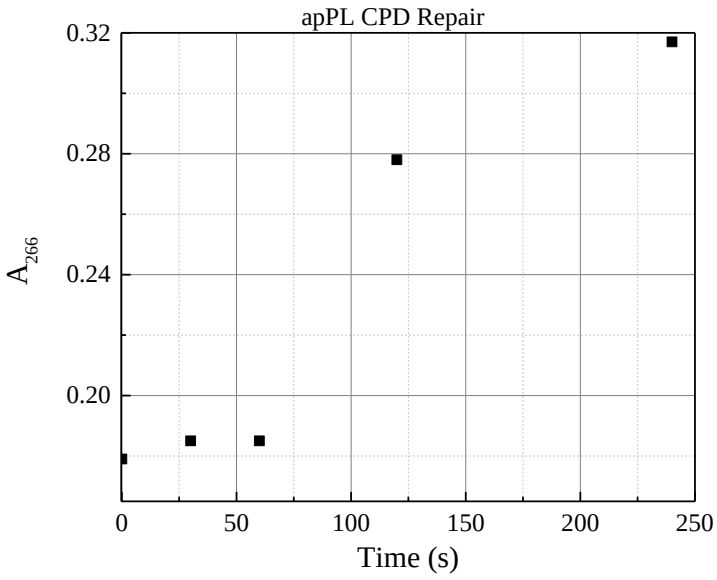

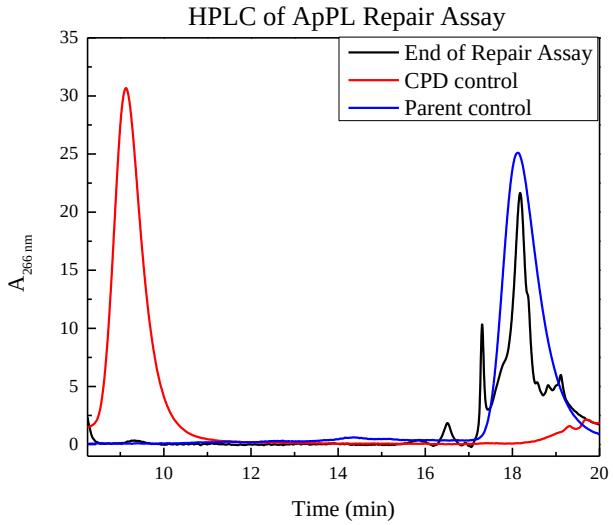

Figure 5.3. CPD repair by ApPL carried out at 25ºC (CPD control and Parent control were obtained by Munshi *et al.*, manuscript submitted).

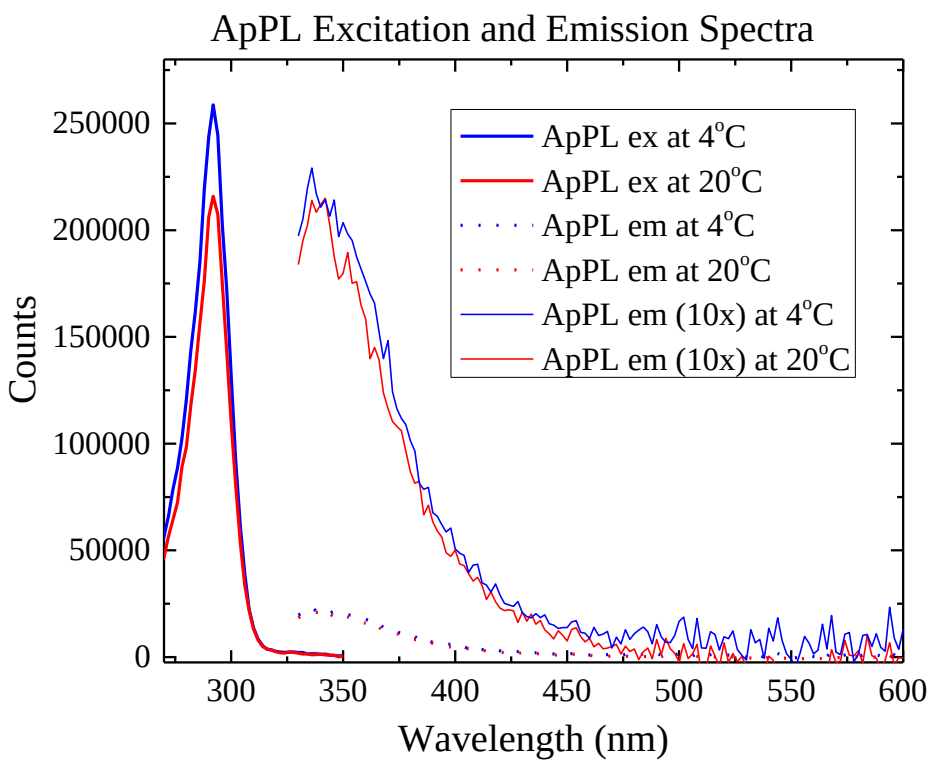

Figure 5.4. Steady-state fluorescence spectra of ApPL at 4° and 20°C. Emission spectra (light solid lines are 10x of the corresponded dotted lines) were taken at λ_{ex}=310 nm. Excitation spectra were taken with λ_{em}=370 nm.

5.5 References

(1) Sancar, G. B.; Sancar, A. *Trends Biochem. Sci.* **1987**, *12(7)*, 259–261.

(2) Johnson, J. L.; Hamm-Alvarez, S.; Payne, G.; Sancar, G. B.; Rajagopalan, K. V; Sancar, A. *Proc. Natl. Acad. Sci. U. S. A.* **1988**, *85* (7), 2046–2050.

(3) MacFarlane Iv, A. W.; Stanley, R. J. *Biochemistry* **2003**, *42* (28), 8558–8568.

(4) Liu, Z.; Tan, C.; Guo, X.; Kao, Y.-T.; Li, J.; Wang, L.; Sancar, A.; Zhong, D. *Proc. Natl. Acad. Sci.* **2011**.

(5) Thiagarajan, V.; Villette, S.; Espagne, A.; Eker, A. P. M.; Brettel, K.; Byrdin, M. *Biochemistry* **2010**, *49* (2), 297–303.

(6) Acocella, A.; Jones, G. A.; Zerbetto, F. *J. Phys. Chem. B* **2010**, *114* (11), 4101–4106.

(7) Medvedev, D.; Stuchebrukhov, A. A. *J. Theor. Biol.* **2001**, *210* (2), 237–248.

(8) Prytkova, T. R.; Beratan, D. N.; Skourtis, S. S. *Proc. Natl. Acad. Sci. U. S. A.* **2007**, *104* (3), 802–807.

(9) Stanley, R. J.; Singh, V.; Narayanan, M.; Jacoby, K.; Munshi, S.; Moravcevic, K. In *Proceedings of the 17th International Symposium on Flavins and Flavoproteins*; Miller, S. M., Hille, R., Palfey, B. A., Eds.; Lulu; pp 403–408.

(10) Gindt, Y. M.; Vollenbroek, E.; Westphal, K.; Sackett, H.; Sancar, A.; Babcock, G. T. *Biochemistry* **1999**, *38* (13), 3857–3866.

(11) Gindt, Y. M.; Vollenbroek, E.; Westphal, K.; Sackett, H.; Sancar, A.; Babcock, G. T. *Biochemistry* **1999**, *38* (13), 3857–3866.

(12) Wang, B.; Jorns, M. S. *Biochemistry* **1989**, *28* (3), 1148–1152.

(13) Schelvis, J. P. M.; Zhu, X.; Gindt, Y. M. *Biochemistry* **2015**, *54* (40), 6176–6185.

(14) Sancar, A.; Smith, F. W.; Sancar, G. B. *J. Biol. Chem.* **1984**, *259* (9), 6028–6032.

(15) Murphy, A. K.; Tammaro, M.; Cortazar, F.; Gindt, Y. M.; Schelvis, J. P. M. *J. Phys. Chem. B* **2008**, *112* (47), 15217–15226.

(16) Jorns, M. S.; Wang, B.; Jordan, S. P.; Chanderkar, L. P. *Biochemistry* **1990**, *29* (2), 552–561.

(17) Masson, J.-F.; Gauda, E.; Mizaikoff, B.; Kranz, C. *Anal. Bioanal. Chem.* **2008**, *390* (8), 2067–2071.

(18) Tamada, T.; Kitadokoro, K.; Higuchi, Y.; Inaka, K.; Yasui, A.; De Ruiter, P. E.; Eker, A. P. M.; Miki, K. *Nat. Struct. Biol.* **1997**, *4* (11), 887–891.